The University of British Columbia

FACULTY OF GRADUATE STUDIES

PROGRAMME OF THE

FINAL ORAL EXAMINATION

FOR THE DEGREE OF

DOCTOR OF PHILOSOPHY

of

LEUNG-KAI NG

B.Sc. (Special), University of Hong Kong, 1961

M.Sc., University of Hong Kong, 1964

FRIDAY, SEPTEMBER 22, 1967 AT 3:30

IN ROOM 301, HENNINGS BUILDING

COMMITTEE IN CHARGE

Chairman: B. N. Moyls

M.P. Beddoes J.W. Bichard
G.M. Griffiths D.L. Livesey
K.C. Mann B.L. White

Research Supervisor: K.C. Mann

External Examiner: G.T. Ewan
Chalk River Nuclear Laboratories
Atomic Energy of Canada Ltd.
Chalk River, Ontario

RE-INVESTIGATION OF THE EXCITED STATES OF Gd 154

ABSTRACT

The excited states of Gd 154 obtained from the decay of Eu 154 have been investigated. Precise measurements of the energies and intensities of the gamma transitions have been made, using Lithium-drifted Germanium detectors. A revised decay scheme is presented in which all the gamma transitional energies agree with the corresponding energy differences between levels to within 1 Kev. A 1263.3 Kev level is established by the presence of a gamma transition of 892.7 Kev. Two other gamma transitions of energies, 903.6 Kev and 582.1 Kev from the negative-parity levels to the 2^+ beta excited level have also been discovered. The proper locations of the 995.9 Kev and 1004.5 Kev in the decay scheme are confirmed by a gamma-gamma coincidence method using a Germanium detector and a NaI(Tl) scintillator. The energies and intensities of the internal conversion electrons and the beta transitions have been measured by an intermediate image spectrometer. Their values are quite consistent with the established decay scheme.

Theoretical values of the energy levels and the branching ratios for gamma transitions have been calculated, using the Asymmetric Rotator Model (J.P. Davidson's treatment). The 'stiffness' parameter of

the nucleus μ and its asymmetry parameter γ obtained are 0.402 and 11.52 degrees respectively. Comparison of the experimental and theoretical energies of seven positive-parity levels gives a root-mean-square deviation of 1.5 %. Three out of the four experimental branching ratios are in good agreement with the theoretical values. The monopole transition probability for the transition from the 0^+ beta excited state to the 0^+ ground state measured also agrees with the present theoretical calculation.

GRADUATE STUDIES

Field of study: Nuclear spectroscopy

Nuclear Physics	J.B. Warren
Theoretical Nuclear Physics	M. McMillan
Special Relativity	H. Schmidt
Electromagnetic Theory	P. Rastall
Elementary Quantum Mechanics	G.M. Volkoff
Advanced Quantum Mechanics	F.A. Kaempffer
Electronic Instrumentation	M.P. Beddoes

AWARDS

1957-60 Hong Kong Government Scholarship

1964-67 Canadian Government Scholarship under the Canadian International Development Assistance Programs.

RE-INVESTIGATION OF THE EXCITED STATES OF Gd 154

by

LEUNG-KAI NG

B.Sc. (Special) The University of Hong Kong, 1961

M.Sc. The University of Hong Kong, 1964

A THESIS SUBMITTED IN PARTIAL FULFILMENT OF

THE REQUIREMENTS FOR THE DEGREE OF

DOCTOR OF PHILOSOPHY

in the Department

of

PHYSICS

We accept this thesis as conforming to the

required standard

THE UNIVERSITY OF BRITISH COLUMBIA

August, 1967

In presenting this thesis in partial fulfilment of the requirements for an advanced degree at the University of British Columbia, I agree that the Library shall make it freely available for reference and Study. I further agree that permission for extensive copying of this thesis for scholarly purposes may be granted by the Head of my Department or by his representatives. It is understood that copying or publication of this thesis for financial gain shall not be allowed without my written permission.

Department of Physics

The University of British Columbia
Vancouver 8, Canada

Date 23rd September, 1967

ABSTRACT

The excited states of Gd 154 obtained from the decay of Eu 154 have been investigated. Precise measurements of the energies and intensities of the gamma transitions have been made, using Lithium-drifted Germanium detectors. A revised decay scheme is presented in which all the gamma transitional energies agree with the corresponding energy differences between levels to within 1 Kev. A 1263.3 Kev level is established by the presence of a gamma transition of 892.7 Kev. Two other gamma transitions of energies, 903.6 Kev and 582.1 Kev from the negative-parity levels to the 2^+beta excited level have also been discovered. The proper locations of the 995.9 Kev and 1004.5 Kev in the decay scheme are confirmed by a gamma-gamma coincidence method using a Germanium detector and a NaI(Tl) scintillator. The energies and intensities of the internal conversion electrons and the beta transitions have been measured by an intermediate image spectrometer. Their values are quite consistent with the established decay scheme.

Theoretical values of the energy levels and the branching ratios for gamma transitions have been calculated, using the Asymmetric Rotator Model (J.P. Davidson's treatment). The 'stiffness' parameter of the nucleus μ and its

asymmetry parameter γ obtained are 0.402 and 11.52 degrees respectively. Comparison of the experimental and theoretical energies of seven positive-parity levels gives a root-mean-square deviation of 1.5 %. Three out of the four experimental branching ratios are in good agreement with the theoretical values. The monopole transition probability for the transition from the 0^+ beta excited state to the 0^+ ground state measured also agrees with the present theoretical calculation.

TABLE OF CONTENTS

		Page
CHAPTER I	INTRODUCTION	1
CHAPTER II	THEORY	6
	1. The Collective Models	6
	2. The Asymmetric Rotator Model	11
	3. The Octupole Case in the Asymmetric Rotator Model	17
	4. Calculations of Reduced E2 Transition Probabilities	19
	5. Other Forms of Electromagnetic Transitions	23
CHAPTER III	THE DESIGN OF EXPERIMENTS	26
CHAPTER IV	THE GAMMA SPECTROSCOPY	29
	1. General Considerations	29
	2. Interaction between Gamma Rays and the the Detectors	32
	3. Gamma-ray Detection Assemblies	34
	4. Source Preparation and Mounting	42
	5. Experimental Procedures	45
	6. Results and Analysis	50
CHAPTER V	GAMMA-GAMMA COINCIDENCE SPECTROSCOPY	62
	1. General Considerations	62

Page

2. The Coincidence System 64

3. Experimental Procedures 70

4. Results 72

CHAPTER VI THE BETA SPECTROSCOPY 74

1. General Considerations 74

2. The Internal Conversion and Pair Production 77

3. The Beta Spectrometer 82

4. Preparation of Beta Sources 86

5. Experimental Procedures 88

6. Results and Analysis 90

CHAPTER VII THE DECAY SCHEME AND MODEL FITTING 103

1. The Decay Scheme 103

2. Model Fitting 108

CHAPTER VIII CONCLUSIONS 114

REFERENCES 117

LIST OF FIGURES AND TABLES

Page

CHAPTER IV

Figure 1. The gamma spectrometer 35

Figure 2. Electronic circuit for the gamma spectrometer 36

Figure 3. Cs 134 spectrum taken from the gamma-spectrometer assembly 38

Figure 4. Germanium detector assembly 40

Figure 5. Input stage of the low-noise preamplifier. 41

Figure 6. Co 60 gamma spectrum from 1.5c.c. Ge detector 43

Figure 7. Co 60 gamma spectrum from 5 c.c. Ge detector 44

Figure 8. Eu 154 gamma spectrum 48

Figure 9. Low-energy gamma peaks of Eu 154 49

Table I. Gamma peaks used for energy calibration . 52

Figure 10. Gamma energy calibration curve 53

Table II. Gamma peaks used for intensity calibration 56

Figure 11. Gamma intensity calibration curve. To follow 56

Table III. Energies and Intensities of Eu 154 spectrum (gamma) 58

Figure 12. Weak gamma peaks in the Eu 154 spectrum . 60

Table IV. Gamma peaks belonging to Eu 152 impurity . 61

CHAPTER V

Figure 13. Illustration of gamma-gamma coincidence. . 63

Figure 14. The gamma-gamma coincidence system 65

Figure 15. Photomultiplier output stages. 67

Figure 16. The tunnel diode discriminator 69

Figure 17a,b,c,d. The gamma-gamma coincidence spectra 73

CHAPTER VI

Figure 18. Beta spectrometer assembly 83

Figure 19. Magnet current control circuit 84

Figure 20a. Beta spectrum of Eu 154, low-energy part. 91

Figure 20b. Beta spectrum of Eu 154, high-energy part 92

Figure 20c. Beta continuum of Eu 154. 93

Table V. Data of beta conversion peaks 95

Figure 20d. Expanded portion of Eu 154 beta spectrum. 98

Table VI. Comparison of K-internal conversion coefficients. 100

Table VII. Energies and relative intensities of beta transitions 101

Figure 21. The Kurie plots 102

CHAPTER VII

Figure 22. The excited states of Gd 154 from the decay of Eu 154 104

Table VIII. Transitional intensities for gammas, conversion electrons and betas. 105

Page

Table IX. Comparison of the experimental and theoretical energies in the quadrupole case. 110

Table X. The branching ratios of gamma transitions between positive-parity levels. 111

ACKNOWLEDGMENTS

I wish to express my gratitude to Dr. K.C. Mann for his guidance, encouragement and help throughout the work.

I am also indebted to Dr. J.P. Davidson of the Physice Department, Kansas University, Dr. T. Katoh of the Nuclear Engineering Department, Nagoya University, and Dr. D. Kiang of the Physics Department, Dalhousie University for valuable information given to me; to the members of the Van de Graaff Group, in particular Dr. G. Jones, Dr. G.M. Griffith and Mr. D.A. Dalby for allowing me the use of some of their equipment; and to the Computing Centre Staff for their help in data processing.

Technical assistance by Mr. T. Walton, Mr. E. Price, Mr. A. Fraser and Mr. J. Lees are highly appreciated.

The present project is supported by the External Aid Office, Government of Canada through a student scholarship and the National Research Council through Grants-in-Aid of Research to Dr. K.C. Mann.

CHAPTER I

INTRODUCTION

The description of a nucleus is essentially a complicated many-body problem which has not reached any precise solution. To simplify this problem, several phenomenological models have been proposed. The commonly known one is the 'single-particle shell model' [1], which views each nucleon (proton or neutron) in a nucleus to be moving under the action of an average potential contributed by the other nucleons. As a quantum-mechanical consequence, the nucleons should be moving in definite 'shells' similar to the electrons in an atom. The number of protons Z or neutrons N which completes a given number of shells is called a magic number.

This model predicts successfully the spins and parities of most nuclei at the ground state. For nuclei whose Z and N values are close to the magic numbers, good quantitative agreement in low-lying energy levels with experiments can be obtained. However, this agreement deteriorates as Z or N runs away from the magic numbers. It is even worse when one considers heavy even-even nuclei whose mass numbers A are within the range 150-190 or greater than 228. In this

case, the individual nucleonic motion gives way to the more predominent motions of the nucleus as a whole, i.e. the collective rotation and vibration. A collective model based on the liquid-drop model was proposed by Bohr [2]. Thus the surface oscillation or vibration of the nucleus is accounted for by the hydrodynamic behaviour of a liquid drop. Also because of the interaction of single particle and closed shells, deformation in the equilibrium shape of the nucleus from spherical symmetry becomes possible [3]. This deformation gives rise to the collective rotation of the nucleus. Consequently, the energy level scheme of the nucleus consists of vibrational levels which are further split into rotational bands.

On the other hand, the nucleus can be considered as a rigid rotator, which gives rise to pure rotational levels. The rotator is then softened to yield surface vibrations, and therefore, vibrational levels. The shape of the rigid rotator is the equilibrium shape, that is the shape at zero vibration.

The collective model described above has been under great theoretical development in the past few years, notably by A. Faessler, W. Greiner, R.K. Sheline, A.S. Davydov and J.P. Davidson [4)-16)]. The current interest lies in the determination of the form and magnitude of the rotation-vibration interaction which accounts for the discrepancy between energy level calculations and experimental measure-

ments. This discrepancy is expected to be more pronounced for nuclei having nuclear masses lying near the ends of the A ranges mentioned above, and Gadolinium 154 is one of the typical examples.

The excited states of Gd 154 are often obtained from the beta decay of Europium 154, the latter isotope being first produced by Scheichenberger using neutron-capture process. Intense investigation on the decay scheme was started in 1957. The first detailed decay scheme was established independently by J.M. Cork et al[17] and F.S. Stephens et al[18], using beta spectral analysis and gamma-gamma coincidence work. Similar investigations have been done by B.S. Dzelepov[19], B.V. Bobilin[20] and O. Nathan et al[21]. The transitional energies determined by the above authors vary appreciably, and their intensities have wide ranges of uncertainty. The reason for these can be easily appreciated when considering the complexity of the decay scheme, and the presence of Eu 152 impurity which has a decay scheme not less complicated than that of Eu 154. It should also be noted that the electron conversion peaks of Eu 152 are similar in energy and intensity to those of Eu 154, and that the neutron-capture process favours the production of Eu 152 over Eu 154. Other methods of source production have so far been unable to eliminate all impurities.

Beta-gamma and gamma-gamma correlation methods have since then been employed in the investigation by several authors [22)-30)], aiming at 1) to confirm or improve the established decay scheme, 2) to determine more precisely the reduced gamma transition probabilities, and 3) to find the forbiddenness of each beta transition in the decay energy continuum. These are essential for verifying any proposed nuclear model and for finding the matrix elements of the beta transitions. Other methods such as life-time measurements for specific gamma transitions [31)], 4π-counting for K-γ coincidence work [32)], investigation of the decay of short-lived Tb 154 to Gd 154 [33)], and Coulomb excitation for producing higher excited levels of Gd 154 [34),35)] have been exploited. However, all experiments performed to date suffer from poor resolution of the gamma detectors (NaI scintillators), which severely hinders the analysis of a complicated gamma spectrum. Although the use of coincidence methods may help in such an analysis, it is only practicable when dealing with relatively strong gamma peaks. Finally, external beta conversion method [36)] (the photoelectron process) has been used. It improves the resolution, but again suffers from lack of intensity.

With the newly developed Lithium-drifted Germanium detectors in the laboratory of the Physics Department, U.B.C., a re-investigation of the decay of Eu 154 becomes more

promising, since the resolution of these detectors is ten times better than that of the usual NaI scintillators. In the present work, the author applied this new tool together with an intermediate-image beta spectrometer to obtain more accurate energy and intensity data for the gamma transitions in the decay of Eu 154. These data were then used to check the validity of the collective model proposed and developed by Davydov, Filippov, and Davidson [10)-16)]. The results, as will be shown later, proved fruitful.

CHAPTER II

THEORY

§1. The Collective Models.

Bohr's hydrodynamical model[2], which borrowed its concept from the liquid-drop model, forms the basis of the present theory. By considering a nucleus to be a drop of charged liquid, the following assumptions immediately apply:

1) the nuclear fluid is incompressible and has constant mass density. Consequently, the nuclear volume is an invariant;

2) the nucleus is capable of surface oscillations which can be described as small simple harmonic motions; and

3) the restoring forces contributing to the oscillation are the surface tension and the Coulomb repulsion.

The surface of the nucleus can be written as an expansion in spherical harmonics as shown,

$$R(\theta,\phi,t) = R_o(1 + \sum_{\lambda,\mu} a(t)_{\lambda,\mu} Y_{\lambda,\mu}(\theta,\phi)) \qquad (1)$$

where R_o is the nuclear radius when in spherical configuration and $a(t)_{\lambda,\mu} \ll 1$ are the distortions from spherical symmetry.

It can be easily seen that $a(t)_{\lambda,\mu}$ represent the dimensionless distance variables; and from expressions of simple harmonic motion, the potential and kinetic energies become,

$$V = \tfrac{1}{2}\sum_{\lambda,\mu} C_\lambda \left| a(t)_{\lambda,\mu} \right|^2 \qquad (2a)$$

$$T = \tfrac{1}{2}\sum_{\lambda,\mu} B_\lambda \left| \dot{a}(t)_{\lambda,\mu} \right|^2 \qquad (2b)$$

respectively, where B_λ is the mass coefficient and C_λ, the constant for restoring forces.

It was shown by Rainwater [3] that a single particle moving in a potential well had a lower energy if the well was deformed than if it was spherical. This "single-particle-shell effect" makes it possible for the 'liquid drop' to be non-spherical at equilibrium. Hence we can assume that a permanently deformed (ellipsoidal) shape exists in the nucleus. Subsequently, we can attach a new set of coordinate axes along the three principle axes of the deformed body. This new coordinate system S' can be related to the laboratory coordinate system S by Eulerian angles, $\theta_1, \theta_2, \theta_3$, such that z'-axis in S' = $z'(\theta_1, \theta_2)$ in S and z-axis in S = $z(\theta_2, \pi-\theta_3)$ in S'. The variables in system S' can then be related to the corresponding variables in system S by a unitary rotation matrix as shown [37), 38)],

$$a'_{\lambda,\nu} = \sum_{\mu} a_{\lambda,\mu} D^{\lambda}_{\mu\nu}(\theta_i), \qquad (\theta_i) = (\theta_1, \theta_2, \theta_3) \qquad (3)$$

It should be noted that the assignment of system S' is not unique. Restricting to right-handed systems, there are 24 ways of choosing system S' with its axes along the principle axes of the nucleus. This will be discussed later (§2).

Considering only the quadrupole case (i.e. $\lambda = 2$), for the time being, and dropping the subscript λ, equation (1) becomes,

$$R = R_o\left(1 + \sum_{\mu=-2}^{2} a_\mu Y_\mu(\theta, \phi)\right) \qquad (4a)$$

or in Cartesian coordinates,

$$R = R_o\left(1+a_{xx}\frac{x^2}{r^2}+a_{yy}\frac{y^2}{r^2}+a_{zz}\frac{z^2}{r^2}+2a_{xy}\frac{xy}{r^2}+2a_{yz}\frac{yz}{r^2}+2a_{zx}\frac{zx}{r^2}\right) \tag{4b}$$

with the relations,

$$\begin{aligned} a_{xx} + a_{yy} + a_{zz} &= 0 \\ a_{\pm 2} &= \sqrt{\frac{2\pi}{15}}\,(a_{xx} - a_{yy} \mp 2ia_{xy}) \\ a_{\pm 1} &= \sqrt{\frac{8\pi}{15}}\,(a_{zx} \mp ia_{yz}) \\ a_{o} &= \sqrt{\frac{4\pi}{45}}\,(2a_{zz} - a_{xx} - a_{yy}) \end{aligned} \tag{5}$$

For the system S',

$$a'_{xy} = a'_{yz} = a'_{zx} = 0$$

Therefore, we can write

$$a'_2 = a'_{-2} = \frac{\beta \sin\gamma}{\sqrt{2}}\ ,\ a'_1 = a'_{-1} = 0,\ a'_o = \beta\cos\gamma \tag{6}$$

where β , γ are newly defined variables indicating the total deformation of the nucleus and the deviation from axial symmetry respectively.

From the equations (2a),(2b) and (3), and making use of the orthonormal and time derivative properties of $D_{\mu\nu}(\theta_i)$ (see ref. 37,p73) the potential and kinetic energies become

$$V = \tfrac{1}{2}C_2\sum_{\mu=-2}^{2}\left|a_\mu\right|^2 = \tfrac{1}{2}C_2\sum_{\nu}\left|a'_\nu\right|^2 = \tfrac{1}{2}C_2\beta^2 \tag{7}$$

$$\begin{aligned} T &= \tfrac{1}{2}B_2\sum_{\mu=-2}^{2}\left|\dot{a}_\mu\right|^2 = \tfrac{1}{2}B_2\sum_{\mu}\left|\sum_{\nu}\left(\dot{a}'_\nu D^*_{\mu\nu}(\theta_i) + a'_\nu \dot{D}^*_{\mu\nu}(\theta_i)\right)\right|^2 \\ &= \underbrace{\tfrac{1}{2}B_2(\dot{\beta}^2+\beta^2\dot{\gamma}^2)}_{T_{vib}} + \underbrace{\tfrac{1}{2}B_2\sum_{k}4\beta^2\sin^2(\gamma-k\tfrac{2\pi}{3})\sum_{j}q^2_{kj}\dot{\theta}^2_j}_{T_{rot}} \end{aligned} \tag{8}$$

where $j,k = 1,2,3$ are the subscripts for coordinate axes, and $Q_k = \sum_j q_{kj}\theta_j$ is the angular velocity component along the principle axis k (see ref. 2,p.12). Also note that the first term of T is the vibrational part and the second term, the rotational part.

The next step is to find the Hamiltonian operator, for which Pauli's method [39] is used as follows:

Let $(\Omega_\mu) = (\beta,\gamma,\theta_1,\theta_2,\theta_3)$ be the 5-dimensional curvilinear space; and

$$I_k = 4B_2\beta^2\sin^2(\gamma-2\pi k/3), \tag{9}$$

which from (8) is just the k-component of moment of inertia. Then the square of the differential interval of action is

$$ds^2 = \sum_{\mu,\nu} G_{\mu\nu}\, d\Omega_\mu d\Omega_\nu = 2Tdt^2$$

and from (8)

$$= B_2 d\beta^2 + B_2\beta^2 d\gamma^2 + \sum_k I_k \sum_j q_{kj}^2 d\theta_j^2 \tag{10}$$

Therefore,

$$G = \begin{bmatrix} B_2 & & & & 0 \\ & B_2\beta^2 & & & \\ & & I_1\sum_j q_{1j}^2 & & \\ & & & I_2\sum_j q_{2j}^2 & \\ 0 & & & & I_3\sum_j q_{3j}^2 \end{bmatrix} \tag{11}$$

The determinant,

$$|G| = 4^3 B_2^5 \beta^8 \sin^2(\gamma-2\pi/3)\sin^2(\gamma-4\pi/3)\sin^2(\gamma-2\pi)\,Q(\theta_i)$$
$$= 4B_2^5\beta^8\sin^2 3\gamma\; Q(\theta_i) \tag{12}$$

where

$$Q(\theta_i) = \left[\sum_j q_{1j}^2\right]\left[\sum_j q_{2j}^2\right]\left[\sum_j q_{3j}^2\right]$$

The Hamiltonian can then be found,

$$\hat{H} = \hat{T} + \hat{V} = -\frac{\hbar^2}{2}\sum_{\mu,\nu}\frac{1}{\sqrt{|G|}}\frac{\partial}{\partial\Omega_\mu}\frac{\sqrt{|G|}}{G_{\mu\nu}}\frac{\partial}{\partial\Omega_\nu} + \hat{V} \tag{13}$$

The potential energy operator,

$$\hat{V} = \tfrac{1}{2}C_2\beta^2 \tag{14}$$

The vibrational energy operator,

$$\begin{aligned}\hat{T}_{vib} &= -\frac{\hbar^2}{2}\sum_{\mu,\nu=1}^{2}\frac{1}{\sqrt{|G|}}\frac{\partial}{\partial\Omega_\mu}\frac{\sqrt{|G|}}{G_{\mu\nu}}\frac{\partial}{\partial\Omega_\nu} \\ &= -\frac{\hbar^2}{2B_2}\left\{\frac{1}{\beta^4}\frac{\partial}{\partial\beta}\beta^4\frac{\partial}{\partial\beta} + \frac{1}{\beta^2}\frac{1}{\sin 3\gamma}\frac{\partial}{\partial\gamma}\sin 3\gamma\frac{\partial}{\partial\gamma}\right\}\end{aligned} \tag{15}$$

The rotational energy operator can be simply expressed as follows without using equation (13),

$$\hat{T}_{rot} = \frac{\hbar^2}{2}\left(\frac{\hat{L}_1^2}{I_1} + \frac{\hat{L}_2^2}{I_2} + \frac{\hat{L}_3^2}{I_3}\right) = \frac{\hbar^2}{8B_2\beta^2}\sum_{k=1}^{3}\frac{\hat{L}_k^2}{\sin^2(\gamma - 2\pi k/3)} \tag{16}$$

where the component angular momentum operator,

$$\hat{L}_k = \hat{I_k Q_k} \tag{17}$$

i.e. moment of inertia X angular velocity, c.f. (8) and (9).

Hence the Schrodinger equation becomes,

$$(\hat{T}_{vib} + \hat{T}_{rot} + \hat{V})\Psi(\beta,\gamma,\theta_i) = E\Psi(\beta,\gamma,\theta_i) \tag{18}$$

Its solution is deferred to §2.

So far, we have only considered $\lambda = 2$ case. $\lambda = 1$ gives no contribution, while $\lambda = 3$ has been treated by Davidson [14], which will be outlined in §3. No evidence exists for any level corresponding to $\lambda > 3$.

Further development in the collective model can be separated into two branches. Faessler and coworkers [4)-9)] considered the deformed nucleus to be an axially symmetric ellipsoid,

while Davydov and coworkers [10)-16)] treated it as axially asymmetric. Only the latter will be discussed, as it is a general case and represents the latest development.

§2. The Asymmetric Rotator Model.

The asymmetric rotator model was proposed by Davydov and Filippov [10)], and developed by Davydov, Davidson and many others [11)-16)]. It is a continuation of Bohr's model. The difference in concept lies on the recognition of a fixed axially asymmetric nuclear shape. This implies that the shape parameter γ is no longer a variable. Hence, in finding the Hamiltonian operator as shown previously (for $\lambda = 2$), we need only a 4-dimensional curvilinear space, i.e. $(\Omega_\mu) = (\beta, \theta_1, \theta_2, \theta_3)$. From equation (13), it follows that the vibrational energy operator is simply,

$$\hat{T}_{vib} = -\frac{\hbar^2}{2B_2}\frac{1}{\beta^3}\frac{\partial}{\partial\beta}\beta^3\frac{\partial}{\partial\beta} \tag{19}$$

Note that

$$G = \begin{bmatrix} B_2 & & \\ & I_1\sum_j q_{1j}^2 & 0 \\ & & I_2\sum_j q_{2j}^2 \\ & 0 & & I_3\sum_j q_{3j}^2 \end{bmatrix} \tag{20}$$

The rotational energy operator is still the same as in equation (16); but the potential energy operator is slightly altered to take into account of the deformation from spherical equilibrium shape, i.e.

$$\hat{V} = \tfrac{1}{2} C_2(\beta - \beta_o)^2 \tag{21}$$

where the constant β_o is the total deformation parameter when the nucleus is not vibrating (i.e. in pure rotational states). Consequently, the Schrodinger equation becomes

$$-\left[\frac{\hbar^2}{2B_2}\left\{\frac{1}{\beta^3}\frac{\partial}{\partial\beta}\left(\beta^3\frac{\partial}{\partial\beta}\right) - \sum_{k=1}^{3}\frac{\hat{L}_k^2}{4\beta^2\sin^2(\gamma-2\pi k/3)}\right\} + \tfrac{1}{2}C_2(\beta-\beta_o)^2\right]\Psi(\beta,\theta_i)$$

$$= E_L\,\Psi(\beta,\theta_i) \tag{22}$$

Since only the operators $\hat{L}_k$ are functions of the Eulerian angles $\theta_i, i = 1,2,3$, the above equation is separable. Let

$$\Psi_L(\beta,\theta_i) = \Phi_L(\theta_i)\,\varphi_L(\beta) \tag{23}$$

then,

$$\left[\tfrac{1}{2}\sum_k \frac{\hat{L}_k^2}{\sin^2(\gamma-2\pi k/3)} - \varepsilon(L)\right]\Phi_L(\theta_i) = 0 \tag{24}$$

and

$$\left[-\frac{\hbar^2}{2B_2}\frac{1}{\beta^3}\frac{\partial}{\partial\beta}\left(\beta^3\frac{\partial}{\partial\beta}\right) + \tfrac{1}{2}C_2(\beta-\beta_o)^2 + \frac{\hbar^2}{4B_2\beta^2}\varepsilon(L) - E_L\right]\varphi_L(\beta) = 0 \tag{25}$$

where $\varepsilon(L)$ gives rotational energies of the asymmetric rotator in units of $\hbar^2/(4B_2\beta^2)$.

To solve equation (24), one needs to choose a set of basis vectors, the simplest of which is that of $D^L_{MK}(\theta_i)$, the rotation matrices, because

$$\hat{L}^2\, D^L_{MK}(\theta_i) = L(L+1)\, D^L_{MK}(\theta_i) \tag{26a}$$

$$\hat{L}_z\, D^L_{MK}(\theta_i) = M\, D^L_{MK}(\theta_i) \tag{26b}$$

$$\hat{L}_3\, D^L_{MK}(\theta_i) = K\, D^L_{MK}(\theta_i) \tag{26c}$$

where the subscript z refers to S system and 3 = z' refers to S' system (see ref. 38 p.64).

Since the basis vectors $|LMK\rangle = D^{L}_{MK}(\theta_i)$ are explicitly known and so are the operators $\hat{L}_j^2$, the matrix elements, $\langle LMK | \hat{L}_j^2 | LMK' \rangle$, for a given value of L and of M can be calculated. Consequently, for a given value of the shape parameter γ,

$$\langle LMK | \hat{H}_{rot} | LMK' \rangle = \frac{1}{2} \sum_{j=1}^{3} \frac{\langle LMK | \hat{L}_j^2 | LMK' \rangle}{\sin^2(\gamma - 2\pi j/3)} \tag{27}$$

can be calculated.

However, since the nucleus is not axially symmetric, K is not a good quantum number. Hence, the state vectors of the nucleus have to be mixtures of the basis vectors, i.e.

$$|LM\rangle = \sum_{K=-L}^{L} A_K |LMK\rangle \tag{28}$$

What is now left is to determine the coefficients A_K and the eigenvalues $\varepsilon_N(L)$ in (24). The eigenvalues can be found by diagonalizing the matrix $\hat{H}_{rot}$. But before doing that, the matrix dimension can be reduced appreciably by considering the symmetry property of the coefficients A_K. As was pointed out in §1 that there are 24 ways of assigning the system S' to the nucleus so that the coordinate axes of S' coincide with the principle axes of the nucleus. The wave function of the nucleus should be independent of the assignment. Therefore, we expect some symmetry relations among the A_K's, which can be found as follows:

The 24 ways of assigning S' can be interrelated by three rotation operators, $\hat{P}_1, \hat{P}_2, \hat{P}_3$, such that $\hat{P}_1$ produces a rotation of π about y'-axis; $\hat{P}_2$, a rotation of $\pi/2$ about z'-axis; and $\hat{P}_3$, a rotation of $2\pi/3$ about the axis equidistant angularly from the three axes (ref. 40, p.110). Apply $\hat{P}_1, \hat{P}_2^2$ on $D^L_{MK}(O_i) = |LMK\rangle$, we have

$$\hat{P}_1|LMK\rangle = \exp i\pi(L+K)\ |LM-K\rangle \tag{29a}$$

$$\hat{P}_2^2|LMK\rangle = \exp(i\pi K)\ |LMK\rangle \tag{29b}$$

As L and K are integers, applying on $|LM\rangle$ gives rise to four cases:

$$\begin{aligned}
&1)\quad \hat{P}_1|LM\rangle = +|LM\rangle\ ,\quad \hat{P}_2^2|LM\rangle = +|LM\rangle \\
&2)\quad \hat{P}_1|LM\rangle = -|LM\rangle\ ,\quad \hat{P}_2^2|LM\rangle = +|LM\rangle \\
&3)\quad \hat{P}_1|LM\rangle = +|LM\rangle\ ,\quad \hat{P}_2^2|LM\rangle = -|LM\rangle \\
&4)\quad \hat{P}_1|LM\rangle = -|LM\rangle\ ,\quad \hat{P}_2^2|LM\rangle = -|LM\rangle
\end{aligned} \tag{30}$$

These four cases belong to the four irreducible representations of a D_2 group, each to each, and therefore cannot be mixed together.

For case 1), from (29b), K must be even and from (28), (29a),

$$A_K = (-1)^L A_{-K} = C_K \tag{31}$$

It follows,

for L=0: K=0, $A_o = +A_o = C_o$, dimension of H_{rot}, N=1, $|LM\rangle = C_o|LM0\rangle$

for L=1: K=0, $A_o = -A_o = 0$, N=0, $|LM\rangle = 0$

for L=2: K=0,2, $A_o = +A_o = C_o$, $A_2 = +A_2 = C_2$, N=2,

$$|LM\rangle = C_o|LM0\rangle + C_2(|LM2\rangle + |LM-2\rangle)/\sqrt{2}$$

etc. (31a)

Similarly, it follows for cases 2),3) and 4). However, from the level structure of even-even nuclei, only cases 1) and 2) apply, i.e. 1) for the quadrupole case ($\lambda = 2$), and 2) for the octupole case ($\lambda = 3$).

Now the eigenvalues $\varepsilon_N(L)$ can be calculated. Then by substituting $\varepsilon_N(L)$ back into the matrix equation, the coefficients C_K can be determined. The solution of equation (24) is thus completed.

(The computations above and what follows were done by the IBM 7040 computer.)

To solve equation (25) for the vibration energy levels, the sole technique is to transform the equation to a simpler standard differential equation by changing the different variables and constants in the equation. This was done in ref. 12 and 15. It proceeds as follows:

Let
$$\varphi_{LN}(\beta) = \beta^{-\frac{3}{2}} U_{LN}(\beta) \tag{32}$$

Then (25) is reduced to

$$\left[-\frac{\hbar^2}{2B}\frac{\partial^2}{\partial\beta^2} + W_{LN}(\beta) - E_{LN} \right] U_{LN}(\beta) = 0 \tag{33}$$

with boundary condition $U_{LN}(0) = 0$, and the potential energy operator,

$$W_{LN}(\beta) = \tfrac{1}{2} C_2(\beta-\beta_o)^2 + \frac{\hbar^2}{4B_2\beta^2} \varepsilon_N(L) + \frac{3\hbar^2}{8B_2\beta^2} \tag{34}$$

Let β_o' be the value of β when $W_{LN}(\beta)$ is a minimum, i.e.

$$\left.\frac{\partial W_{LN}(\beta)}{\partial \beta}\right|_{\beta=\beta_o'} = C_2(\beta_o'-\beta_o) - \frac{\hbar^2}{2B_2\beta_o'^3}(\varepsilon_N(L) + 3/2) = 0$$

or

$$\beta_o' = \beta_o + \frac{\hbar^2}{2B_2C_2\beta_o'^3}(\varepsilon_N(L) + 3/2) \tag{35}$$

Then β_o' is a new total deformation parameter at equilibrium. It differs from β_o by $\hbar^2(\varepsilon_N(L)+3/2)/(2B_2C_2\beta_o'^3)$ which is obviously due to the rotation-vibration interaction.

Further, define

$$\mu^4 = \hbar^2/(B_2C_2\beta_o^4) \tag{36}$$

and

$$Z = \beta_o'/(\beta_o\mu) \tag{37}$$

(35) becomes

$$Z^4 - \frac{1}{\mu}Z^3 - (\varepsilon_N(L) + 3/2)/2 = 0 \tag{38}$$

The parameter μ measures the stiffness of the nucleus against vibration, and is characteristic of a nucleus. After choosing a suitable value for μ, (38) can be solved numerically for Z. Also, introducing

$$Z_1^4 = Z^4 + \frac{3}{2}(\varepsilon_N(L) + 3/2) \tag{39}$$

$$y = Z_1(\beta - \beta_o')/\beta_o' \tag{40}$$

$$D_\nu(\sqrt{2}\,y) = U_{LN}(\beta) \tag{41}$$

the equation (33) is reduced to a standard form,

$$\frac{d^2D_\nu(\sqrt{2}\,y)}{dy^2} + (2\nu + 1 - y^2)D_\nu(\sqrt{2}\,y) = 0 \tag{42}$$

where $\nu_n = \nu_n(Z_1)$ is a quantum number determined by the boundary condition $U_{LN}(0) = 0$ or $D_\nu(-\sqrt{2}\,Z_1) = 0$. (43)

The eigenvalues for (42) are

$$E_{LNn} = \hbar\omega_o \left\{ (\nu_n + \tfrac{1}{2})(Z_1/Z)^2 + \frac{\varepsilon_N(L)+3/2}{4Z^2} \left[1 + \frac{\varepsilon_N(L)+3/2}{2Z^2} \right] \right\} \qquad (44)$$

where $\omega_o = \sqrt{C_2/B_2}$.

The values ν_n for n = 1 and for n = 2 were computed and tabulated as functions of Z_1 in refs. 14 and 41. Here n = 1 refers to all the levels belonging to the ground state beta band, and n = 2, to the levels in the first excited beta band. It is also clear that N is the level order for a given L. The levels corresponding to $N \geq 2$ and n = 1 are often called the gamma vibrational levels in another model [9]. The eigenvalues E_{LNn} calculated are in arbitrary energy scale. Therefore, in the present calculation, the following ratio was chosen for each level LNn ,

$$\frac{E_{LNn} - E_{011}}{E_{211} - E_{011}} .$$

§3. The Octupole Case in the Asymmetric Rotator Model.

The treatment of the octupole case ($\lambda = 3$) in the asymmetric rotator model is completely in parallel with the quadrupole case ($\lambda = 2$). There are only two points which give rise to different mathematical expressions:

a) Instead of the expressions for a'_μ (μ=-2,-1,0,1,2) given in equation (6) of §1, we have

$$a''_{\pm 1} = a''_{\pm 3} = 0, \quad a''_o = \beta'' \cos\gamma'' \quad a''_{\pm 2} = (\beta''/\sqrt{2}) \sin\gamma'' \qquad (45)$$

Therefore, the three moments of inertia become

$$I_1'' = 4B_3\beta''^2(\sin^2\gamma'' + \frac{\sqrt{15}}{2}\sin\gamma''\cos\gamma'' + \frac{3}{2}\cos^2\gamma'')$$
$$I_2'' = 4B_3\beta''^2(\sin^2\gamma'' - \frac{\sqrt{15}}{2}\sin\gamma''\cos\gamma'' + \frac{3}{2}\cos^2\gamma'') \quad (46)$$
$$I_3'' = 4B_3\beta''^2\sin\gamma''$$

and the rotational energy operator,

$$\hat{T}_{rot} = \frac{\hbar^2}{2}\sum_{j=1}^{3}\frac{\hat{L}_j^2}{I_j''} \quad (47)$$

b) As mentioned in §2, the symmetry condition of the coefficients A_K's in octupole case is derived from the case 2) of equation (30). Hence, from equations (28), (29a), (29b) again, K must be even and

$$A_{-K} = (-1)^{L+1} A_K \quad (48)$$

The forms of the potential and vibrational energy operators are the same as in equations (19) and (21), i.e.

$$\hat{V} = \tfrac{1}{2} C_3(\beta'' - \beta_o'')^2 \quad (49)$$

$$\hat{T}_{vib} = -\frac{\hbar^2}{2B_3}\frac{1}{\beta''^3}\frac{\partial}{\partial\beta''}\left(\beta''^3\frac{\partial}{\partial\beta''}\right) \quad (50)$$

The methods of calculation following this are exactly the same as in §2.

Finally, it should be noted that the shape parameter γ'' and the stiffness parameter $\mu'' = \hbar^{\frac{1}{2}}\left[\beta_o''(B_3C_3)^{\frac{1}{4}}\right]^{-1}$ are in general different in values from γ and μ in the quadrupole case, as these two cases are quite unrelated. Also the parities of

the quadrupole and octupole cases are necessarily positive and negative respectively.

§4. Calculations of Reduced E2 Transition Probabilities.

Since we are considering deformed even-even nuclei, large quadrupole moments are to be expected. This should lead to very favourable electric quadrupole (E2) transitions between the various energy levels. The results of these calculations when compared with experimental data should provide a sensitive test of the validity of this model.

The general expression for the gamma transition probability per unit time is

$$T(\ell)_{i\to f} = \frac{8\pi(\ell+1)}{\ell\{(2\ell+1)!!\}^2\hbar} \left(\frac{\omega}{c}\right)^{2\ell+1} B(\ell, L_i \to L_f) \qquad (51)$$

where the emitted photon has energy $\hbar\omega$ and angular momentum ℓ; the angular momentum of the initial and final levels are given by L_i and L_f respectively; and $B(\ell, L_i \to L_f)$ which is energy independent is called the reduced transition probability. For E2 transitions due to the quadrupole moment $Q_{2\mu}$ from a state $|LMNn\rangle$ to a state $|L'M'N'n'\rangle$,

$$B(E2; LMNn \to L'M'N'n') = |\langle L'M'N'n' | Q_{2\mu} | LMNn \rangle|^2$$

Summing over all final states with respect to M' and averaging the initial states with respect to M, in order to omit polarisation,

$$B(E2; LNn \to L'N'n') = \frac{1}{2L+1} \sum_{M,M'} |\langle L'M'N'n' | Q_2 | LMNn \rangle|^2 \qquad (52)$$

The electric quadrupole moment $Q_{2\mu}$ should be in the laboratory system (S-system), but it takes a simpler form in the body-fixed system (S'-system), the transformation from S' to S being as usual

$$Q_{2\mu} = \sum_{\nu} Q'_{2\nu} D^*_{\mu\nu}(\theta_i) \qquad (53)$$

(c.f. equation (3)). Now assuming that the nuclear charge density is a constant in the nucleus, i.e. $\rho = ze/(4\pi R_0^3/3)$, then the quadrupole moment in the S'-system is just

$$Q'_{2\nu} = \frac{3ze}{4\pi R_0^3}\int r^4 Y_{2\nu}(\theta',\phi') \sin\theta' \, d\theta' \, d\phi' \, dr$$

$$= \text{constant} \int \frac{R'^5}{5} Y_{2\nu}(\theta',\phi') \sin\theta' \, d\theta' \, d\phi'$$

where $R'(\theta',\phi',t) = R_0\left[1 + \sum_{\nu} a'_{2\nu}(t)\, Y_{2\nu}(\theta',\phi')\right. \qquad (54)$

(c.f. equation (1)). Therefore, neglecting higher order terms of $a'_{2\nu}(t)$ than the first, we obtain

$$Q'_{2\nu} = \frac{3ze}{4\pi R_0 3} \; R_0^5 \, a'_{2\nu}(t)$$

and from (6) $$= \frac{3ze}{4\pi} R_0^2 \beta \begin{cases} \cos\gamma \\ 0 \\ \sin\gamma/2 \end{cases} \qquad \text{for } \nu = \begin{cases} 0 \\ \pm 1 \\ \pm 2 \end{cases} \qquad (55)$$

From (53) therefore,

$$Q_{2\mu} = \frac{3ze}{4\pi} R_0^2 \beta \left[D^*_{\mu 0}\cos\gamma + (D^*_{\mu 2} + D^*_{\mu -2}) \sin\gamma/2\right]$$

$$= \frac{3ze}{4\pi} R_0^2 \beta \, F_\mu(\gamma) \qquad (56)$$

Subtituting into (52), we have

$$B(E2: LNn \rightarrow L'N'n') =$$

$$\frac{9z^2e^2}{16\pi^2(2L+1)} R_0^4 \sum_{M;M} \left| \varphi_{L'N'}(\beta) \middle| \beta \middle| \varphi_{LN}(\beta) \right\rangle \left\langle L'M'N' \middle| F_\mu(\gamma) \middle| LMN \right\rangle \Big|^2 \qquad (57)$$

where the last two factors represent the vibrational and the

rotational parts respectively.

From equations (31a), we have

$$|LMN\rangle = C_0^{LN} D_{M0}^{L*} + \sum_{K=2}^{L} C_2^{LN} (D_{MK}^{L*} + (-1)^L D_{M-K}^{L*})/\sqrt{2} \qquad (58)$$

Hence the rotational part can be calculated. The expression in terms of Clebsch-Gordan coefficients $C(j_1 j_2 j_3 ; m_1 m_2 m_3)$ when properly normalized is as follows

$$\langle L'M'N'|F_\mu(\gamma)|LMN\rangle = C(L2L';M\mu M')\sqrt{\frac{2L+1}{2L'+L}}$$

$$\left\{\left[C_0^{L'N'}C_0^{LN}\,C(L2L';000) + \sum_{K=2}^{L} C_K^{L'N'}C_K^{LN}\,C(L2L';K0K)\right]\cos\gamma +\right.$$

$$\tfrac{1}{2}\left[(1+(-1)^{L'})\,C_0^{L'N'}C_2^{LN}\,C(L2L';2,-2,0) + (1+(-1)^L)C_0^{LN}C_2^{L'N'}C(L2L;02\right.$$

$$\left.\left.+\sqrt{2}\sum_{K=2}^{L} C_{K+2}^{L'N'}C_K^{LN}C(L2L';K,2,K+2) + \sqrt{2}\sum_{K=4}^{L} C_{K-2}^{L'N'}C_K^{LN}C(L2L';K-2,K-2)\right]\sin\right.$$

(59)

For the vibrational part, we must evaluate $\langle\varphi_{L'N'}|\beta|\varphi_{LN}\rangle = S^{\frac{1}{2}}_{\nu'\nu}$ in the notation of Davidson [15]. Recalling equations (32), (37), (40) and (41), we can write

$$\varphi_{LN}(\beta) = \beta^{-3/2}D_\nu(\sqrt{2}y) \quad \text{and} \quad \varphi_{L'N'}(\beta) = \beta^{-3/2}D_{\nu'}(\sqrt{2}y')$$

where $y = Z_1(\beta/\mu\beta_o Z - 1)$ and $y' = Z_1'(\beta/\mu\beta_o Z' - 1)$.

Thus, $$\varphi_{LN} = \beta^{-3/2}D_\nu\left[\sqrt{2}\left(\frac{Z_1\beta}{\mu\beta_o Z} - Z_1\right)\right] = \beta^{-3/2}D_\nu\left[\sqrt{2}\left(\frac{Z_1 Z'}{Z Z_1'}X - Z_1\right)\right] \qquad (60)$$

and $$\varphi_{L'N'} = \beta^{-3/2}D_{\nu'}\left[\sqrt{2}(x - Z_1')\right] \qquad (61)$$

with $$x = Z_1'\beta/\mu\beta_o Z' \qquad (62)$$

Therefore, the matrix element $\langle\varphi_{L'N'}(\beta)|\beta|\varphi_{LN}(\beta)\rangle =$

$$N_{\nu'}N_\nu\int_0^\infty \beta^{-3}D_{\nu'}\left[\sqrt{2}(x - Z_1')\right]\beta\, D_\nu\left[\sqrt{2}\left(\frac{Z_1 Z'}{Z Z_1'}x - Z_1\right)\right]\beta^3 d\beta$$

$$= N_{\nu'}N_\nu(\mu\beta_o Z'/Z_1')\, I_{\nu'\nu} \qquad (63)$$

where $\beta^3 d\beta$ is the volume element, and the function

$$I_{\nu'\nu} = \int_0^\infty D_{\nu'}\left[\sqrt{2}(x - Z_1')\right] \times D_\nu\left[\sqrt{2}\left(\frac{Z_1 Z'}{Z Z_1'}x - Z_1\right)\right] dx \qquad (64)$$

The normalizing constants $N_{\nu'}$ and N_ν are defined from

$$N_\nu^2 \int_0^\infty D_\nu^2(\sqrt{2}y)d\beta = (\mu\beta_o Z/Z_1)\int_0^\infty D_\nu^2(\sqrt{2}y)dy = 1$$

Thus, $N_\nu^2 = (Z_1/\mu\beta_o Z I_\nu)$ (65)

with $I_\nu = \int_{-Z_1}^\infty D_\nu^2(\sqrt{2}y)dy$ (66)

Hence

$$\left|\langle\varphi_{L'N'}(\beta)|\beta|\varphi_{LN}(\beta)\rangle\right|^2 = (Z_1' Z_1/Z'Z)(\mu\beta_o Z'/Z_1')^4 \frac{I^2_{\nu'\nu}}{I_{\nu'} I_\nu}$$

$$= (\mu\beta_o)^2 (Z_1/Z)(Z'/Z_1')^3 \frac{I^2_{\nu'\nu}}{I_{\nu'} I_\nu} \qquad (67)$$

The explicit expressions for $I_{\nu'\nu}$ and I_ν were worked out by Davidson as shown below and programmed [41].

$$I_{\nu'\nu} = \left[2^{\frac{1}{2}(\nu+\nu')}\right]\pi \int_{-Z_1}^\infty \exp\left\{-\tfrac{1}{2}(x^2 + R_Z(x+Z_1) - Z_1'\right\}^2 (x+Z_1) X_\nu(x)$$
$$X_{\nu'}(R_Z(x+Z_1)-Z_1')\, dx \qquad (68)$$

where $R_Z = Z_1 Z'/ZZ_1'$,

and $X_\nu(x) = \dfrac{1}{\Gamma(-\frac{1}{2}\nu)\Gamma\frac{1}{2}(1-\nu)} \sum_{k=0}^\infty \dfrac{(-1)^k \frac{1}{2}(k-\nu)(2x)^k}{k}$

$$I_\nu(Z_1) = I_{\nu e} + \tfrac{1}{2}\sqrt{\pi}\,\Gamma(\nu+1) + \sqrt{\pi}\left[H\left(\frac{1+\nu}{2}\right) - H(1+\nu/2)\right] / 4\Gamma(-\nu) \qquad (69)$$

where $H(x) = d/dx(\ln\Gamma(x))$

and $I_{\nu e} = \dfrac{Z_1 2^\nu \pi}{10} \sum_{j=1}^{10} \exp\left\{-Z_1^2\left(\dfrac{j-0.5}{10}\right)^2 X^2\left(Z_1 \dfrac{0.5-j}{10}\right)\right\}$

Thus, returning to equation (57), the ratio of two transition probabilities can be computed. Of course, this is only applicable to E2 transitions, corresponding to the $\lambda = 2$ case. For the $\lambda = 3$ case, discussion is omitted on the ground that no transition between $\lambda = 3$ states is observed in the present experiment.

§5. Other Forms of Electromagnetic Transitions.

Two possible forms of electromagnetic transitions that can compete with E2 transition are the M1 and E0. It was shown by Davydov et al [10] that M1 transition was forbidden in a symmetric rotator (i.e. when $\gamma = 0$), but not in an asymmetric rotator. The latter was then pointed out by Tamura et al [42)-44)] to be incorrect, that is both cases are forbidden. Therefore, only E0 transition needs to be considered.

An E0 transition is only possible between two states of the same spin L. Since no photon carries an angular momentum zero, the E0 transition only works through the internal electron conversion process. The absolute transition probability per unit time was given by Church et al [45)] as

$$T(E0) = \Omega \rho^2 \tag{70}$$

where Ω is the electronic factor involved in the transition and ρ^2 the nuclear factor. Only the K-conversion is important in this case, and hence Ω_K was plotted against the transition energy by the above authors. ρ is just the matrix element corresponding to the vibrational part of the E2 transition* (no rotation). For E0 transition from a beta band (i.e. the first excited state, n = 2) to a ground rotational state (n = 1), (see ref. 16)

$$\rho = \langle \varphi_{LNn'}(\beta) | \beta^2 | \varphi_{LNn}(\beta) \rangle \frac{3z}{4\pi} \tag{71}$$

---

* Only consider transitions from beta vibrational band.

where z = atomic number.

Thus $\rho = (3z/4\pi)\int_0^\infty \varphi_{L'N'n'}(\beta)\beta^2 \varphi_{LNn}(\beta)\beta^3 d\beta$

$= (3z/4\pi)N_{\nu'}N_{\nu}\int_0^\infty D_{\nu'}\left[\sqrt{2}\left(\frac{Z_1'\beta}{\mu\beta_o Z'} - Z_1'\right)\right]\beta^2 D_{\nu}\left[\sqrt{2}\left(\frac{Z_1\beta}{\mu\beta_o Z} - Z_1\right)\right] d\beta$

and with the same substitutions which led to equation (67) but with $Z = Z'$, and $Z_1 = Z_1'$, we obtain

$$\rho = (3z/4\pi)(\mu\beta_o Z/Z_1)^3 N_{\nu'}N_{\nu}\int_0^\infty D_{\nu'}\left[\sqrt{2}(x-Z_1)\right]\ x^2\ D_{\nu}\left[\sqrt{2}(x-Z_1)\right] dx$$

$$\text{or} \quad \rho^2 = (3z/4\pi)^2\ (\mu\beta_o Z/Z_1)^4\ \frac{I^2_{\nu'\nu}(0)}{I_{\nu'}(0)I_{\nu}(0)} \qquad (72)$$

The overlap integral $I_{\nu'\nu}(0)$

$$= \int_0^\infty D_{\nu'}\left[\sqrt{2}(x-Z_1)\right]\ x^2\ D_{\nu}\left[\sqrt{2}(x-Z_1)\right] dx$$

$$= \left[2^{\frac{1}{2}(\nu+\nu')}\right]\pi\int_{-Z_1}^\infty (x+Z)^2 X^2(x)dx \qquad \text{(c.f.equation (68).}$$

Functions $I_{\nu'}(0)$ and $I_{\nu}(0)$ are given in (69).

The monopole transition probability T(E0) is usually compared with the E2 transition probability from the same state, $T(E2;0+ \rightarrow 2+)$. From (51)

$$T(E2) = \frac{8\pi \cdot 3}{2(5.3.1)^2\hbar}\left[\frac{\hbar\omega}{\hbar c}\right]^5 B(E2;\ 0+ \rightarrow 2+)$$

$$= \frac{4\pi}{75\hbar^6 c^5}\ E_\gamma^5\ B(E2;\ \underset{\uparrow\uparrow\uparrow}{012}\ \ \underset{LNn}{}\ \ \underset{\uparrow\uparrow\uparrow}{011}\ \underset{LNn'}{})$$

where E_γ is the energy of the emitted photon. With E_γ in Mev and with equations (57), (67), and (72), we can write

$$\frac{T(E0)}{T(E2)} = \frac{(\mu\beta_o)^2\ \Omega}{2.53\times10^9\ A^{4/3}E_\gamma^5}\ (Z/Z_1)^5(Z_1'/Z')^3\ \frac{I_{\nu'}(2)\ I^2_{\nu'\nu}(0)}{I_{\nu'}(0)\ I^2_{\nu'\nu}(2)\ P_{rot}} \qquad (78)$$

where P_{rot} is the rotational part of the transition probability computed by (59).

Since E0 transitions may also occur between any two states of the same spin and parity, equation (78) may easily be altered to apply to these. For example, for transitions between states of the first beta band and similar spin states of the ground state band, we can write for the ratio of the transition probabilities between the same states,

$$\frac{T(E0)}{T(E2)}\,(L^{+}_{\beta} \rightarrow L^{+}_{gnd}) = \frac{(\mu\beta_0)^2\ \Omega}{2.53\times10^{9}\,A^{4/3}E_{\gamma}^{5}}\,(Z/Z_1)^2\,\frac{I^2_{\nu'\nu}(0)}{I^2_{\nu'\nu}(2)\ P_{rot}}$$

(see reference (16)). (78a)

Although several transitions from the negative parity levels ($\lambda = 3$) to positive parity levels ($\lambda = 2$) have been observed, no theoretical transition probabilities have so far been worked out to account for these.

CHAPTER III

THE DESIGN OF EXPERIMENTS

In nuclear spectroscopy, the types of problems that are commonly involved are: to construct the nuclear decay scheme of a radioactive isotope, to determine mechanisms of transitions from one nuclear state to another, and consequently to understand the nucleus by model fitting. The energy levels in the decay scheme of a nucleus cannot be measured directly. They can only be determined by making use of the energy transfer in transitions between states. The physical observables involved in a transition, which are usually measured, are the kinetic energies of the emitted particles during the transitions, the intensities of emission of the particles either in polarised or unpolarised conditions, and the time correlation or directional correlation between a pair of emitted particles. The particles referred to here are alpha-particles, beta-particles (electrons and positrons), neutrinos and photons.

In the present experiment, we are concerned with the decay of Eu 154 from its ground state to the excited states of the daughter nucleus, Gd 154. During each transition in the decay, an electron and a neutrino are emitted. The de-excitation of each excited state so formed may result in the

emission of a photon, or an electron through an internal conversion process (see §2, Chapter 6), or a positron-electron pair if the energy transfer is greater than 1.022 Mev. Since the neutrino cross-section of nucleons is next to zero ($\sim 10^{-44}$ cm^2), the only measurable particles using conventional techniques are the betas and the gammas (photons).

The methods for investigating the beta and gamma transitions vary from one experiment to another. The determining factors for using the different methods lie primarily in the nature of the transitions of the chosen isotope (e.g. the energies of the emitted particles), the specific need for further examination of the isotope, and the technical limitations such as exist on the efficiencies and resolutions of the detectors available and on the speed of the electronic system. Strong emphasis has to be placed at the last point, because spectroscopic work relies essentially on the precision of measurement.

As stated in the Introduction, the decay of Eu 154 has been investigated by several workers, and consequently a rough skeleton of the decay scheme has been established for some time. The problems left over now are:

1) to determine the energies and intensities of all the transitions accurately enough so as to make a meaningful identification with an appropriate theoretical model.

2) to search for new weak transitions that have not been found before, and, if any, to assign them to their proper positions in the decay scheme; and

3) to check those parts of the decay in which there are disagreements or uncertainties in earlier investigations.

With the above considerations in mind, three methods of investigation were employed for the present work, the gamma singles spectroscopy, gamma-gamma coincidence work, and beta spectroscopy. They are separately discussed in the following three chapters.

CHAPTER IV

THE GAMMA SPECTROSCOPY

§1. General Considerations.

It was mentioned in the previous chapter that the de-excitation of an excited state of Gd 154 to a lower state may be carried out by the direct emission of a photon, or by an internal conversion process, or by internal pair production. In this chapter, only the direct gamma emission will be treated. The other two processes will be considered along with beta transitions in Chapter 6.

The change of states in a nucleus in the process of de-excitation corresponds to the sudden alteration of the charge-current distribution of the nucleus in order to acquire a lower potential energy. In general, this alteration is equivalent to sudden switching on and off of a combination of electromagnetic oscillators, and thus sending out a series of electromagnetic waves with various multipole orders. These waves or radiations can be separated into two groups, the electric multipoles (EL) and the magnetic multipoles (ML). The multipole order L is just the angular momentum in units $\hbar$ carried away by each quantum of radiation (a photon). The parity of an electric multipole radiation is defined as

$\pi^E = (-1)^L$. From Maxwell's equation,

$$\vec{\nabla}(\vec{r}) \times \vec{E}(\vec{r}) = -\frac{1}{\mu}\dot{\vec{H}}(\vec{r})$$

and $\vec{\nabla}(-\vec{r}) \times \vec{E}(-\vec{r}) = -\frac{1}{\mu}\dot{\vec{H}}(-\vec{r})$, (79)

and since $\vec{\nabla}(-\vec{r}) = -\vec{\nabla}(\vec{r})$, it implies that for the same L, the electric field and the magnetic field are of opposite parity. Hence, the parity of a magnetic multipole radiation is $\pi^M = -(-1)^L$.

Not all the components of the multipole radiations are equally preferred in each transition. Their presence is restricted by a few selection rules as shown below:

1. In order to conserve angular momentum, the following triangular rule must hold,

$$|I_i - I_f| \leq L \leq [I_i + I_f] \tag{80}$$

where I_i, I_f are the total angular momenta in units $\hbar$ of the initial and final levels in the transition respectively.

2. Conservation of parity during the transition must be observed.

3. From the expression for transition probabilities with multipole order L (c.f. equations (51) and (56) in Chapter 2), the following factor can be extracted,

$$\left[\frac{\omega}{c}\right]^{2L} \left[R_o^L\right]^2 = \left[\frac{R_o}{\lambda}\right]^{2L} \tag{81}$$

where λ is the wave length of the emitted radiation. Since the ratio R_o/λ is very small even for several Mev transfer

of energy, only the term with lowest order of L is significant in each transition.

4. Again from equation (51), when $L = 0$, the transition probability, $T_{i-f}(L)$ becomes infinite, which is impossible. Hence, no electromagnetic radiation can be expected with zero multipole order.

5. For the same L, it can be shown that the magnetic radiation is weaker than the electric radiation by a factor of $(v/c)^2$ (see ref.47 p.592), where v is the speed of motion of the charges in the nucleus.

In collective models, another selection rule due to rotational quantum number K is added, i,e.

$$L \geq |K_i - K_f| \tag{82}$$

However, in asymmetric rotator model, since K is not a good quantum number, this K-forbiddenness only hinders the transition but does not forbid it. The hindrance is expressed as,

$$\nu = |K_i - K_f| - L \tag{83}$$

According to the asymmetric rotator model described in Chapter 2, the predominant multipole radiations in the gamma transitions of Gd 154 are again limited to E2, consistent with the above selection rules. Experimental determination of the types of multipole radiation requires the knowledge of internal conversion data, and hence will be treated in Chapter 6.

Meanwhile, we will proceed to deal with the means of measuring the energies and intensities of these gamma rays.

§2. Interaction between Gamma Rays and the Detectors.

When a photon enters a detector, several things can happen. The photon energy may be completely absorbed by an electron in the detector. This electron then moves about in the detector producing ion pairs or luminescence until it comes to rest with its energy spent. The ion pairs if collected by a pair of electrodes will give a charge pulse whose magnitude is linearly proportional to the electron energy. Similarly, the luminescence if collected by a photomultiplier will give a pulse proportional to the luminiscent energy. This process of complete energy transfer from a photon to a detector is called photo-absorption. The peaks in an energy spectrum obtained from this process arethus named photo-absorption peaks. If the gamma rays are mono-energetic, a single peak should be observed which is ideally Gaussian in shape.

On the other hand, if a photon interacts with an electron and is itself scattered out of the detector, then the energy of the photon absorbed by the electron is partial. The amount of this partial energy (i.e. the electron recoil energy, E_e) varies with the scattering angle θ as given in the equation [48],

$$E_e(\theta) = E_\gamma\left[1 - 1/\left(1 + \frac{E_\gamma}{mc^2}(1-\cos\theta)\right)\right] \qquad (84)$$

where E_γ is the initial photon energy and θ is defined as shown below.

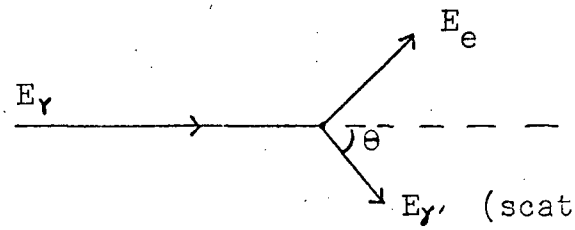

The recoil electron then meets the same fate as that described in the previous paragraph. This process of partial transfer of energy is called Compton scattering. Since θ can be any value between 0^o and 180^o, the energy spectrum thus obtained for mono-energetic incident gamma rays is known as the Compton continuum. This continuum extends from $E_e(\theta^o) = 0$ to $E_e(180^o)$. Hence, the Compton edge (upper edge of the continuum) corresponds to the case in which the photons are back-scattered.

Another process which has been mentioned before is pair production. When a photon with energy greater than two electron mass enters the EM-field of a nucleus in the detector, the energy may be converted into matter by lifting an electron from a negative energy state to a positive energy state and leaving a 'hole' or positron behind. Thus an electron-positron pair is created. The positron is often stopped and annihilated with an electron in the detector yielding a pair of photons of energy 0.511 Mev each. Therefore, a double-escape peak of energy,

$$E_{de} = (E_\gamma - 1.022)\ \text{Mev} \qquad (85)$$

can be obtained, if both photons escape from the detector. However, if one of them is re-absorbed in the detector, a single-escape peak of energy,

$$E_{se} = (E_\gamma - 0.511)\ \text{Mev} \qquad (86)$$

is formed.

§3. Gamma-ray Detection Assemblies.

The first gamma-ray detection assembly constructed and intended for the present work is shown in figure 1. It makes use of the principle of Compton back-scattering. Gamma rays from the source S were collimated by the cylindrical lead blocks A and B, and travelled through the aluminium tubing to a Lithium-drifted Silicon detector which has a depletion depth of 3 mm. and an active volume of 0.15 c.c. Some of the photons were stopped by the detector and back-scattered to the block of plastic scintillator molded in the shape of a cylinder. The Silicon detector was cooled by a copper brush dipped in a Dewar of liquid nitrogen so as to achieve optimum resolution. The plastic scintillator was viewed by four photomultipliers which were adjusted to yield the same charge multiplication factor. The outputs of the photomultipliers were tied to one cathode follower stage as shown in figure 2. Each event was defined by the coincidence between a pulse from the detector

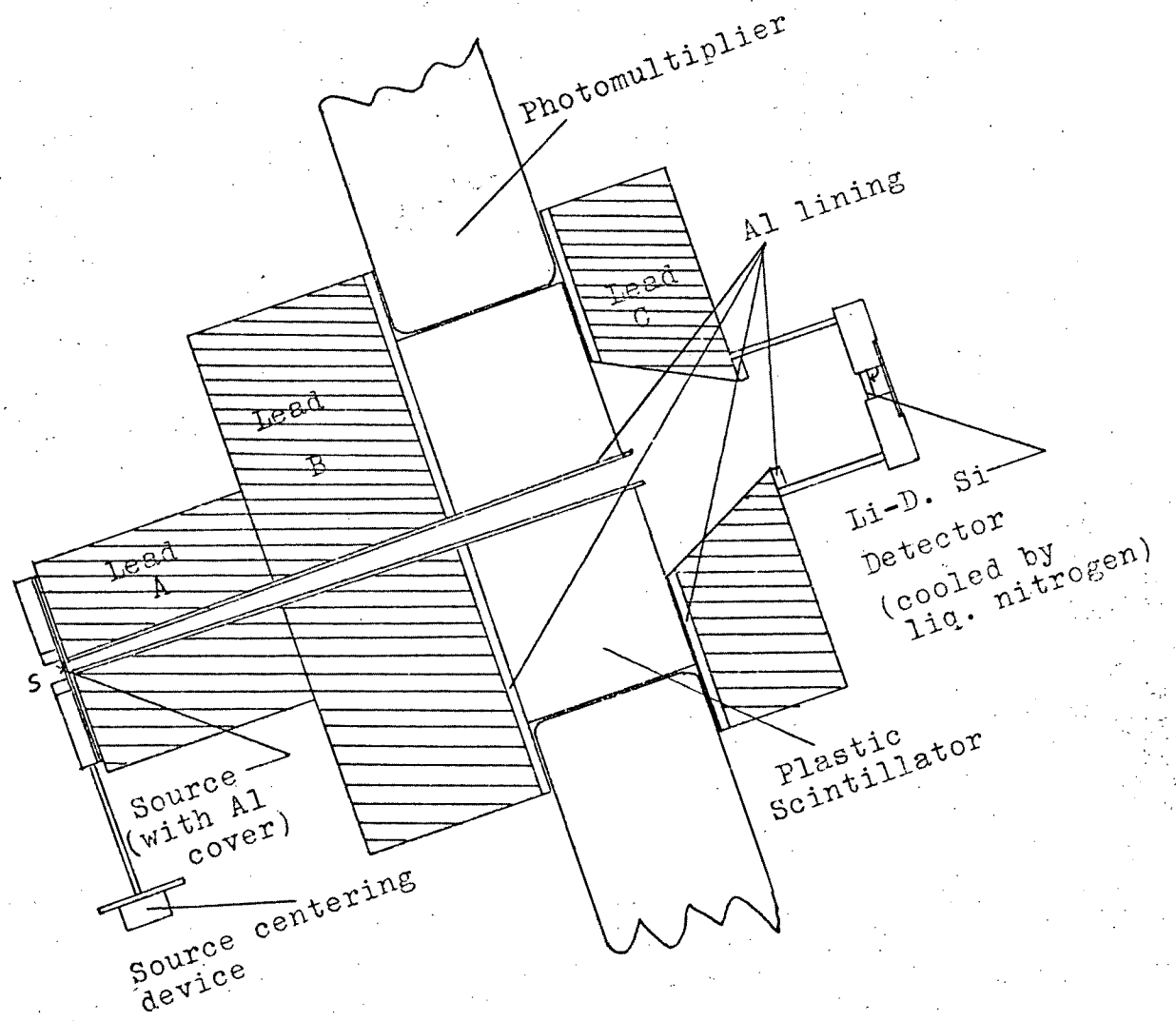

Fig.1 The Gamma Spectrometer.

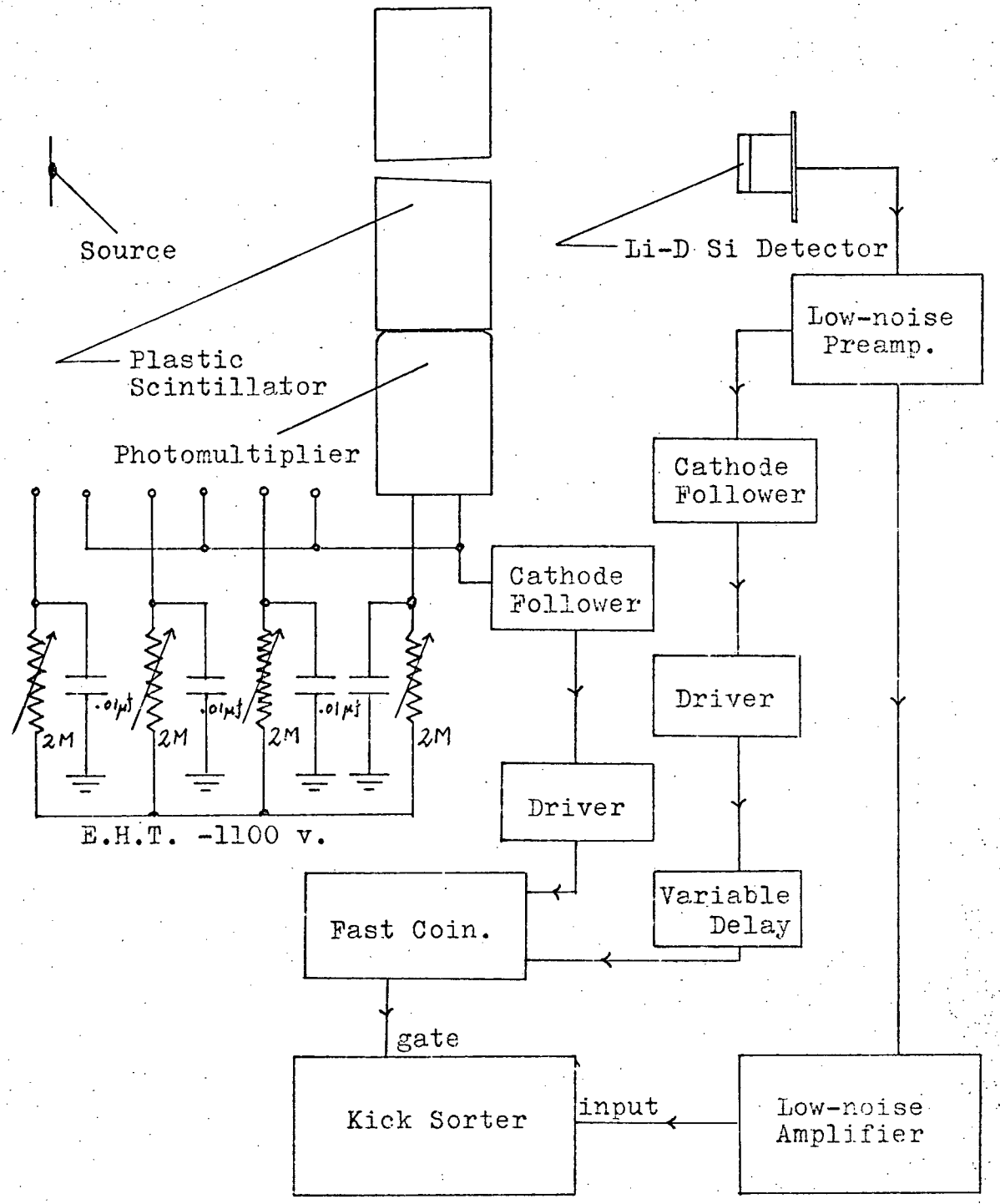

Fig.2 Electronic circuit for the gamma spectrometer.

and a pulse from the photomultipliers. The output from the detector corresponds to the recoil energies of the electrons in the depletion region. This output was stored in a 128-channel kick sorter after being gated by the coincidence pulses. Therefore, each count recorded by the kick sorter corresponds to a back-scattering event, the back-scattering angle being limited to a range 157°-180° by the cone in the lead block C. A spectrum of Cs 134 was then taken as shown in figure 3. From §2, the peak positions of the spectrum are almost at the positions of the original Compton edges. It can be seen from the spectrum that the rest of the Compton continuum is highly suppressed by the coincidence system, which is the beauty of this assembly. The resolution as quoted on the figure is fairly good. It is achieved because in the range of back-scattering angles accepted, the energy of scattered electron is almost independent of scattering angle. The only drawback in this assembly is low efficiency.

By the time the above assembly was tested, Lithium-drifted Germanium detectors were available in this laboratory. Since the latter far exceed the former in resolution and efficiency, the gamma experiments were then performed by using the Germanium detectors instead. However, it is interesting to note that the above assembly provides a method of gamma

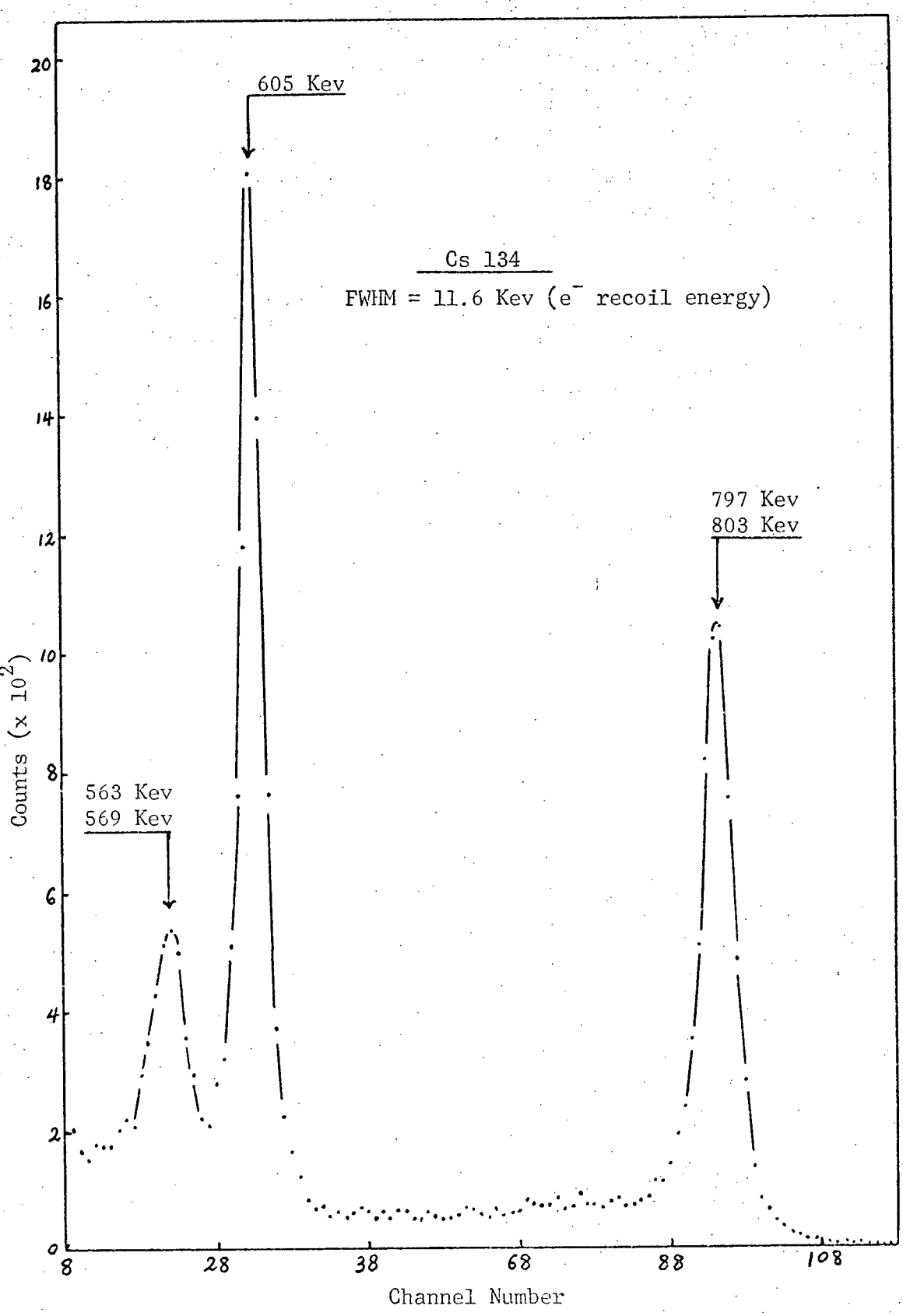

Fig. 3 Cs 134 spectrum taken from the gamma-spectrometer assembly.

detection based on a quite different principle.

The Germanium detector assembly is shown in figure 4. Two planar-type detectors prepared and mounted by D.A. Dalby have been used one after the other. The first detector has a depletion depth of 5 mm. and active volume, 1.5 c.c., while the second one is much bigger, having a depletion depth of 7.5 mm. and active volume, 5 c.c. As usual, each detector was mounted in a vacuum chamber and cooled by a cold finger. In this case, because of the special preamplifier circuit used, the detector bias had to be negative. Thus the P surface of the detector resting on the cold finger was electrically insulated from the latter by a thin sheet of nylon. The N surface (i.e. the Li surface) was in spot contact with the gate terminal of a field effect transistor (2N3823) and a feedback lead through a 500 MΩ resistor as shown in figure 5. This figure presents the first stage of the low-noise preamplifier used. The super-high input impedence provided by the field effect transistor significantly increased the peak-to-noise ratio when compared with other low-noise preamplifiers using cathode follower input stages (e.g. Ortec 101XL and Simtec P-10). The preamplifier output was connected to a Time Constant Box with 1 μsec. rise time and 10 μsec. decay time, and then to a low-noise amplifier and a 1024-channel kick sorter. Using a detector bias of -600 v.

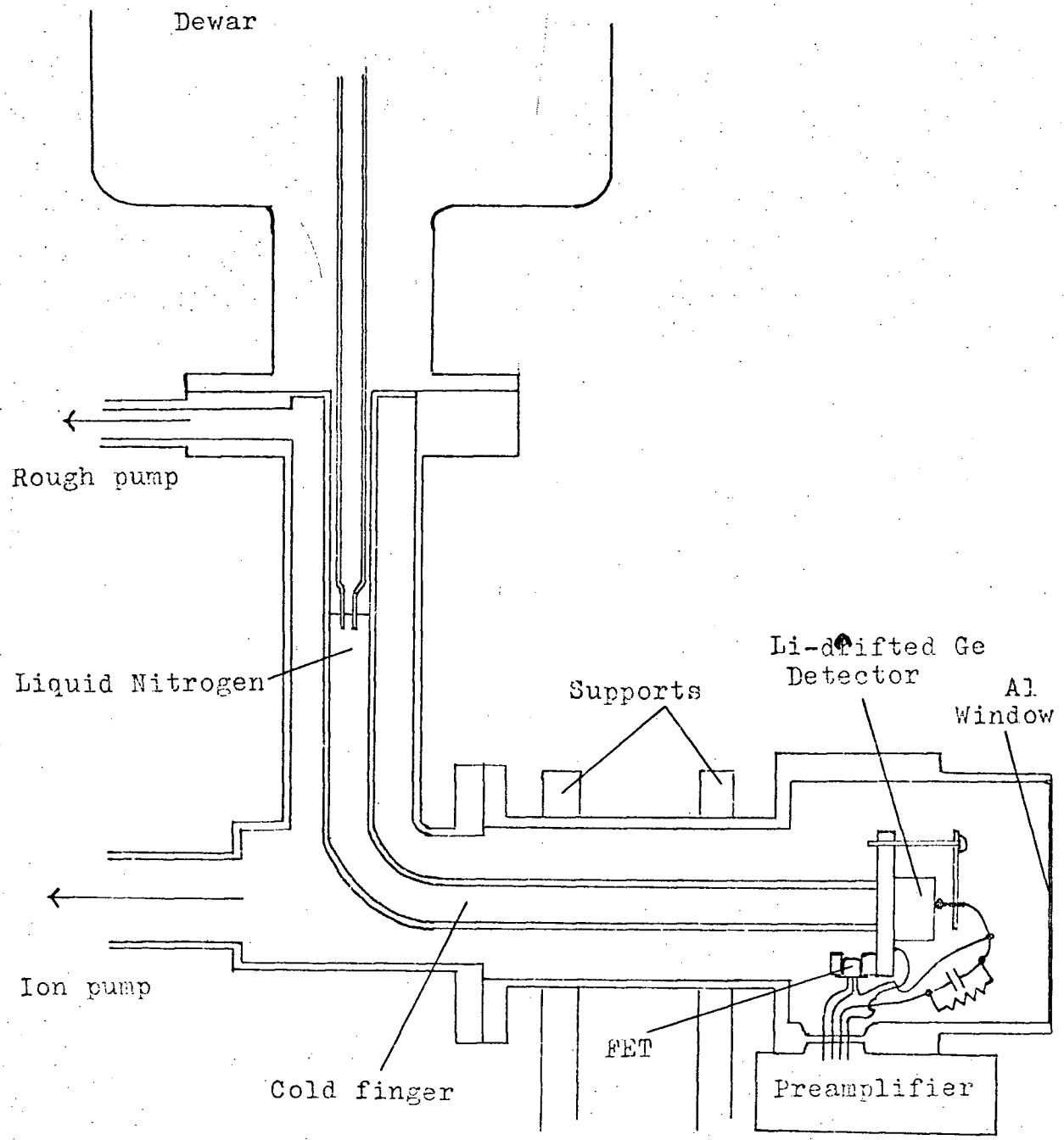

Fig. 4 The Germanium detector assembly.

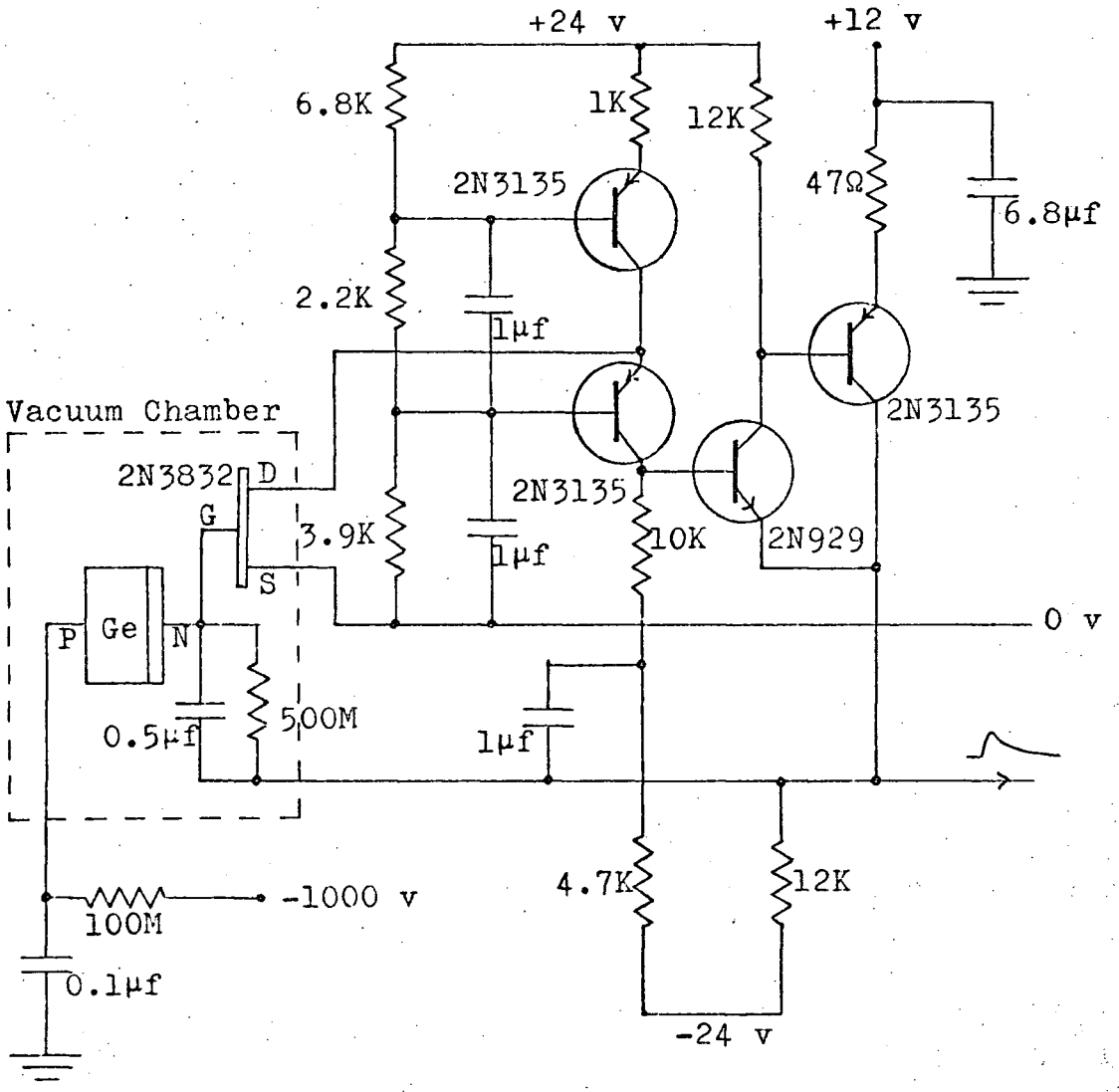

Fig.5 Input stage of the low-noise preamplifier connected to the Germanium detector.

for the first detector, we obtained a resolution of 4 Kev at about 1.3 Mev of energy or below; while with a bias of -1000 v. for the second detector, the resolution was 3.5 Kev in the same energy range. These are illustrated in figures 6 and 7. It is also clear that the second detector having a larger active volume gave a much better ratio of photo-absorption peak to Compton continuum.

§4. Source Preparation and Mounting.

The Eu 154 source was prepared from 2 milligrams of Europium in oxide form, which was enriched to 98.76% of Eu 153. The oxide was sealed in a quartz capsule and irradiated for 7 days in the Oak Ridge National Laboratory reactor to yield about 5 millicuries of Eu 154 by neutron-capture process. A small quantity of the irradiated source was introduced into a miniature beaker and a few drops of pure concentrated hydrochloric acid were added to obtain a chloride solution. The solution was evaporated to dryness under a tungsten lamp to remove the excess acid, and when cool the chloride was dissolved in distilled water. It was re-evaporated and then dissolved in distilled water again.

The purpose of changing the insoluble oxide into the soluble choride is mainly for preparing the beta sources.

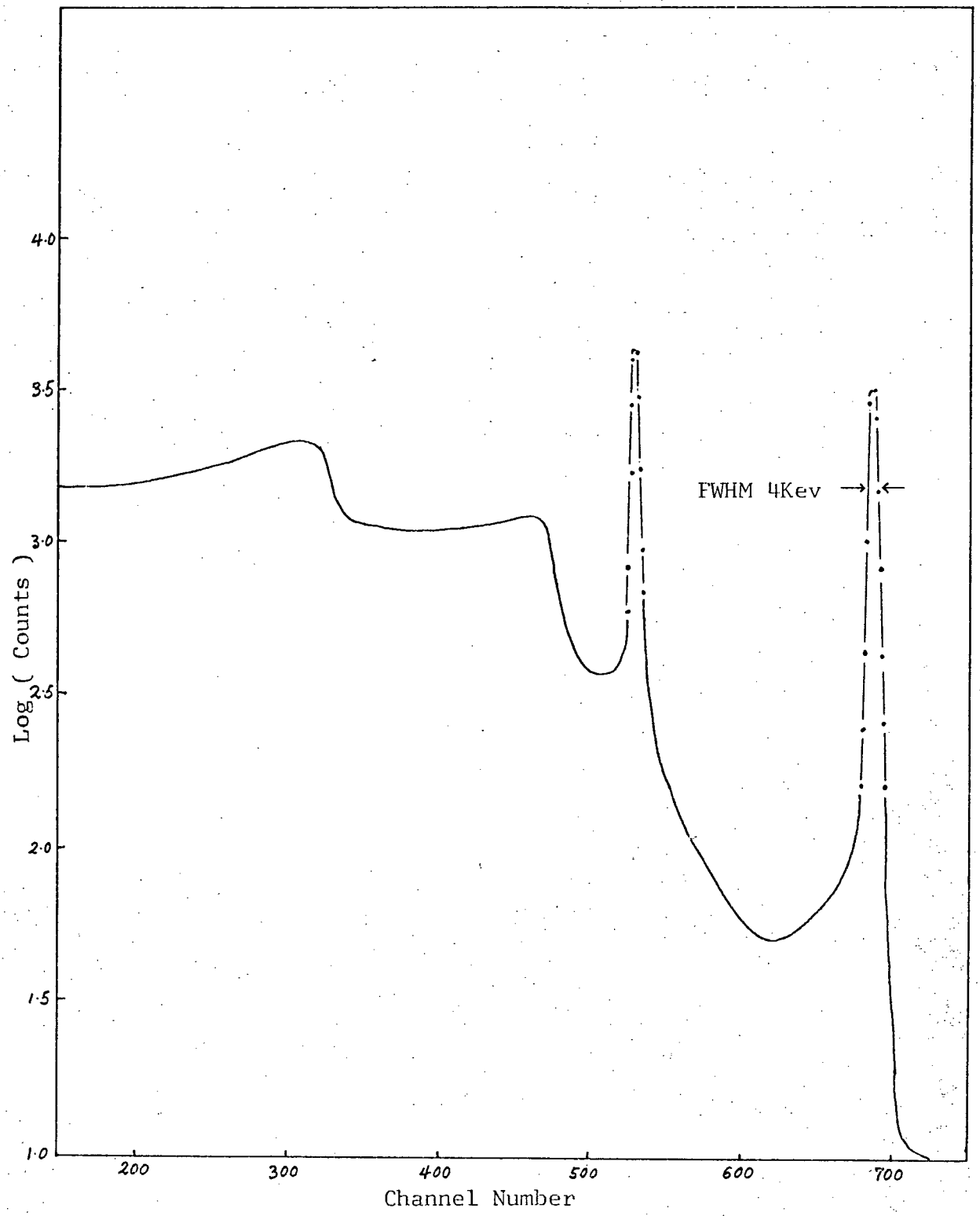

Fig.6 Co 60 gamma spectrum obtained from the 1.5 c.c. Ge detector.

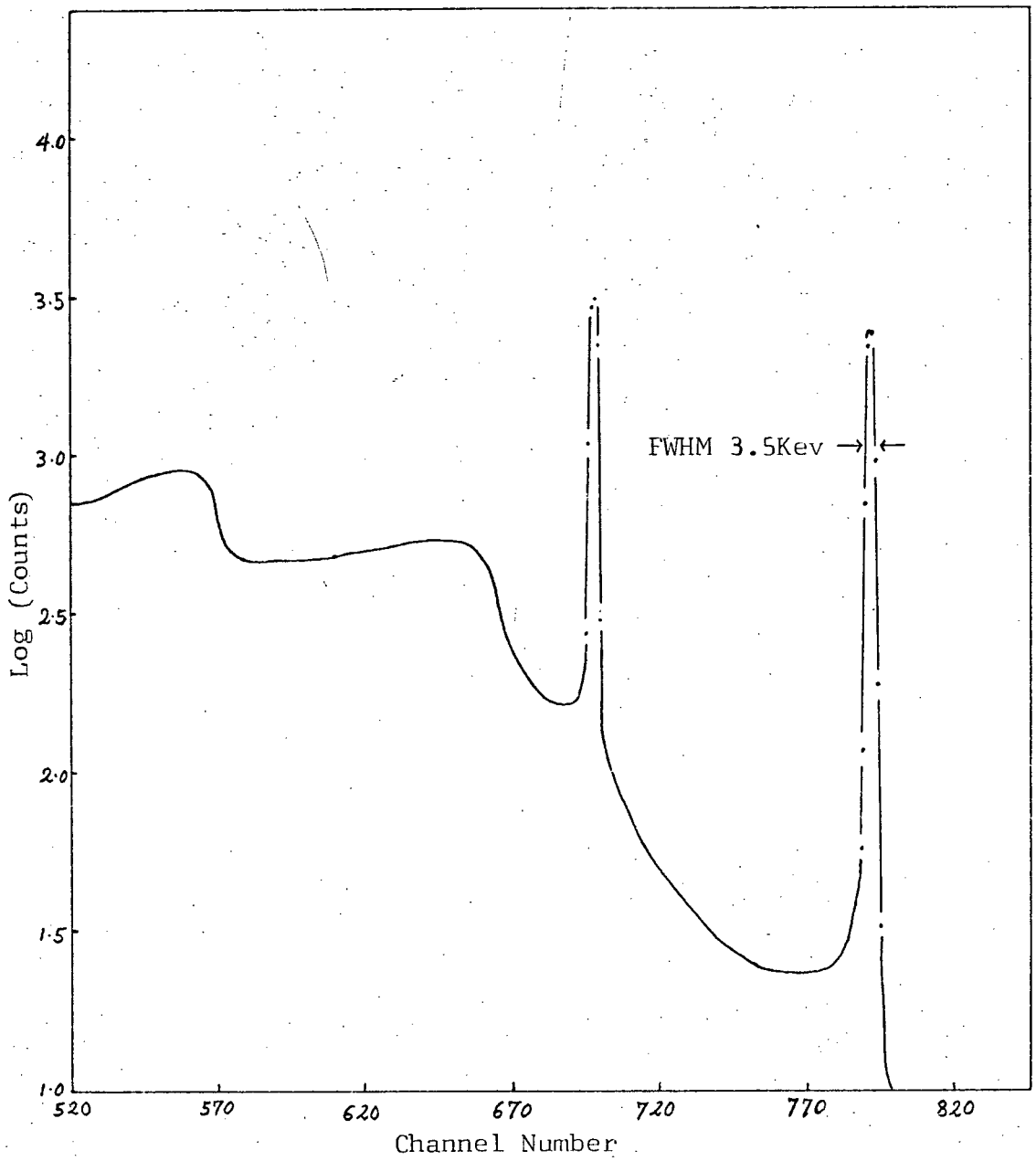

Fig.7 Co 60 gamma spectrum obtained from the 5 c.c. Ge Detector.

But it is also convenient to prepare gamma sources from liquid form, because the radioactive strength can be easily controlled in this way.

A drop of the liquid was dried on an IBM card cut into a circular disc of 1 inch diameter with the drop at the centre. The source was then sealed with scotch tape and mounted on a lucite ring as shown. Several sources were prepared with various strengths.

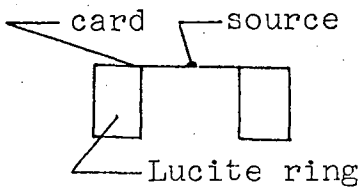

The other sources used for energy calibration were also prepared in the similar way.

§5. Experimental Procedures.

The experiments were carried out at three separate times using the Germanium detectors described in §3, and the gamma sources prepared as described in §4. At each time, a 40-minute run was taken to obtain the gamma spectrum of Eu 154 in a 1024-channel kick sorter. This was followed by 10-minute runs for various calibration sources including Co 57, Co 60, Cs 137, Na 22, Mn 54, Ba 133, Cs 134, Y 88, RdTh, Hg 203, and Am 241. The position of the source holder relative to the detector was fixed on an aluminium frame, so that every source could be placed at exactly the same position. Hence, no correction for the detector geometry was necessary. (Actually, there is

no way to do this, as every Germanium detector has its own peculiar effective geometry.) Then, in order to obtain better information on the weak peaks, an over-night run of the Eu 154 spectrum was repeated, and so also a longer-period run for each of the weaker calibration sources. From the beginning to the end, the conditions of the electronic system such as the amplification, threshold and bias voltage were kept constant. The loss percentage indicated on the kick sorter was not allowed to exceed 5 in all the runs. If it did, a new source position had to be located. Special care was taken to ensure no time shift in the electronic system when the short-period runs were taking place. This was done by using a suitable calibration source as a probe. (Na 22 was chosen for this purpose.) Spectra of this 'probe' were taken at the beginning and the end of the short-period runs and also before the 40-minute run of Eu 154. Any shift in the two Na 22 peaks (i.e. the 511.0 Kev and 1274.6 Kev) would indicate instability in the system and the spectra then had to be re-taken. The output data from the kick sorter were photographed in polaroid films for immediate inspection, and punched out in paper tapes for further processing.

The first experiment was done in October, 1966, in which the Eu 154 spectrum was taken in two portions by means of a bias amplifier. Each channel of the kick sorter then corresponds

to slightly less than 1 Kev. These spectra gave a fine picture of the number and locations of the peaks to be expected. Also similar spectra of Eu 152 were taken to check for the impurity of this isotope in Eu 154. The peaks belonging to Eu 152 were soon sorted out. Unfortunately, the smaller detector (1.5 c.c. effective volume) was used in this case, so that the intensity measurement was not very reliable.

In the second and third experiments which were done in December, 1966 and April, 1967 respectively, the bigger detector (5 c.c. effective volume) was employed, and much better results were obtained. Figure 8 shows a typical Eu 154 spectrum on logarithmic plot. In this case, each channel of the kick sorter corresponds to about 1.7 Kev of energy. It can be seen from the figure that the threshold of the kick sorter was set at a fairly high level. This was done so as to be able to eliminate the very high counting rate of the low energy pulses.
In order to be free from any possible distortion in energy and intensity at the low-energy peaks due to the threshold setting, the lower portion of the spectrum was recalibrated in a 400-channel kick sorter as shown in figure 9, and the intensities were normalised to the main spectrum.

The standard sources for intensity calibration were obtained from the International Atomic Energy Agency, Vienna.

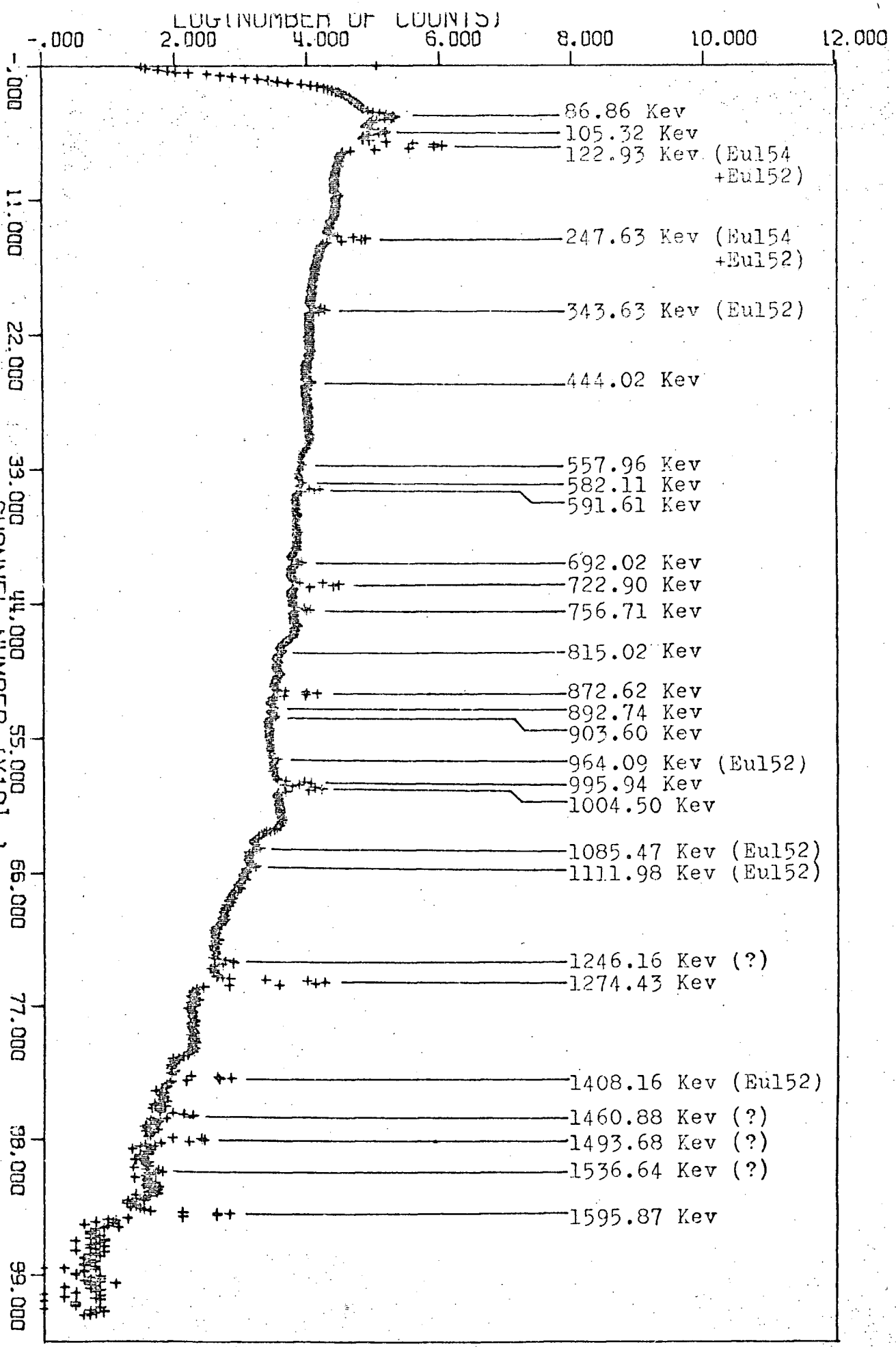

Fig.8 Eu 154 gamma spectrum.

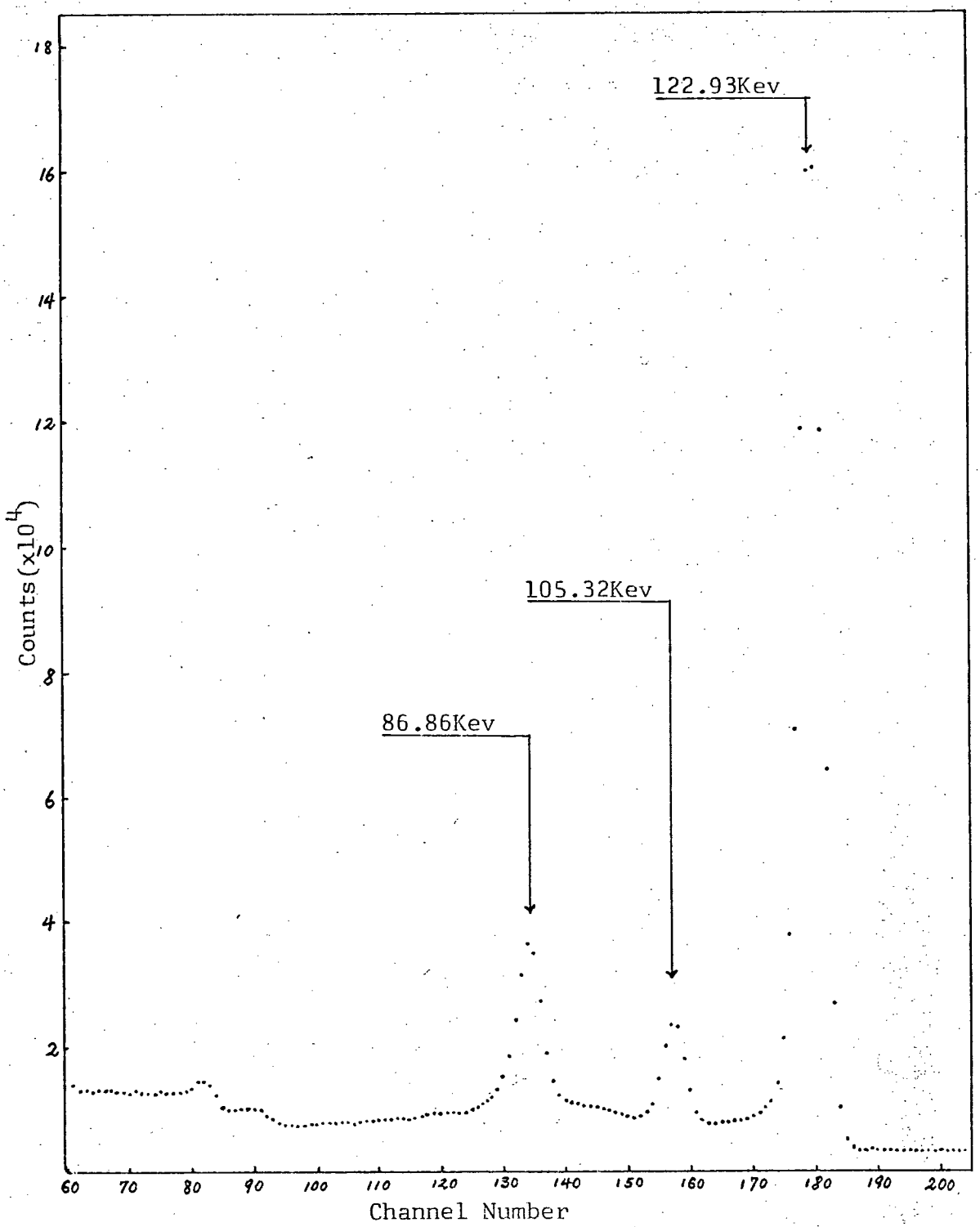

Fig.9 Low-energy gamma peaks of Eu 154.

They include Am 241, Hg 203, Co 57, Na 22, Cs 137, Mn 54, Co 60, and Y 88, covering an energy range from 59.57 Kev to 1841 Kev. They were all spot sources, and, when the calibration was being performed, these sources were again placed at exactly the same position as the Eu 154 source.

One important reason for performing the experiments at three separate times has not yet been mentioned. By examining the Eu 154 spectra taken at the three different periods, we found that some of the peaks were shrinking with respect to the others, indicating the presence of some short-lived impurities. These peaks, of course, had to be excluded.

The analysis of the spectra taken will be discussed in the next section.

§6. Results and Analysis.

After the vast amount of spectral data were plotted out by the IBM computer, the peak positions and the peak counts were estimated by graphical methods. It should be noted that the peak shapes were not Gaussian, so that the standard Gaussian fitting could not be applied in the hope of obtaining more accurate results. In spite of the only 3.5 Kev full width at half maximum, a long tail existed at the lower energy side of each peak as shown in figure 7 in §5. This was probably due

to dislocations or impurities in the Germanium crystal, which occasionally trapped some electrons causing incomplete collection of charges in each event. These tails gave some difficulty in the intensity estimation. However, the counts in a tail are only about 5 per cent of the counts under the relevant peak. Assuming the tail counts are proportional to the peak counts, the error should not be too serious even if part of the tail is neglected.

Another point to be mentioned is that, since there are so many peaks over the entire Eu 154 spectrum, it is quite possible that some of these peaks might sit on some Compton edges, or single or double escape peaks. For this, all the positions of the Compton edges, single and double escape peaks related to those prominant peaks were computed by using the simple equations (84),(85), and (86) given in §2. Care was taken in analyzing those few peaks in the vicinity of the mentioned positions.

For the energy calibration, the known-energy peaks used are listed in table I. From figure 10, which shows one calibration curve for the Eu 154 spectrum, we see that the electronic system is fairly linear. However, we did not assume any simple functional dependence of the energy on the channel number. Since the calibration curve is fairly linear, the

Radionuclide	Energy(Kev)	Radionuclide	Energy(Kev)
Am 241	59.57	Cs 134	569.0
Hg 203	73.0	RdTh	583.0
Ba 133	81.0	Cs 134	604.65
Co 57	122.0	Cs 137	661.59
Co 57	136.4	RdTh	727.0
Hg 203	279.1	Cs 134	796.0
RdTh	238.6	Mn 54	835.0
Ba 133	276.0	RdTh	860.0
Ba 133	302.0	Y 88	897.5
Ba 133	355.0	Co 60	1173.3
Ba 133	383.0	Na 22	1274.6
RdTh	511.0	Co 60	1333.0
Na 22	511.0	RdTh	1592.4
Cs 134	563.0	Y 88	1841.0

Table I Peaks used for energy calibration (obtained from ref. 49 and other sources).

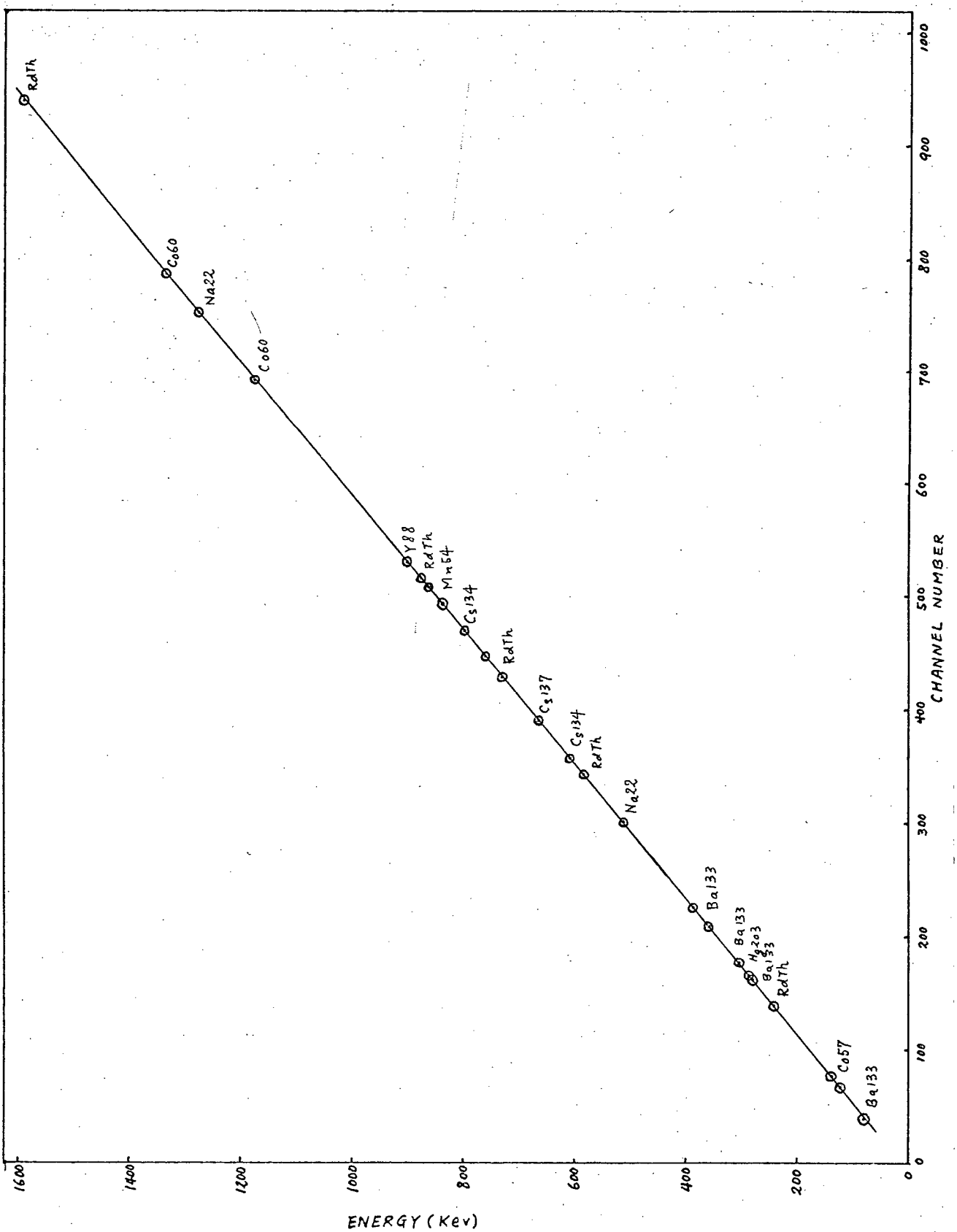

Fig.10 Gamma energy calibration curve.

following method of linear interpolation was considered to be the best way:

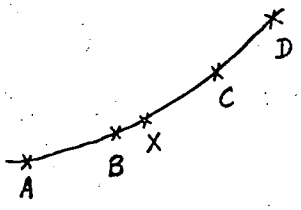

Let A,B,C,D be the known energy points and X, the point to be calibrated. Linear interpolations were computed using the pairs of known energy points, (B,C), (A,C) and (B,D), and these gave the results for X as X(1), X(2) and X(3) respectively. If these three values for X agree to within 1 Kev, then X = X(1). If otherwise, that section of the curve was expanded in a graph paper and X was determined by curve fitting.

The above method, of course, depends considerably on the accuracy of the individual calibration peaks. However, because so many known energy peaks were being used, it was not difficult to check whether any individual peak value was up to the standard or not. No pulser was used in the present case, as better accuracy was not expected from it. Provided that the energies listed in table I are correct to within 0.5 Kev, the peaks calibrated in this way should be within 1 Kev.

The energies of those well-defined peaks in each 40-minute spectrum of Eu 154 were thus calibrated. As for the

weak peaks, calibration had to be done on the over-night-run spectra. In this case, the strong peaks of the same spectrum acted as substandards. Consequently, any time shift would not affect the calibration, since the whole spectrum would have shifted altogether.

The characteristics of the standard sources for intensity calibration are given in table II, which were calibrated at zero hour GMT, January 1, 1967. The relative strength of each source at the time when its spectrum was half taken was calculated, and so were the relative intensities corresponding to its gamma energies. The observed intensities of the gamma peaks were directly measured from each spectrum. The ratios of relative intensity to observed intensity were then plotted as a function of gamma energy as shown in figure 11*. The curve is fairly smooth and is just the inverse of the efficiency curve. The window effect sets in at about 80 Kev. It is due to the obstruction of the N layer of the detector (about 0.5 mm. thick) and the aluminium window of the vacuum chamber (0.25 mm. thick). Using the graph plotted,

---

* The intensity ratio at 81.0 Kev was obtained by taking a Ba 133 spectrum. The relative intensity of 355 Kev of Ba 133 was found from the graph. Then we multiplied it by 0.52 (see ref. 46) to obtain the relative intensity of the 81 Kev peak and hence its intensity ratio.

Isotope	Strength (μC)	Half-life	γ-energy (Kev)	γ-ray per disintegration (%)
Am 241	10.66	485.1±0.5 years	59.57±0.02	35.9±0.6
Co 57	10.78	271.6±0.5 days	122.0	85.3±1.5
Hg 203	21.77	46.57±0.03 days	279.1±0.05	81.55±0.15
Na 22	11.46	2.603±0.005 years	511.0 1274.6±0.3	179.7±0.8 99.94
Cs 137	10.68	29.82±0.11 years	661.59 ±0.076	84.6±0.6
Mn 54	10.70	313 ±1 days	835.0±0.3	100
Co 60	10.87	5.263±0.003 years	1173.3±0.3 1333.0±0.3	100±0.012 100±0.00
Y 88	10.64	106.6±0.1 days	897.5±0.5 1836.2 0.3	92 100

Table II Peaks used for intensity calibration.

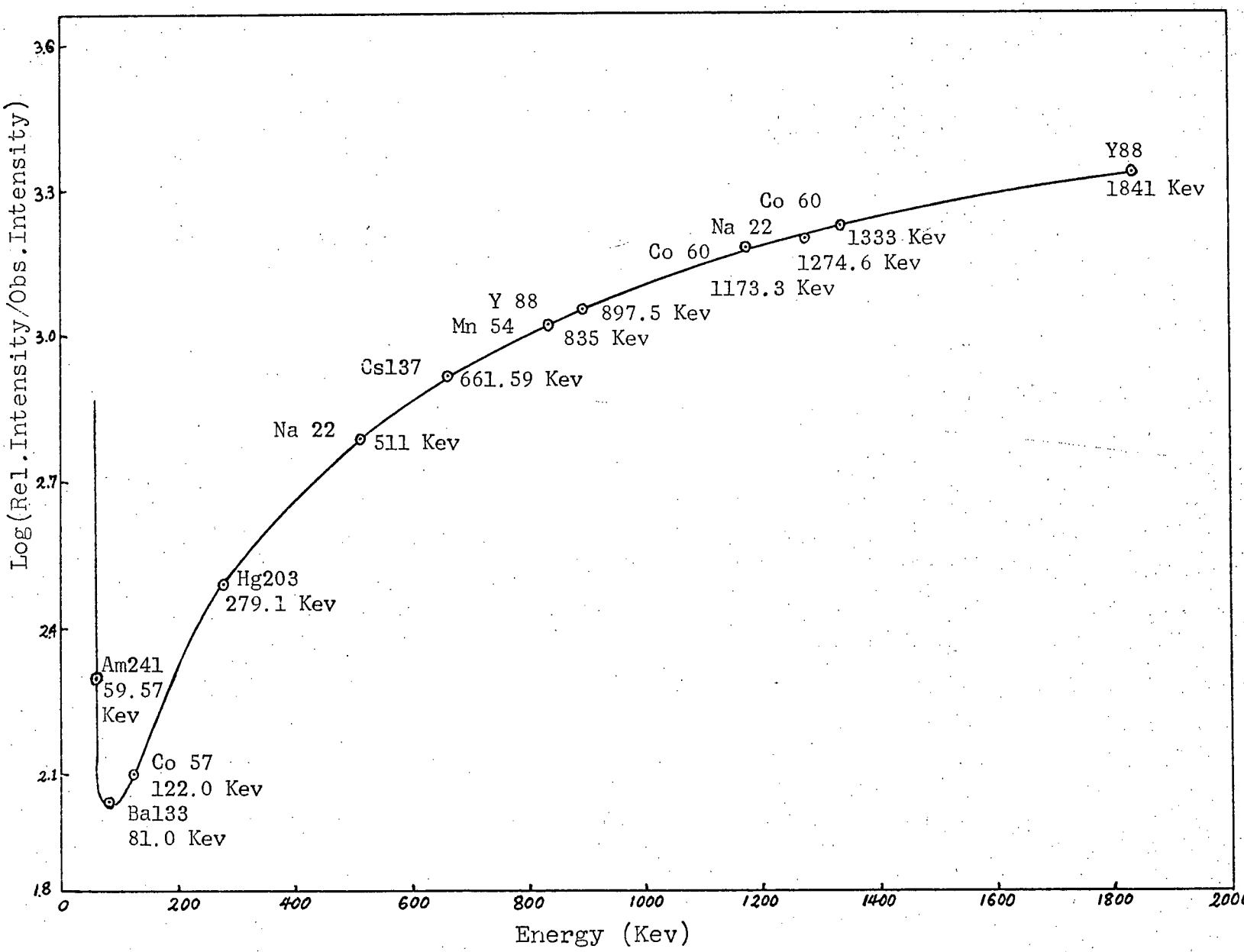

Fig. 11. Gamma intensity calibration curve.

To follow p. 56.

the relative intensities for the corresponding Eu 154 spectrum were found by multiplying the observed intensities to the corresponding ratios in the graph.

The calibrated energies and the relative intensities with error limits were then presented in table III. The energies given are accurate to within 1 Kev. This accuracy is revealed in Chapter 7 when constructing the decay scheme. The relative intensities determined are far more complete than those of previous workers. The accuracies of the energy measurements compare very favourably with those from conversion lines measured with high resolution spectrometers.

Scanning through table III, in addition to the well-established strong peaks, we find that there are a few partially familiar peaks, i.e. 86.86 Kev, 105.32 Kev, 444.02 Kev, 557.96 Kev, 692.02 Kev, 815.02 Kev, and 892.74 Kev. Among them, the 557.96 Kev and 892.74 Kev peaks have been observed by Harmatz et al[33] in the decay of Tb 154 to Gd 154, but have never been observed in the decay of Eu 154. The gamma intensity of the 692.02 Kev was barely measured by Hamilton et al[36] using the external conversion method. The rest of the transitions were known from the internal conversion data[20),36)].

In addition to the above, there are completely unfamiliar peaks, i.e. 582.11 Kev, 903.60 Kev, 1246.16 Kev, 1460.88 Kev and 1493.68 Kev. It is quite interesting to find

γ-energy (Kev)	Relative Intensity	Remark
86.86	15.42 ±1.31	*
105.32	9.70 ±0.84	*
122.93	100.00 ±2.44	Eu152 Int. subtracted
247.63	15.86 ±0.72	Eu152 Int. subtracted
343.63	3.76 ±0.29	Eu152
444.02	1.56 ±0.14	
557.96	0.867±0.163	
582.11	1.73 ±0.16	
591.61	10.51 ±0.54	
692.02	3.80 ±0.29	
722.90	47.30 ±2.05	
756.71	10.36 ±0.60	
815.02	1.31 ±0.22	
872.62	29.38 ±1.36	
892.74	1.23 ±0.20	
903.60	2.04 ±0.23	
964.09	1.82 ±0.25	Eu152
995.94	24.69 ±1.12	
1004.50	43.85 ±1.92	
1085.47	1.67 ±0.22	Eu152
1111.98	2.40 ±0.24	Eu152
1246.16	2.27 ±0.21	**
1274.43	92.00 ±4.13	
1408.16	3.29 ±0.20	Eu152
1460.88	0.386±0.052	**
1493.68	1.71 ±0.11	**
1536.64	0.125±0.022	**
1595.87	4.67 ±0.22	

* Transitions known to be belonging to the decay of Eu154 [20], but cannot be fitted into the decay scheme.

** Weak peaks with unknown origin.

Table III Energies and Intensities of Eu154 Spectrum.

(The second figure after each decimal in column one is physically insignificant.)

that the first two peaks fit perfectly into the decay scheme in Chapter 7. The others still cannot be fitted to the known levels.

Among the very weak peaks, 444.02 Kev is shown distinctly in figure 8, §5. The others were plotted again in an enlarged scale as shown in figure 12. They are all well above the statistical fluctuation.

It was noted in table III that a few Eu 152 peaks were present due to a small percentage of this impurity. Comparison of their intensities with those given in Nuclear Data Sheets[49] is shown in table IV. They agree fairly well. We also expected a small impurity mixing in the peaks 122.93 Kev and 247.63 Kev due to the 121.8 Kev and 244.7 Kev peaks of Eu 152. The contribution to the intensity by this impurity in each peak has already been subtracted. This was done by using internal conversion data calculated in Chapter 6 (since the 121.8 K- peak of Eu 152 was separable from the 122.93 K- peak in the beta spectrum).

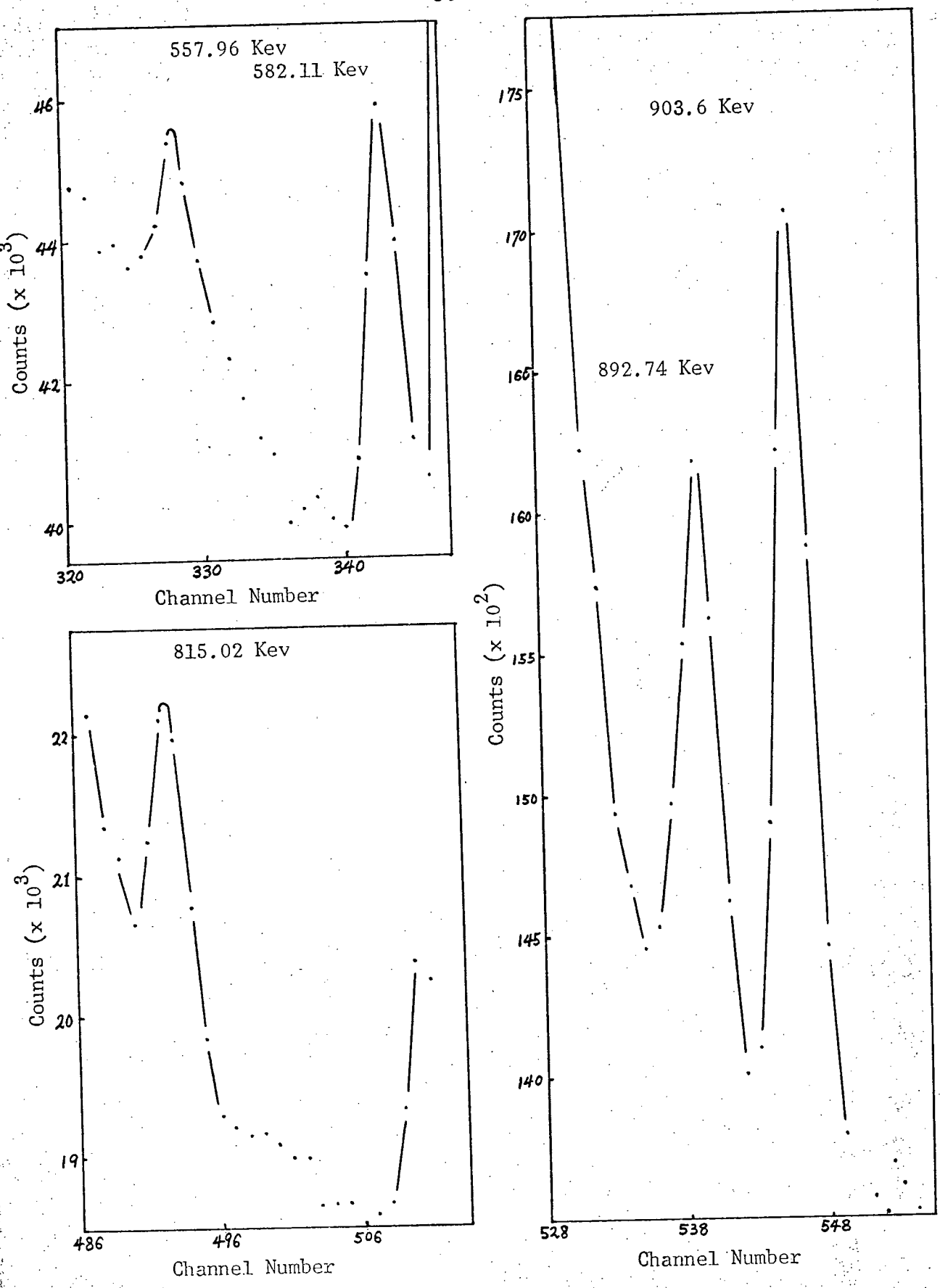

Fig.12 Weak gamma peaks in the Eu 154spectrum (see fig.8).

Gamma-energy (Kev)	Rel. Intensity obtained	Rel. Intensity from ref.49
343.63	3.76±0.29 (29%)	24%
964.09	1.82±0.25 (14%)	14%
1085.47	1.67±0.22 (13%)	11%
1111.98	2.40±0.24 (18%)	15%
1408.16	3.29±0.20 (26%)	25%

Table IV. Gamma peaks belonging to Eu 152 impurity.

CHAPTER V

GAMMA-GAMMA COINCIDENCE SPECTROSCOPY

§1. General Considerations.

The results from the last chapter provide many interesting aspects which require further investigation. They can be stated as follows,

1) The 995.94 Kev and 1004.50 Kev peaks which have never been separated by previous workers are well resolved. Therefore, if gamma-gamma coincidence should be performed again, we expect to get conclusive results regarding the proper locations of these two transitions in the decay scheme.

2) New peaks such as 903.60 Kev and 582.11 Kev were found, which, as will be shown later, have suitable places in the decay scheme. But they need to be confirmed.

3) New peaks such as 1246.16 Kev, 1460.88 Kev and 1493.68 Kev were found, but their origins are unknown.

4) Weak peaks such as 872.62 Kev, 815.02 Kev and 444.02 Kev which have been reported from beta spectroscopic measurements (e.g. refs. 20 and 36),have also been seen in this gamma spectrum. Their positions in the decay scheme need to be confirmed.

All the above points can be examined by gamma-gamma coincidence at least in principle. However, in practice,

one requires much sophistication in the detection and electronic systems such as an increase in the active volume of the Germanium detectors, the use of multiparameter kick sorters etc. In view of the time consumption in doing gamma-gamma coincidence work and the present equipment available, we have for the time being limited our coincidence experiments to the first of the above four points. Results obtained are quite conclusive. The experimentswill be described in the next sections.

The idea of gamma-gamma coincidence is simple and straight-forward. Suppose there are two gamma transitions in cascade as shown in figure 13a, and the directions of

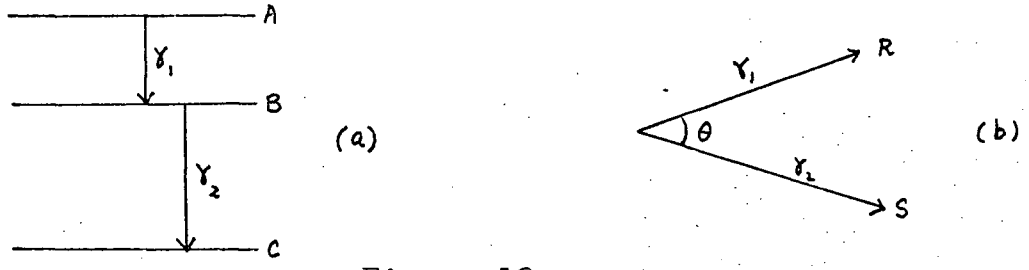

Figure 13.

emission of these gammas are related by the angle θ as in figure 13b. Now if we place two counters or detectors at the positions R and S respectively, the two gammas will be recorded either simultaneously or in a small fixed interval of time. However, the most probable angle of θ varies with different pairs γ_1 and γ_2, so that the position of S relative to R has to be determined in order to gather a maximum number of pairs in a given period of time. If the two gammas were uncorrelated, then any position of the counter S

relative to R will give equal probability in counting the pairs. In the correlated case, the probability is given by [50]

$$W(\theta) = \sum_{n=0}^{N} A_{2n} P_{2n}(\cos\theta) \qquad (87)$$

where A_{2n} are constant coefficients, and $P_{2n}(\cos\theta)$ are the Legendre polynomials, given explicitly by

$$P_0(\cos\theta) = 1$$
$$P_2(\cos\theta) = \tfrac{1}{2}(3\cos^2\theta - 1)$$
$$P_4(\cos\theta) = (35\cos^4\theta - 30\cos^2\theta + 3)/8 \qquad \text{etc.}$$

Theoretical evaluation of the true counting rates is not a problem in this investigation, because no variation of the correlation angle θ is involved in the experiment, and in any case, the results that will be presented later are so unambiguous that reliance upon a theoretical analysis is entirely unnecessary.

2. The Coincidence System.

The experimental arrangements are shown in figure 14. The source was placed between a Germanium-Lithium detector and a 1X1½ in. diameter NaI(Tl) scintillator. The 1.5 cc Ge detector was used in this case. (It would have been preferable to use the 5 cc detector, except that it was being used in other

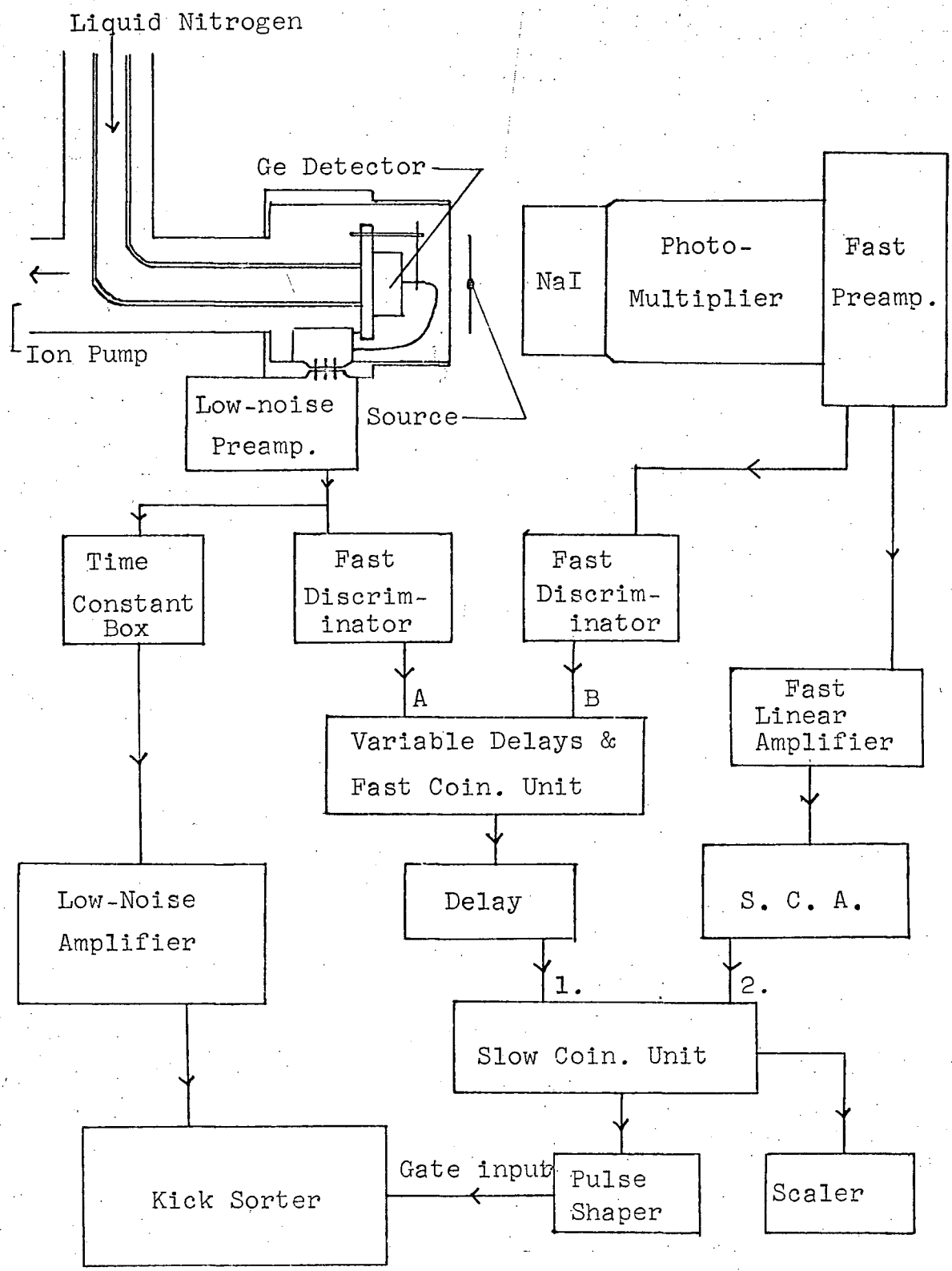

Fig. 14. The gamma-gamma coincidence system.

experiments.) As usual , the scintillator was in photo contact with a photomultiplier (RCA 5819) which was biased at a voltage of -1100 volts. Outputs from the photomultiplier were obtained from the anode and the eighth dynode as shown in figure 15. The reasons for using the eighth dynode instead of the last dynode are to have the output pulse height comparable to the corresponding one from the anode output and to achieve better linearty. The negative output from the anode was used for the purpose of fast coincidence. It was connected to a cascade emitter follower in order to acquire enough power to drive the fast discriminator in the following stage. This emitter follower does not need good linearty, all that was demanded of it was a fast rise time ($<$ 50 nsec.) and a low impedance output.

The positive output from the eighth dynode was fed to a white cathode follower, which has a linearity better than 1%. With the given input RC-coupling, the rise time and decay time were found to be 0.2 μsec. and 30 μsec. respectively. This circuit accepts both positive and negative pulses equally well, and hence any overshoot will not cause cut off or other distortion at the output. The output pulses were then amplified by a fast linear amplifier with double-delay-line clipping. These pulses were clipped to 1 μsec. in width and were then fed to an anti-walk single channel analyser (S.C.A.), which

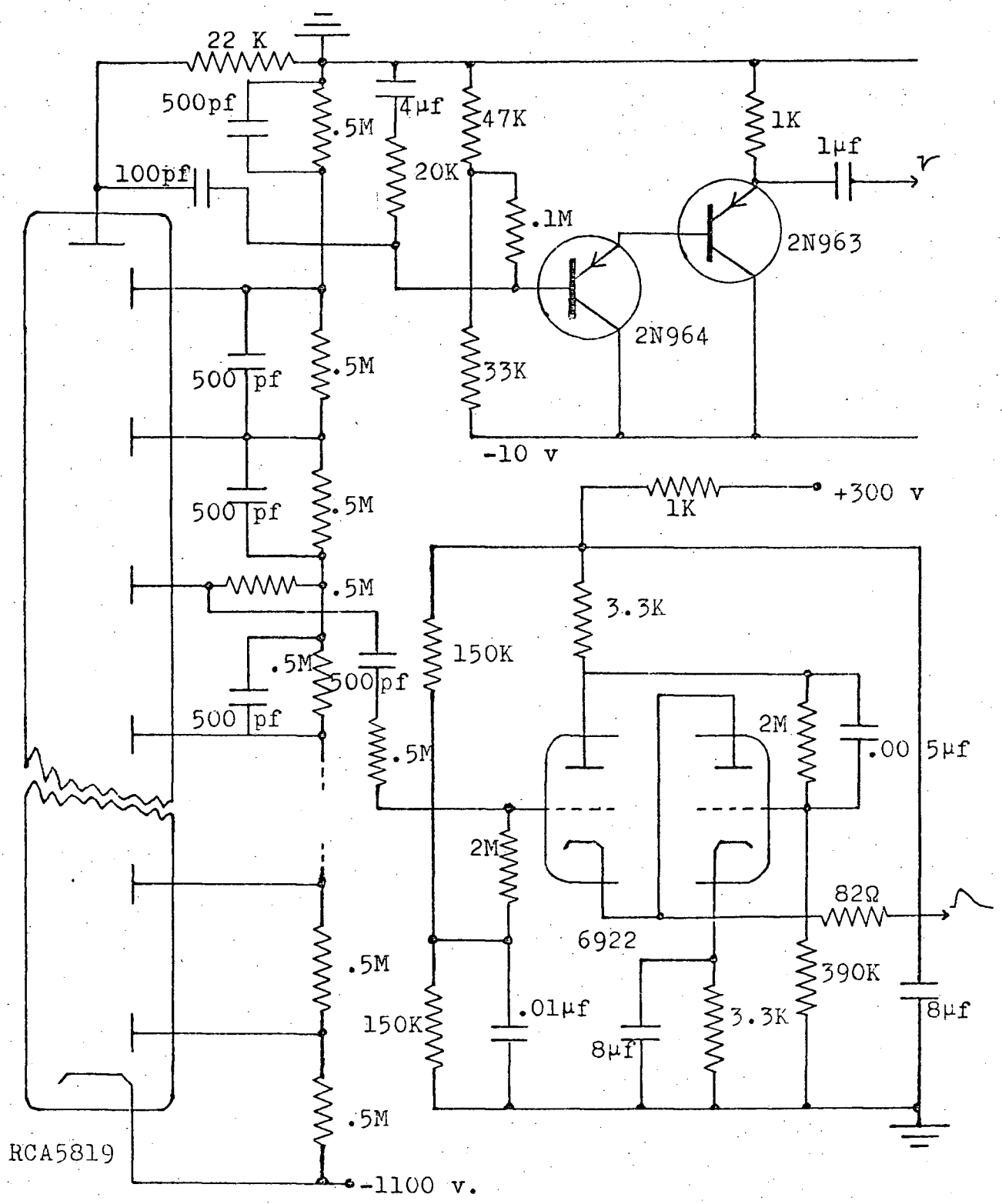

Fig. 15 Photomultiplier output stages.

selects the pulses corresponding to the desired energy in the spectrum taken by the scintillator.

The fast discriminator connected to the cascade emitter follower output is shown in figure 16. The negative input pulse was amplified by the first two transistor stages . The discrimination is controlled by the 2.5 KΩ potentiometer. The resultant current triggered the tunnel diode (1N3716) and brought about a square pulse of rise time less than 10 nsec. The low impedance output was then obtained from the two emitter followers in series. The Zenor diode 1N752A was used to limit the pulse height in order to match the input requirement of the fast coincidence unit.

The low-noise preamplifier attached to the Germanium detector assembly is the same as that described in Chapter 4. The pulses for fast coincidence on the detector side were obtained directly from the preamplifier output before being shaped by the time constant box. These pulses being positive, an inverter stage was installed at the input of the following fast discriminator. The shaped pulses from the time constant box were fed to a 128-channel kick sorter via a low-noise amplifier.

The rest of the units in figure 14 constitute a fast-slow coincidence system, which chooses the gate pulses for the kick sorter.

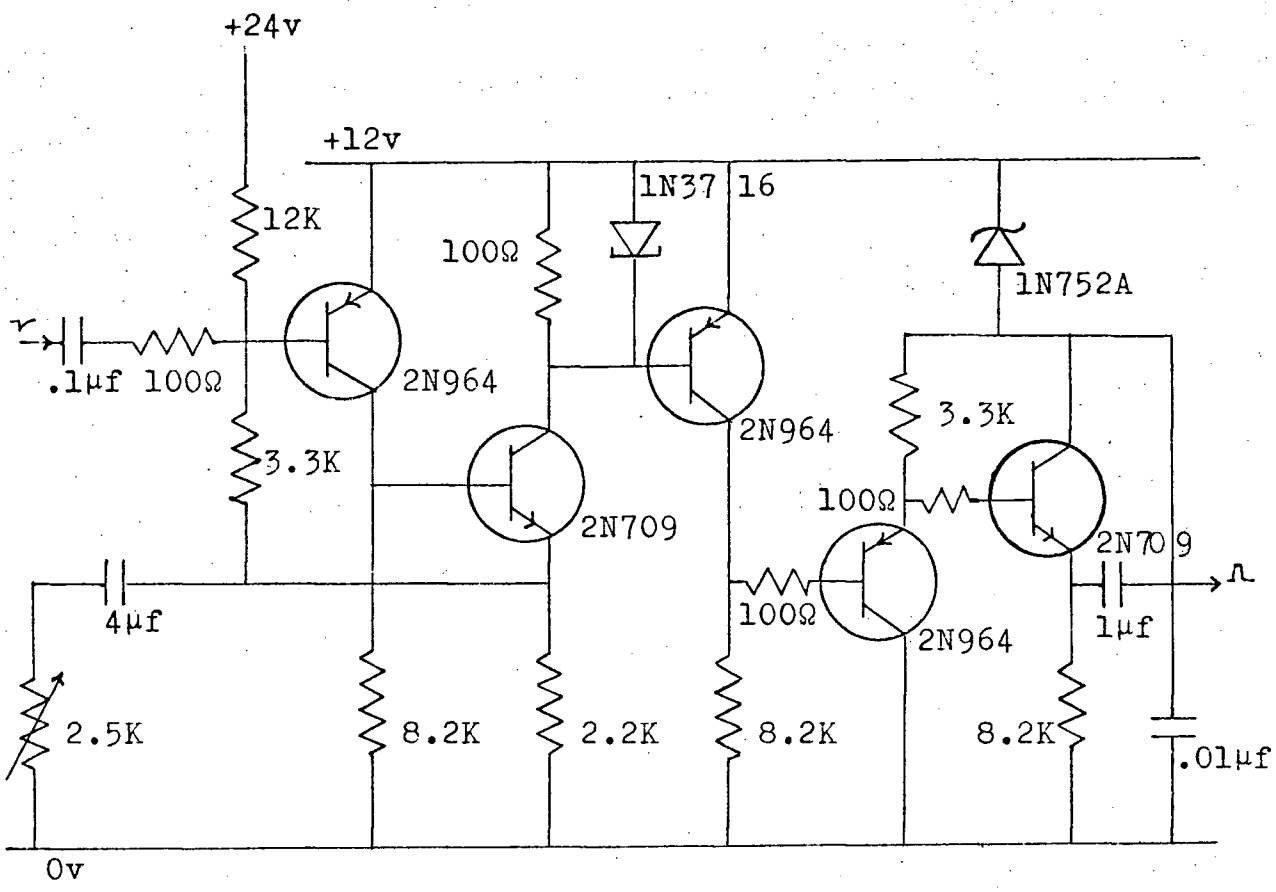

Fig. 16 The tunnel diode discriminator.

§3. Experimental procedures.

A source of Eu 154 with suitable strength was selected from among those prepared earlier, and mounted on a lucite support. The distances of the source from the Germanium detector and the scintillator were chosen by taking the single count rates from the detector and the scintillator respectively. With the source close to the aluminium window of the detector assembly and at a distance of 5 cm. from the scintillator, the single count rates from the detector and the scintillator were 0.7×10^6 cpm and 1.1×10^6 cpm respectively. These count rates were about the maximum the system can tolerate. Higher than these would result in poor resolution on both sides.

The potentiometer of each fast discriminator was adjusted to eliminate most of the base line fluctuations with the help of an oscilloscope. The coincidence pulse width of the fast coincidence unit was set at 50 nsec. With channel 2 input of the slow coincidence unit switch off, the delays in the fast coincidence unit were varied until a maximum counting rate was obtained in the scaler. Then the channel 2 input was switched on again, while the channel A input of the fast coincidence unit was switched off. Also the output of the fast linear amplifier was connected to the kick sorter input in

place of the low-noise amplifier. With this arrangement, the required energy peak from the scintillator to be used as the kick sorter gate control (hereafter referred as the gate peak) could be located. This was done by varying the base line(from zero up) of the S.C.A. and at the same time watching the display in the kick sorter, until the desired peak position is reached. Then the window of S.C.A. was narrowed down to about 20 Kev in width and the base line was again adjusted to acquire the peak position and to obtain maximum scaler counts. Finally, the connections were restored to that shown in figure 14 and the experiment was set going.

The system was allowed to run for 24 hours a day, and all together four runs were done corresponding to different gate settings. The total time taken was approximately 300 hours.

It was checked once in a while for any time shift by counting the fast coincidence output and the S.C.A. output and by printing out the kick sorter data. If time shift took place, the variable delays in the fast coincidence unit or the base line of S.C.A. would have to be adjusted. However, the amplifications, bias voltages and the kick sorter threshold never were altered throughout the four runs.

§4. Results.

Results of the four runs are shown in the figures 17a,b,c,d. Figure 17a used 722.90 Kev peak as the gate peak, and the spectrum shows clearly that 872.62 Kev and 995.94 Kev were in coincidence with 722.90 Kev. The time for this run was 77 hrs. 26 mins.

When the gate setting was brought down to the base of the 722.90 Kev peak on the lower energy side, we got the spectrum shown in figure 17b in 61 hrs. 33 mins. This background spectrum was composed of the accidental counts plus the counts in coincidence with the Compton events.

Similarly, the spectrum in figure 17c corresponds to the gate peak of 591.61 Kev run for 85 hrs. 2 mins., and that in figure 17d corresponds to its background spectrum run for 67 hrs. 37 mins. It leaves no doubt that the 1004.50 Kev peak in the spectrum is in coincidence with the 591.61 Kev peak.

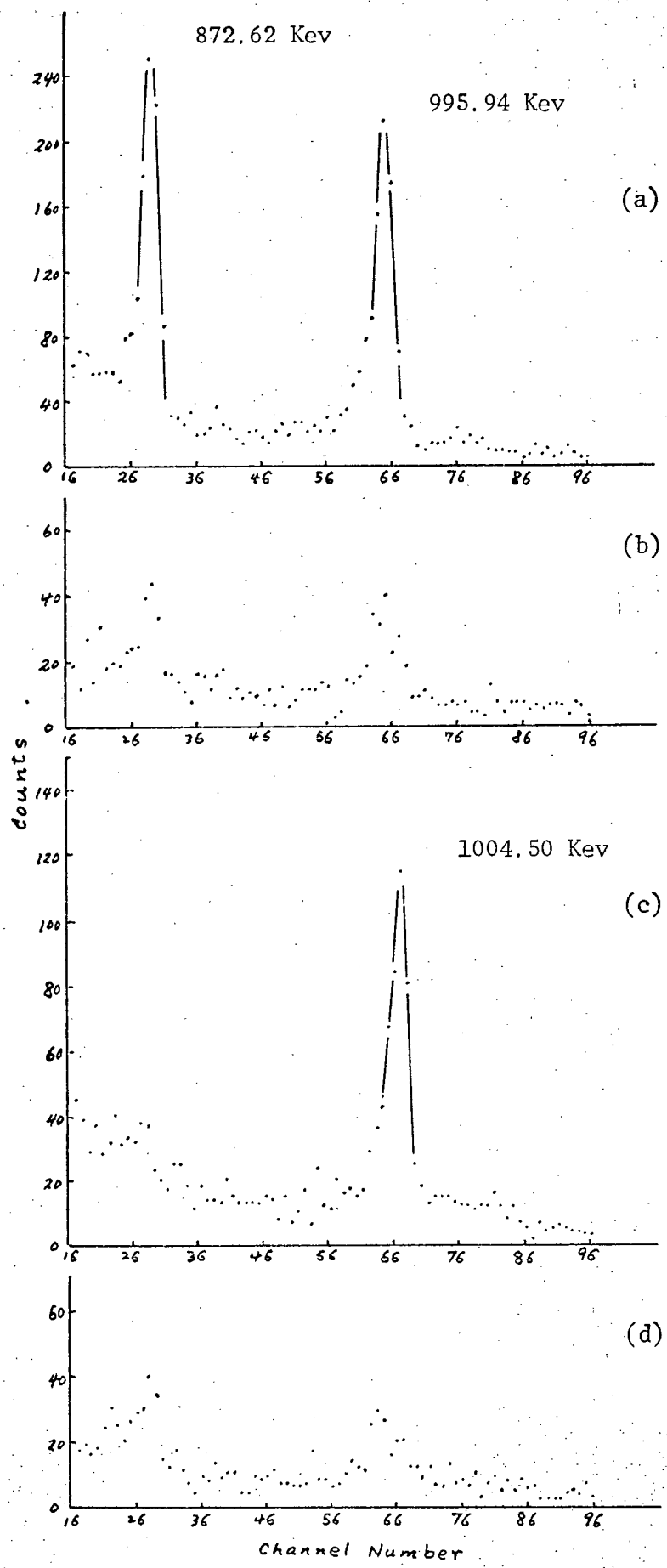

Fig. 17. The gamma-gamma coincidence spectra (see text).

CHAPTER VI

THE BETA SPECTROSCOPY

§1. General Considerations

The theory presented in Chapter 2 did not include beta transitions. The reasons for this are two-fold. Firstly, the measurements made with the beta spectrometer give information on both the primary beta radiations between parent and daughter nuclei and the internal conversion electrons. We are mainly concerned with the internal conversion electron peaks. Evaluation of the energies and intensities from the beta continuum are only for the purpose of establishing the decay scheme and as a check upon the transition intensities. No attempt has been made to determine the transition matrix elements in the beta decay, since this requires directional correlation work as well. Secondly, the beta transitions in this case are from an odd-odd nucleus (Eu 154) to an even-even nucleus, while the gamma transitions discussed in Chapter 2 using the Asymmetric Rotator Model are concerned with an even-even nucleus only (Gd 154). The two cases are not the same.

In this section, we will outline some of the features of the beta transitions of an odd-odd parent nucleus and then

pass to the discussion of the internal conversion process.

Since Eu 154 is also a deformed body, the selection rules given in Chapter 4,§1 also apply. In addition, we have to take into account an odd proton and an odd neutron. Because of this, the Nilsson Model for individual nucleons in strongly deformed nuclei is required [51]. In this model, Nilsson considers the Hamiltonian for a single nucleon in a deformed nucleus to be

$$H = H_o + C\vec{l}.\vec{s} + D\vec{l}^2 \tag{88}$$

where

$$H_o = -\frac{\hbar^2}{2M}\Delta' + \frac{M}{2}(\omega_x^2, X'^2 + \omega_y^2, Y'^2 + \omega_z^2, Z'^2) \tag{89}$$

is the oscillator Hamiltonian, and the other two terms are the spin-orbit and orbit-orbit coupling terms. As a crude approximation, consider the deformation to be axially symmetric, i.e.

$$\begin{aligned} \omega_{x'} &= \omega_{y'} = \omega_o(1 + \tfrac{1}{2}\varepsilon) \\ \omega_{z'} &= \omega_o(1 - 2\varepsilon/3) \end{aligned} \tag{90}$$

where ε is a deformation parameter. The variables are then changed to

$$(X'',Y'',Z'') = \left(X'\sqrt{\frac{M\omega_{x'}}{\hbar}}, Y'\sqrt{\frac{M\omega_{y'}}{\hbar}}, Z'\sqrt{\frac{M\omega_{z'}}{\hbar}}\right)$$

It follows that

$$H_o = H_{x''} + H_{y''} + H_{z''} \tag{91}$$

where

$$H_{x''} = \tfrac{1}{2}\hbar\omega_{x'}\left(-\frac{\partial^2}{\partial X''^2} + X''^2\right), \text{ etc.} \tag{91a}$$

Hence H_o is diagonal in the representation, $|n_1\rangle|n_2\rangle|n_3\rangle$ such that

$$H_{x''}|n_1\rangle = (n_1+\tfrac{1}{2})\hbar\omega_{x'}|n_1\rangle \text{ ,etc.} \tag{92}$$

Consequently $$H_o |n_1\rangle|n_2\rangle|n_3\rangle = E_o |n_1\rangle|n_2\rangle|n_3\rangle \quad (93)$$

with $$E_o = (n_3 + \tfrac{1}{2})\hbar\omega_{z'} + (n_1 + n_2 + 1)\hbar\omega_{x'} \quad (94a)$$

Define $N = n_1 + n_2 + n_3$, $n_\perp = n_1 + n_2$, $n_{z''} = n_3$ and from (90)

$$E_o = \hbar\omega \left[(N+3/2) + \varepsilon (n_\perp - 2n_{z''})/3)\right] \quad (94b)$$

This solution is known as the asymptotic solution in the limit of strong deformation, and it is obvious that the energy levels rely on the quantum numbers $N, n_\perp$, and $n_{z''}$ for a given deformation parameter ε. Now let Λ be the z"-component of the orbital quantum number, then

$$\Lambda = n_\perp, n_\perp - 2, \ \ldots\ , -n_\perp + 2, -n_\perp \quad (95)$$

Thus for an odd-A nucleus, we expect that some selection rules on the quantum numbers N, Λ and $n_\perp$ would appear. This is indeed the case, and the selection rules were tabulated by Alaga for the matrix elements often used in calculating the β-transition probabilities as shown in reference 52.

For an odd-odd nucleus, the selection rules mentioned apply to both the odd proton and odd neutron. In addition, the coupling relations between these two odd nucleons in the initial and final states would also give rise to new selection rules. The details were given by Gallagher[53].

However, if one compares the reduced transition probabilities of two transitions from the same initial state to different members of a rotational family, then the intrinsic wave functions of the odd nucleons are cancelled out in the ratio shown below, and hence the selection rules involving

N, Λ and $n_\perp$ do not enter. Thus (ref. 54),

$$\frac{B(L,I_i\to I_f)}{B(L,I_i\to I_{f'})} = \left[\frac{C(I_iL\ I_f;K_i,K_f-K_i,K_f)}{C(I_iL\ I_{f'};K_i,K_{f'}-K_i,K_{f'})}\right]^2 \qquad (96)$$

This equation is for axially symmetric nuclei. For the asymmetric case, mixtures of K terms should be included, i.e.

$$\frac{B(L,I_i\to I_f)}{B(L,I_i\to I_{f'})} = \left[\frac{\sum_m A_{Km}C(I_iLI_{fm};K_i,K_m-K_i,K_m)}{\sum_n A_{Kn}C(I_iLI_{fn};K_i,K_n-K_i,K_n)}\right]^2 \qquad (97)$$

It is well known that the energy E_0 of each beta transition is shared between the emitted electron and neutrino in all possible ways. As a result, the beta spectrum for a single beta transition is a continuum with a definite shape and an energy range, $0-E_0$. For more than one transition, the spectrum is a superposition of all the continua. Experimental determination of E_0 is usually done by the method of Kurie plot (c.f. ref. 55). From the Kurie plot, the component continua can also be resolved. Hence the transition intensities can be found.

§2. The Internal Conversion and Pair Production.

In Chapter 3, we have discussed the processes of de-excitation, which include internal conversion and internal pair production. The internal conversion process involves the transfer of energy from the nucleus to an extranuclear electron by direct interaction between the nuclear charge and the electromagnetic field of the electron (Coulomb interaction).

This was shown by Taylor and Mott [56] by calculation, that the probability for internal conversion by photoelectric effect (i.e. by emission and absorption of a photon) is very small compared to the probability for internal conversion by direct energy transfer. It can also be visualized from the presence of the EO transitions in the conversion spectrum, as in this case there is no gamma counterpart. Consequently, we may conclude that direct gamma emission and internal conversion are two independent processes of de-excitation.

The energy carried by the emitted electron in internal conversion is related to the de-excitation energy, W by

$$E_e = W - B_X \qquad (98)$$

where B_X is the electron binding energy for orbit X from which the electron was ejected. Since B_X is different for different X, there is more than one value of E_e for a given W. Therefore, the conversion peaks in an energy spectrum corresponding to one W are classified into X = K,L,M,N, etc. Also since each of the L,M,N, etc has more than one electron orbit, X may be redefined as X = K,L1,L2,L3,M1, etc. The ratio of the emission rate of the conversion electrons to that of the gamma photons in a given energy transition is called the internal conversion coefficient α, which may be expanded in terms of X's as below

$$\alpha = \alpha_K + \alpha_{L1} + \alpha_{L2} + \alpha_{L3} + \alpha_{M1} + \cdots\cdots\cdots \qquad (99)$$

Also, since the transitions depend on the angular momentum L carried away and the change of parity π, α can be expressed as a linear combination of the terms arising from different electric multipoles EL and magnetic multipoles ML as shown,

$$\alpha = \sum_L \delta_\alpha^2(L) \sum_X \alpha_X(L) + \sum_L \delta_\beta^2(L) \sum_X \beta_X(L) \qquad (100)$$

where $\alpha_X(L)$ and $\beta_X(L)$ are the conversion coefficients referred to EL and ML respectively, and the δ^2's are the relative contributions corresponding to the respective EL's and ML's.

The coefficients $\alpha_X(L)$ and $\beta_X(L)$, which are functions of energy, were calculated and tabulated by Rose [57], and Sliv et al [58] for the first few values of X and L. Rose's calculation was based on the assumption of a point nucleus taking into account the effect of screening by the atomic electron cloud, while in the case of Sliv et al, a finite-sized nucleus with modifications on the initial and final electron wave functions were adopted. Thus the second calculation included the penetration effect(that is the interaction when the electron is inside the charge distribution of the nucleus), and was considered to be more accurate. In general, it agrees with experimental data to within a few per cent.

Experimental evaluation of internal conversion coefficients can be done in several ways [59]. In the present work, we used the so-called normalized peak to gamma method. From

the gamma single spectrum and the β spectrum, a suitable gamma peak (e.g. 122.93 Kev) and a corresponding beta conversion peak were chosen as standards. Let $(I_\gamma)_{st}$ and $(I_{eX})_{st}$ be their respective relative intensities and $(\alpha_X)_{st}$ be the conversion coefficient. Using the tables of theoretical values of α_X, $(\alpha_X)_{st}$ can be obtained by interpolation. Then the experimental internal conversion coefficient for any other transition may be calculated from

$$\alpha_{X'} = \frac{I_{eX'}}{I_\gamma} \frac{(I_\gamma)_{st}}{(I_{eX})_{st}} (\alpha_X)_{st} \qquad (101)$$

where $I_{eX'}$ and I_γ are the relative intensities of the pair.

After a K-orbit electron is internally converted, the unoccupied orbit must be filled up eventually. This is done by dropping another electron from a free or bound state down to the K-orbit. The radiation thus released is called the K x-ray. Therefore, a knowledge of the K x-ray intensity together with the gamma intensity offers a method of absolute determination of the internal conversion coefficients [32]. However, not all K-shell vacancies are filled by emission of K x-rays. A small fraction of the events goes through a different channel. The energy released, instead of in the form of a K x-photon, may be used to eject another electron from a higher orbit, thus emitting a so-called Auger electron. The fraction of the events

going through the x-ray channel (known as the fluorescent yield) is a constant for a given atom and can be evaluated.

There are, of course, other x-rays, L,M,N, etc., but they are much lower in energy and intensity.

In Chapter 4, we have described pair production in a detector. The process of internal pair production follows the same principle as the process of internal conversion. The basic difference is that in the second case, the nuclear energy is transferred directly to a bound atomic electron, while in the first process, the energy is transferred to an electron in a 'negative energy' state. However, similar to the internal conversion coefficients, the emission rate of the internal pair production is also expressed in ratio with that of the gamma photons, and is known as the pair production coefficients, $\pi(L)$. For transition energies exceeding several Mev, this process should be taken into acccunt. However, the transition energies in the present investigation are all below 2 Mev, and the corresponding $\pi(L)$ are less than 5×10^{-4} [60] . Hence, they are within the experimental error and can be neglected. For an energy less than 1.022 Mev, such processes cannot even occur.

§3. The Beta Spectrometer.

An intermediate image beta spectrometer (also known as a double-lens spectrometer) was used in the present work. As shown in figure 18, it consists of two water-cooled magnetic lenses, a cylindrical vacuum chamber, baffles A,B,C, and externally adjustable holders for the source and the detector. The magnetic lenses, as the name implies, focus the beta particles with an appropriate momentum from the source onto the detector. The appropriate momentum referred to is directly proportional to the magnetic field strength in the vacuum chamber, which is in turn proportional to the current in the lenses, The current was supplied by a 150 volt d.c. generator and controlled by a current regulator. The latter consists of two trays of 6AS7 triodes, a standard resistor of low temperature coefficient and a feedback bias control system (figure 19) with a high precision potentiometer for varying the d.c. current. Thus the momenta of the beta particles can be expressed in terms of the potentiometer setting.

To avoid the effect of the earth magnetic field, the spectrometer was placed with its axis along the magnetic meridian and between two compensating coils to reduce the vertical component of the field.

The source position together with that of baffle A can be varied in the plane perpendicular to the chamber axis by

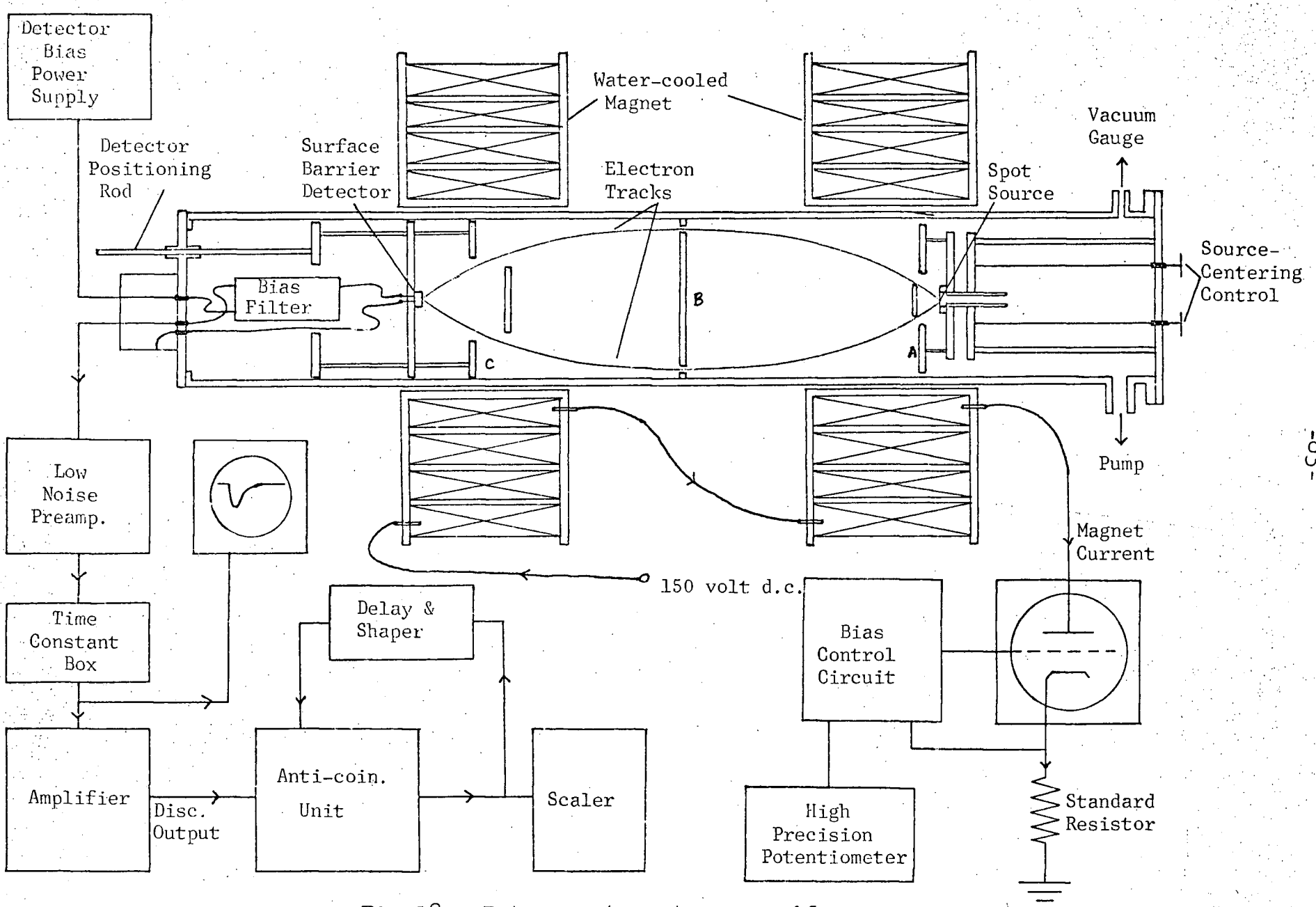

Fig.18 Beta spectrometer assembly.

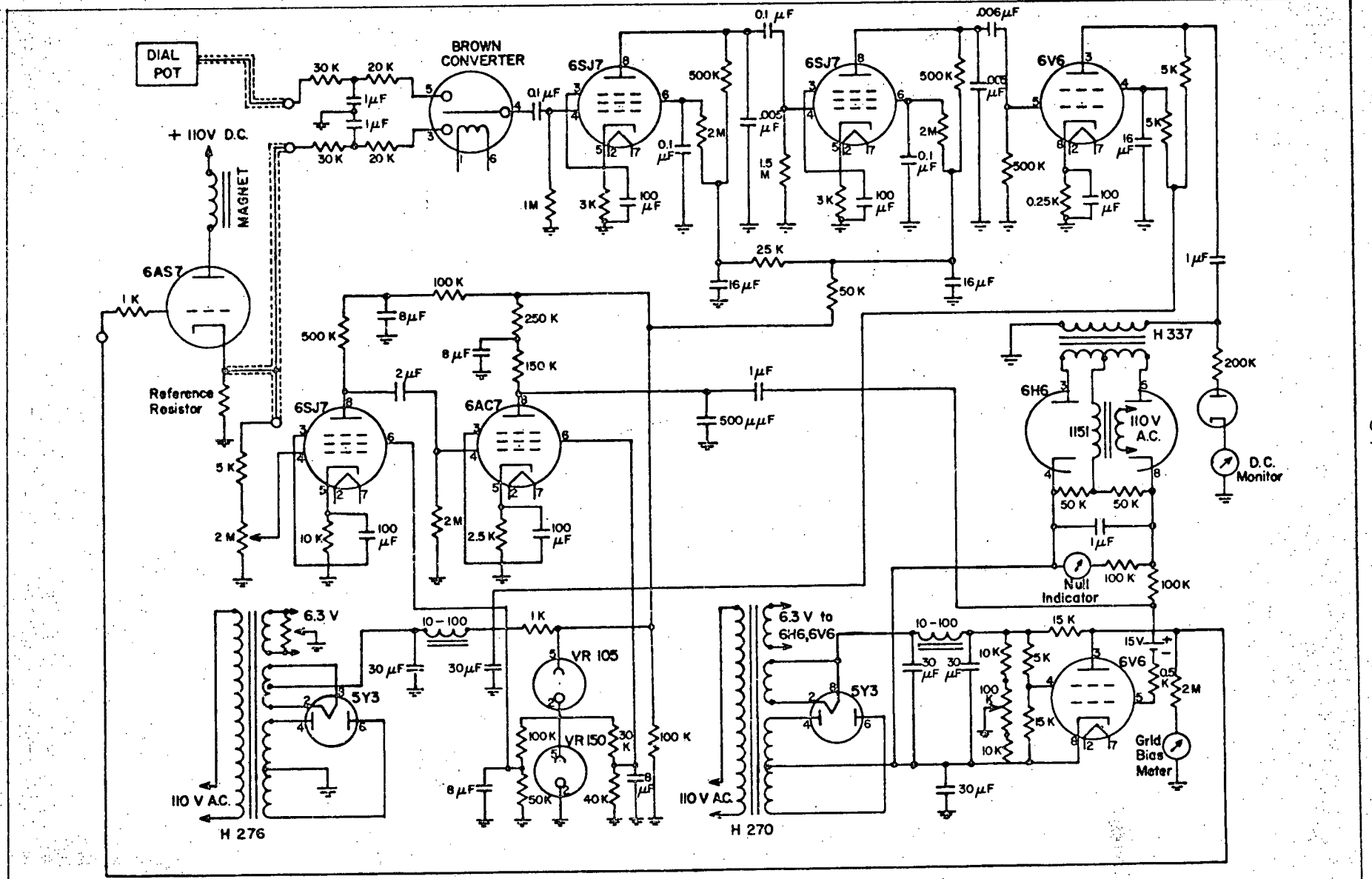

Fig.19 Magnet current control circuit

means of the two centering dials, while the detector is movable along the chamber axis by the positioning rod. The annular slit in baffle A defines the initial angle of the beta tracks and limits the beta intensity to the detector. The central baffle B controls the momentum spread of the passing beta particles. The detector baffle C protects the detector from those betas not following the proper paths. The resolution of this spectrometer depends on the curvature of the beta tracks and on the d.c. current stability. The former is determined by magnetic field strength, and the latter, by the sensitivity of the current regulator.

The detector mentioned above is a thin surface barrier type with surface diameter of 1cm. The use of this type of detector in the present case is particularly advantageous if one compares it with the conventional scintillators or gas-filled counters. Firstly, because of the thin depletion layer of the detector, it is practically insensitive to gamma radiation originating either in the source or in the background. Therefore, no lead shielding in the chamber is necessary. Secondly, the surface barrier detector is unaffected by the magnetic field in the chamber, whereas in the case of a photomultiplier which must accompany a scintillator, the presence of this strong field would be intolerable. The signal output of the

detector is, however, relatively small. Therefore, a low-noise preamplifier with a time constant box was required to increase the peak-to-noise ratio.

The introduction of an anti-coincidence unit and a feedback device shown in figure 18 was only for the sake of minimizing the effect of noisy surroundings. Sudden bursts of pulses occasionally were observed in the monitor oscilloscope. Each of these bursts of pulses, after entering the anti-coincidence unit, were reduced to just one leading pulse. Consequently, the effect became insignificant when considering the higher beta counting rate. The delay and shaper unit produced the required blocking pulse for the anti-coincidence unit.

§4. Preparation of Beta Sources.

The preparation of a spot source for beta spectroscopy with minimum possible source scattering but with maximum possible radioactive strength is a challenging task. Several methods have been tried by previous workers, such as vacuum evaporation, molecular deposition, electrostatic spraying, electroplating, liquid drop deposition etc [61)-64)]. Each method has its own advantages and disadvantages. But by far, the liquid drop deposition method is the simplest and most

frequently used among them all. It has the disadvantages of limited strength and comparatively poor surface uniformity. But, in addition to being easy to prepare, it accepts almost any kind of thin backing. Therefore, having tried some other methods without satisfactory results, this method was finally chosen.

Before starting the source preparation, a thin backing had to be prepared first. Vinyl films were selected for this purpose. About 10 gms. ofBakelite vinyl resin powder (called VYNS) were mixed with 100 ml. of cyclohexanone solution in a bottle and stirred until most of the powder had dissolved. It was left for a few days with occasional stirring. When all the powder had disappeared, a small quantity of the solution was diluted by an equal amount of cyclohexanone on a watch glass. By using a glass rod, a drop of the solution was introduced to the surface of a tray of clean water. The solution quickly spread into a tough thin film. The uniform part(judging from the reflecting colours) was picked up by a copper wire loop and placed on an aluminium ring. The film thus prepared was estimated to be less than 10 $\mu g/cm^2$ thick. When the film was dry, a trace of aluminium was evaporated in vacuum onto the film to serve as a charge conducting layer. Great care was taken not to overheat the film during evaporation. Several

backings were prepared in this way.

To prepare the source, a small glass jet with a clean and plane-cut nozzle was connected to a system such that the internal pressure of the jet could be varied conveniently. A tiny quantity of the chloride solution of Eu 154 with suitable concentration was sucked into the jet. A source backing was then placed under the nozzle on an adjustable base. By carefully controlling the pressure, a small well-defined spot source could be deposited onto the centre of the vinyl film. This was done with repeated trials, and a fairly intense and uniform source was finally obtained. The source was then dried in a desiccator (since Europium Chloride is a hygroscopic compound). Then a very dilute solution of collodion in dry ether was prepared, and a drop of it was introduced onto the surface of the dried source to protect the source from flaking off. The source was again replaced in the desiccator, ready to be mounted in the vacuum chamber.

§5. Experimental Procedures.

Preliminary adjustments to the spectrometer consisted of changing baffles, and repeated variation of the source and detector positions as well as the orientation of the chamber, until optimum intensity with best possible resolution was obtained. A beta source of Cs 137 was used for this purpose.

Details of the adjustments and calibration of the spectrometer are given in ref. 65. The best resolution achieved was 0.7 % in terms of potentiometer setting or momenta with 0.96% transmission.

The Cs 137 source was then replaced by a beta source of Eu 154 chosen from among those prepared, and the chamber was continuously pumped down to keep away the water vapour. (Unfortunately, in the later runs, because of repeated removal and replacement of the source, a small quantity of water vapour was absorbed by the source and trapped in the collodion film. This caused deterioration of resolution in the low energy portion of the spectrum, but did not affect the higher energy part.)

In each run of the experiment, the pressure of the chamber was kept at about 10^{-6} mm. of Hg. The potentiometer reference voltage was calibrated against a standard cell every five or ten minutes. The shape of the output pulses from the time constant box was observed constantly with an oscilloscope. The counting time for each potentiometer setting varied from half a minute to eight minutes depending on the counting rate. One section of the spectrum was taken each time with repeated runs, until enough counts were accumulated such that the statistics for each data point was within the

required limits (i.e. 1 % for the energy continuum and less for the peaks).

Three experiments have been performed at different periods of time. The first two experiments were mainly concerned with the internal conversion peaks. A typical spectrum was plotted out in two portions as shown in figures 20a,b. The third experiment was designed to investigate the beta continuum near the high energy end. In this experiment, a stronger beta source was used to obtain a greater counting rate and better statistics. The spectrometer was set up to use a larger source-detector distance and smaller initial trajectory angles. This was necessary in order to reach energies near the end point of the Eu 154 spectrum with the maximum available magnetic current. The spectrum for the beta continuum was shown in figure 20c.(Note that the counts are divided by the momentum.)

§6. Results and Analysis.

The beta spectrum shown plotted in figures 20a,b in the previous section was obtained after all short-lived peaks had decayed to negligible size. They were plotted in logarithmic values in order to show as much as possible of the features of all the conversion peaks.

Since the beta spectrometer was first calibrated using a Cs 137 source, the energy correspondence of each potentiometer

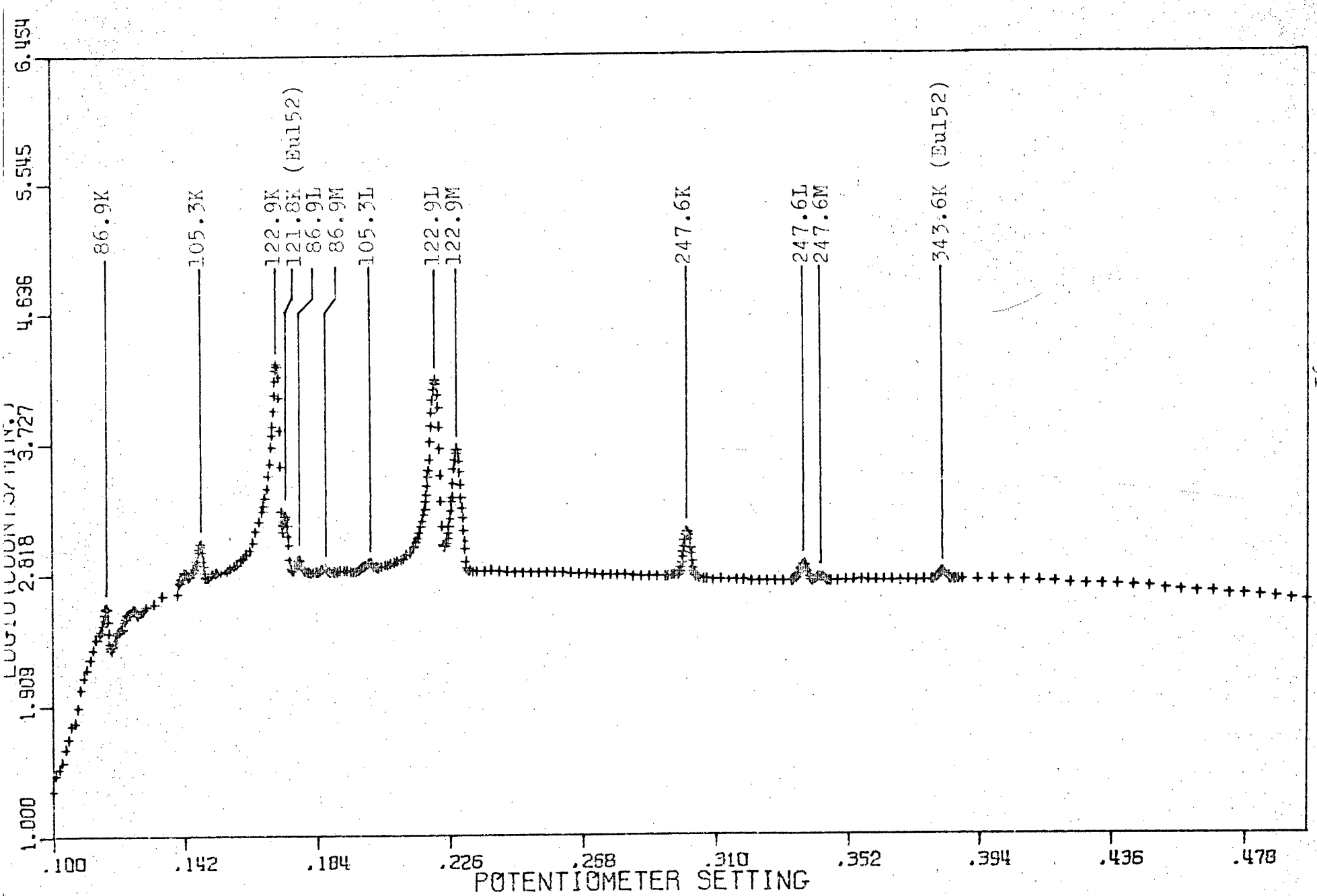

Fig.20a Beta spectrum of Eu 154, low-energy part.

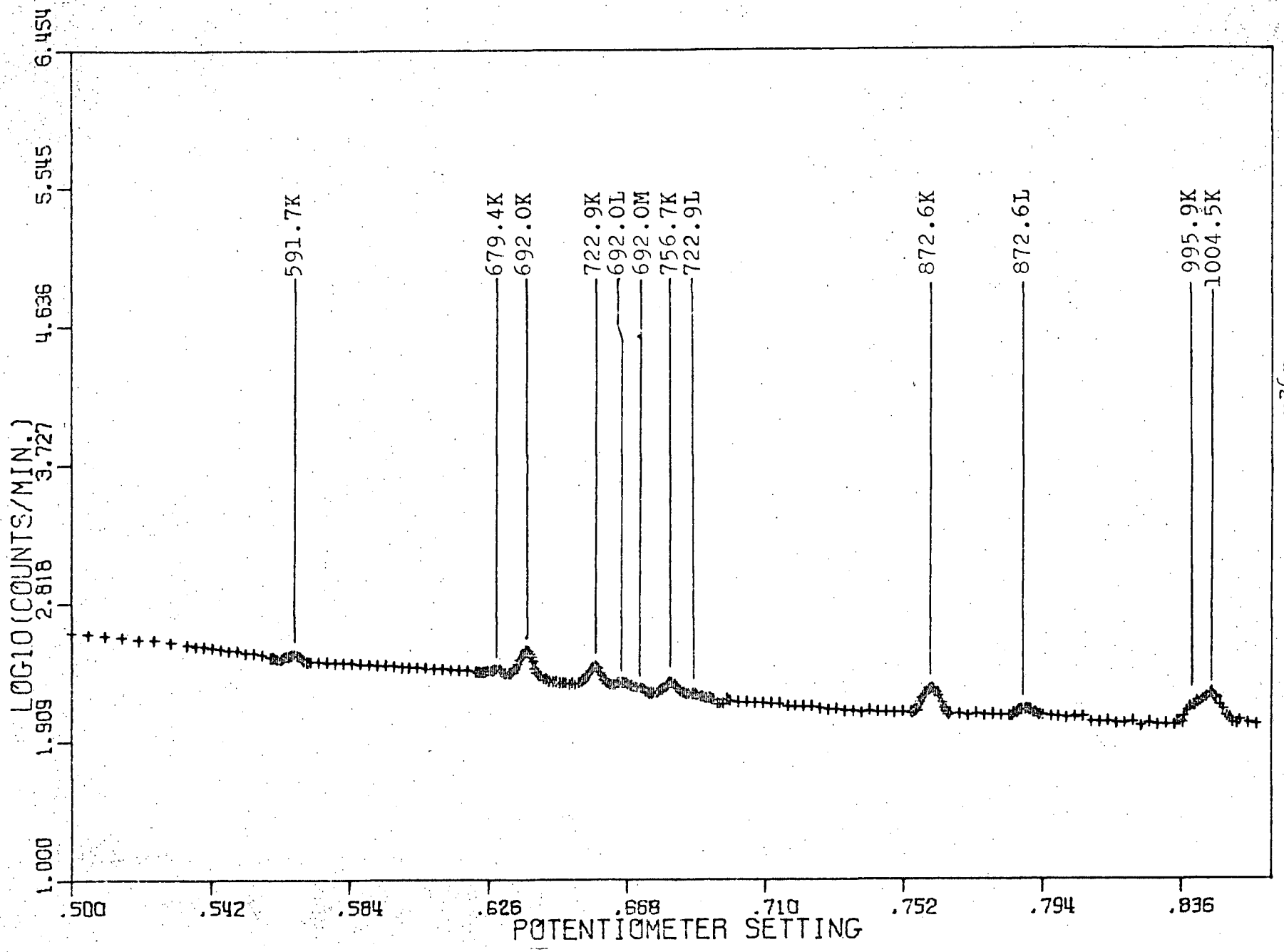

Fig.20b Beta spectrum of Eu 154, high-energy part.

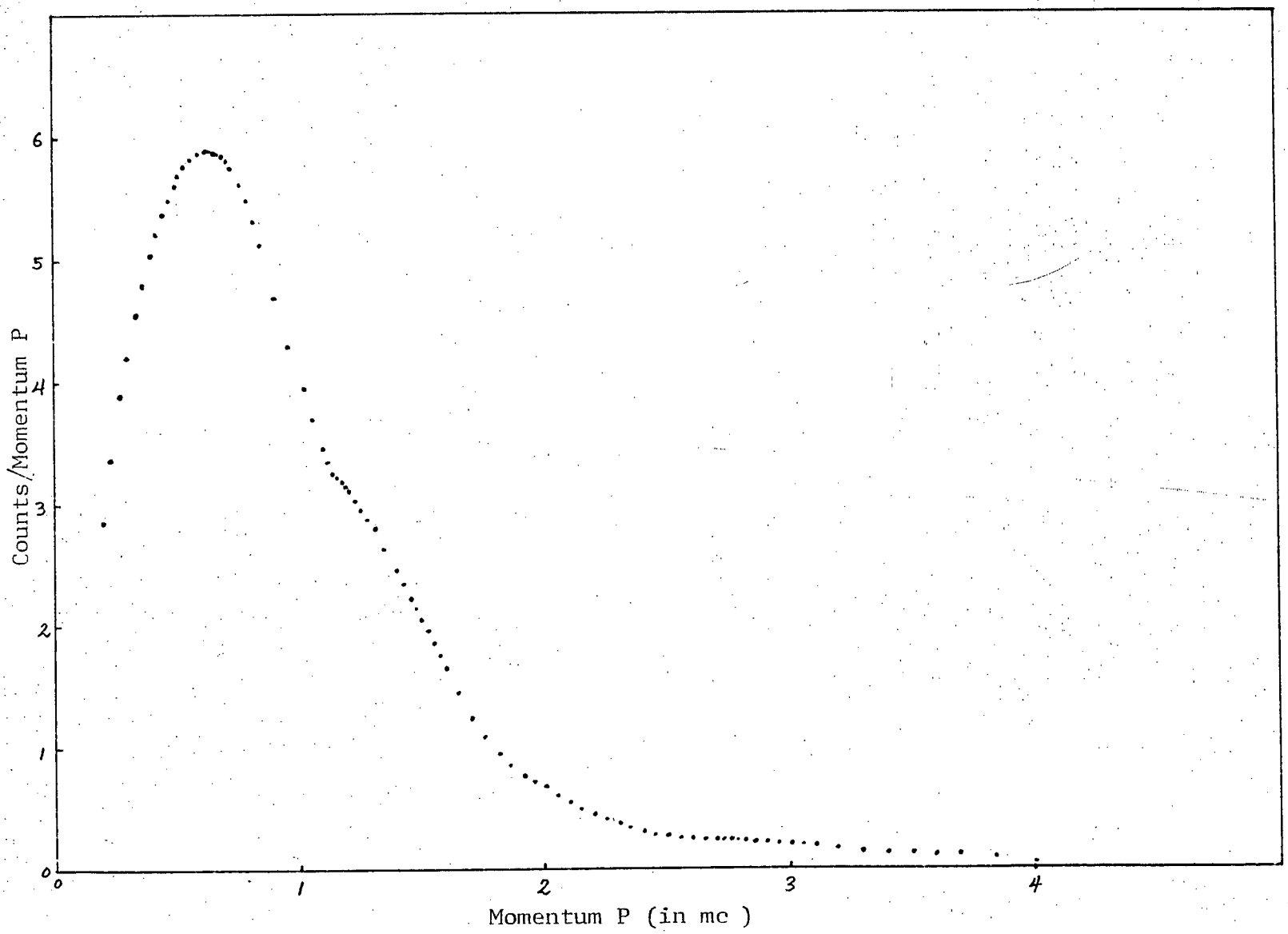

Fig.20c Continuum for beta transitions of Eu 154.

setting was roughly known. Hence, the conspicuous conversion peaks in the Eu 154 spectrum were soon recognized. The 722.90K conversion peak was then selected as a standard to calibrate the electron energies of all the other conversion peaks. The intensity measurement was done by estimating the area under each peak in an enlarged linear plot after the continuum was subbracted, and then dividing the area by the momentum or potentiometer setting at that peak. The full width at half maximum was also determined graphically in each case. The particulars for the conversion peaks are presented in table V.*

Figure 20a shows that the lower portion of the beta spectrum is dominated by the 122.9 Kev conversion peaks. The the asymmetry of the peak shape indicates slight source scattering in this energy range. The tails at the lower energy side of these strong peaks did interfere with the intensity measurement of the weaker peaks between them as well as the beta continuum beneath them. However, source scattering begins to

---

* Column 1 of the table gives the energies of the transitions as determined by the gamma-ray measurements together with the atomic shells. Column 5 gives the transition energies calculated by adding Column 2 to the appropriate shell binding energies B_X (i.e. B_K = 50.22 Kev etc for Eu 154, and B_K = 46.85 etc for Eu 152). Column 6 compares the transition energies from gamma and conversion electron data.

Peak Name (from γ)	Electron Energy (Kev)	Relative Intensity	FWHM (%)	Trans. Energy (Kev)	γ-energy Deviation (%)
86.9K	37.28	---	1.4	87.5	0.69
105.3K	54.54	10.5 ±0.4	1.21	104.8	0.48
122.9K	72.49	260.0±2.6	1.0	122.7	0.16
121.8K	74.6	10.7 ±2.1	1.0	121.5	0.25
86.9L	77.85	1.90 ±0.22	1.0	85.7	1.4
86.9M	83.05	0.37 ±0.08	1.0	84.6	2.6
105.3L	96.18	1.21 ±0.25	1.45	104.0	1.2
122.9L	115.20	170.3±3.5	1.0	123.0	0.081
122.9M	121.30	48.8 ±1.8	1.0	122.8	0.081
247.6K	196.56	5.71 ±0.12	0.7	246.8	0.32
247.6L	239.33	1.46 ±0.15	0.77	247.2	0.16
247.6M	245.78	0.30 ±o.03	0.74	247.3	0.12
343.6K	293.94	0.58 ±0.02	0.67	340.8	0.82
591.7K	540.57	0.26 ±0.03	0.78	590.8	0.15
679.4K	629.2	0.135±0.014	0.73	679.4	--
692.0K	642.1	0.839±0.017	0.67	692.3	0.04
722.9K	672.68	0.477±0.019	0.66	722.9	0.
692.0L	684.5	0.127±0.025	0.80	692.3	0.04
692.0M	690.9	0.097±0.019	0.80	692.4	0.058
756.7K	706.57	0.238±0.020	0.67	756.8	0.013
722.9L	718.0	0.048±0.010	0.67	725.8	0.40
872.6K	824.0	0.408±0.018	0.70	874.2	0.18
872.6L	868.0	0.084±0.017	0.67	875.8	0.37
995.9K	945.0	0.234±0.047	0.71	995.2	0.07
1004.5K	953.2	0.393±0.080	0.66	1003.4	0.11
1274.4K	1227.9	0.259 ± 0.070	1.64	1278.1	0.29

Table V Data of β Conversion Peaks in figures 20a,b, (Explanation given in the foot note *, p. 94).

disappear when the energy is above 121.30 Kev (i.e. above the 122.9M peak), and all the conversion peaks having energies greater than this are fairly symmetrical. This can also be seen from the values of the FWHM presented in table V. The intensity of the 86.9K peak could not be estimated, because it is barely above the noise level and the tail due to scattering certainly extends below the discrimintor level of the amplifier. The two humps between the 86.9K and 105.3K peaks are suspected to be Auger electron lines but have not been positively identified. It is interesting to note that the 121.8K peak belonging to Eu 152 impurity is separated from the 122.9K peak of Eu 154, and that the former is only 4.12 % of the latter. Since these peaks are respectively the strongest peaks in Eu 152 and Eu 154, the percentage ratio was made use of in calculating all the other Eu152 peak intensities present in the spectrum. For example, the intensity of the 244.7K of Eu152 expected to be present in the 247.6K peak of Eu 154 was calculated. This intensity was subtracted from that of the latter peak in order to find the experimental value for the internal conversion coefficient. The procedure was also applied to the gamma peaks 122.93 Kev and 247.63 Kev as mentioned previously.

From figure 20b, the main interest lies in the group of peaks from 679.4K to 722.9L shown in an expanded scale

in figure 20d. According to Hamilton et al [36], two conversion peaks namely 678K and 682K were found lying close to each other. In this spectrum, we only found a single peak labelled 679.4K and FWHM of 0.73 %. If there are in fact two peaks as reported, the peak width would have been much larger than those of the neighbouring peaks. This is not the case. Further discussion will be given in the next chapter. The next point that needs to be mentioned is that we have not found any gamma or beta conversion peak corresponding to the 626 Kev transition given in the same reference. Finally, it should be noted that the 1274.4K peak given in table V was not included in the figures 20a,b,d, because this peak was obtained in the third run of the beta experiments, while the above figures were from the second run.

From the last column of table V, the agreement for the K peaks of Eu 154 is good. The relative intensities in the same table have not been corrected for the Eu 152 impurity. The correction was done later only for the K peaks in order to find the K-conversion coefficients.

To find the K-conversion coefficients, the 122.93 Kev transition, which was considered to be purely E2, was chosen as the standard. From the intensity data given in tables III and V, and the table of Sliv et al [58], we have from equation (101),

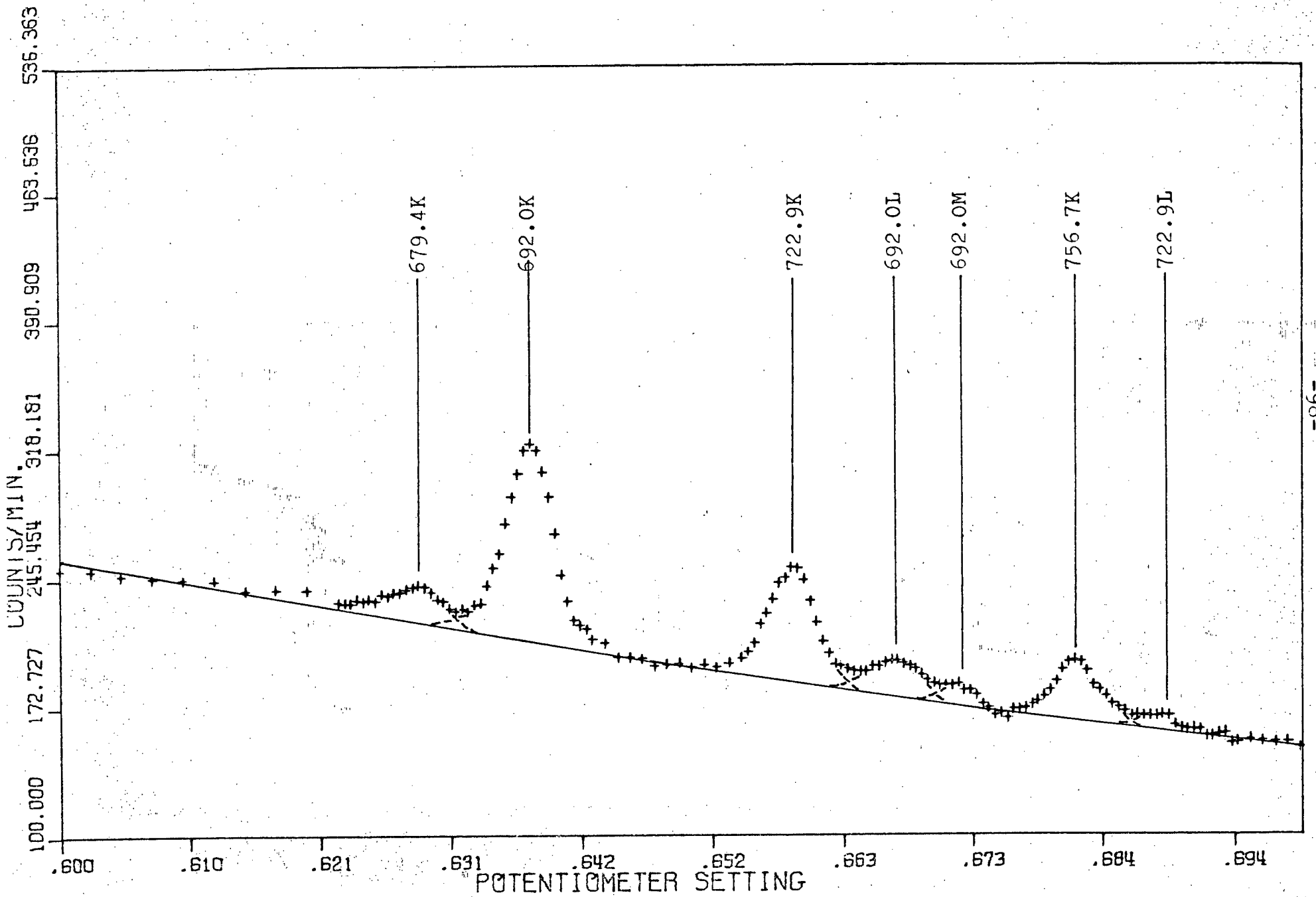

Fig.20d Expanded portion of Eu 154 beta spectrum.

$X = K$

$(I_\gamma)_{st} = 100.00$ (from Table III)

$(I_{eK})_{st} = 260.0$ (from Table V)

$(\alpha_K)_{st} = 0.652$ (E2 conversion-122.9 Kev)

With these values and equation (101), the experimental K-conversion coefficients were calculated, and are listed in Table VI together with the theoretical values for E1, M1, and E2 transitions.

The data in Table VI confirms the expected E2 nature of all but one of the transitions between positive parity states. The one exception is the transition of energy 692 Kev, which has a conversion coefficient ten times the theoretical E2 value. This suggests an E0 component. The magnitude of this component (calculated on the assumption that the E2 conversion coefficient is indeed 0.0052) is approximately 6 percent of the total E0 + E2 transition probability. The 591.7 Kev gamma-ray has an α_K whose limits of uncertainty do not quite encompass the theoretical E2 value, although M1 and E1 can be ruled out. This conversion peak received a lot of attention experimentally, and many counts were accumulated in an effort to attain good statistics. It is possible of course, that the error limits were somewhat underestimated.

The 722.9 Kev and the 1274.4 Kev transitions both involve negative parity levels, and are most probably E1, assignments that are consistent with the decay scheme shown in Figure 22. The 105.3 Kev transition has not been fitted into the decay scheme, but it appears also to be E1.

Peak Name	K- Internal Conversion Coefficients			
	Experimental	(E2)	(M1)	(E1)
105.3K	0.272 ± 0.033	1.002	1.469	0.216
122.9K	0.652 ± 0.022	0.652	0.941	0.142
247.6K	0.085 ± 0.006	0.0815	0.135	0.0218
591.7K	0.0065± 0.0011	0.00803	0.0140	0.00281
692.0K	0.056 ± 0.0055	0.00519	0.00954	0.00201
722.9K	0.00254±0.00021	0.00471	0.00857	0.00183
756.7K	0.0058 ±0.0010	0.00426	0.00766	0.00167
872.6K	0.00347±0.00031	0.00314	0.00542	0.00127
995.9K	0.00238±0.00058	0.00238	0.00395	0.000988
1004.5K	0.00225±0.00056	0.00234	0.00388	0.000971
1274.4K	0.00071±0.00023	0.00145	0.00219	0.000631

Table VI Comparison of K-Internal Conversion Coefficients with the Theoretical Values for E1, M1, and E2 transitions taken from reference (58).

The analysis on the beta continuum was done by using Kurie-plot method (see figure 21), and the results are presented in table VII. (For details of the analysis, see reference 65.)

Beta Energy (Mev)	Transition Intensity (%)
1.866 ± .012	10.8 ± 0.12
1.198 ± .060	0.67 ± 0.49
0.976 ± .030	4.6 ± 3.8
0.843 ± .015	17.0 ± 3.9
0.579 ± .005	37.8 ± 3.5
0.274 ± .010	29.1 ± 2.5

Table VII. Energies and relative intensities of the beta transitions.

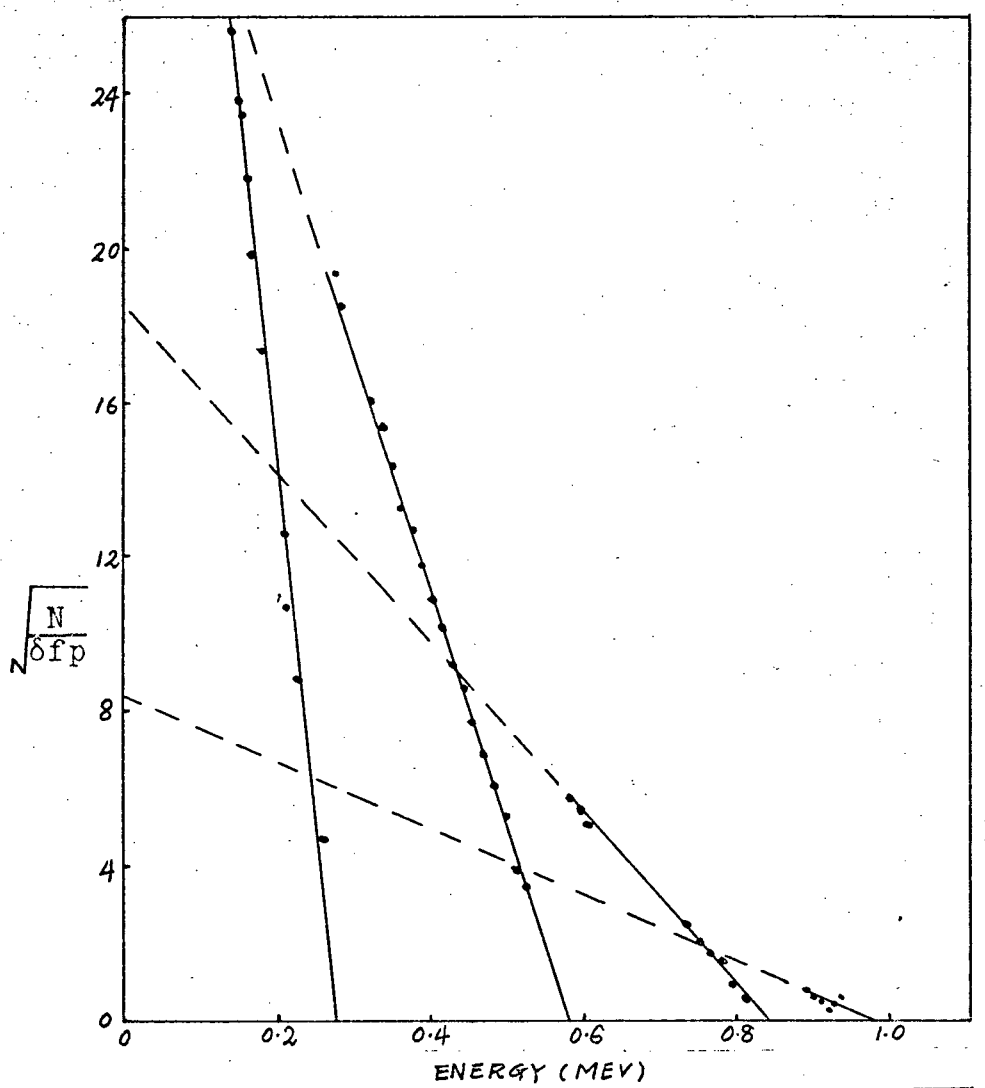

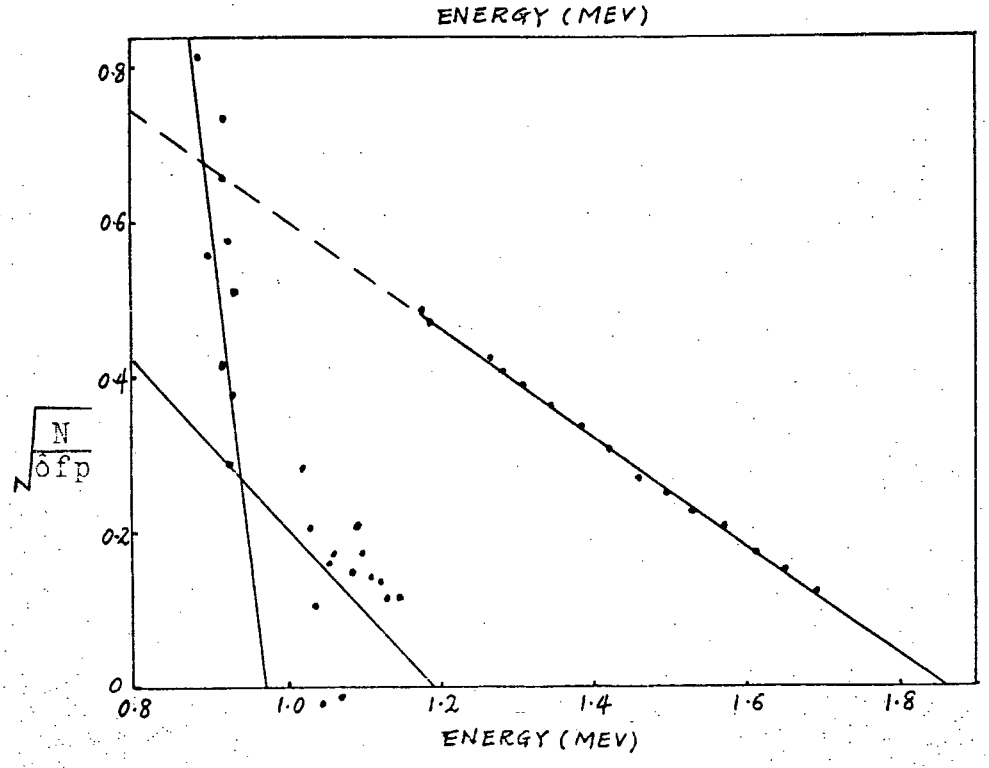

Fig. 102

The Kurie plots

N=counts/min.
p=momentum(mc)
f=reduced Fermi function
δ=correction factor (see ref. 55)

CHAPTER VII

THE DECAY SCHEME AND MODEL FITTING

§1. The Decay Scheme.

Summing all the results obtained so far from the beta- and gamma-spectroscopic work as well as the gamma-gamma coincidence investigation described in the previous three chapters, the decay scheme of Eu 154 to Gd 154 was constructed, and the excited states of Gd 154 resulting from this decay areshown in figure 22. The relative input and output transitional intensities with respect to each level are provided in table VIII.

The level structure presented in the figure is as a whole in agreement with those constructed by the previous workers, in particular by Hamilton et al [36], although there are important differences. In general, there is a marked improvement in the accuracy of the level energies, which can be easily perceived from the fact that all the experimentally determined values for the gamma transitional energies fit into the decay scheme with energy deviations less than 1 Kev.

The two new weak transitions discovered, i.e. 903.60 Kev and 582.11 Kev, were assigned to the transitions from the levels 1718.80 Kev and 1397.36 Kev to the level 814.77 Kev respectively. (These levels were all assigned from other more

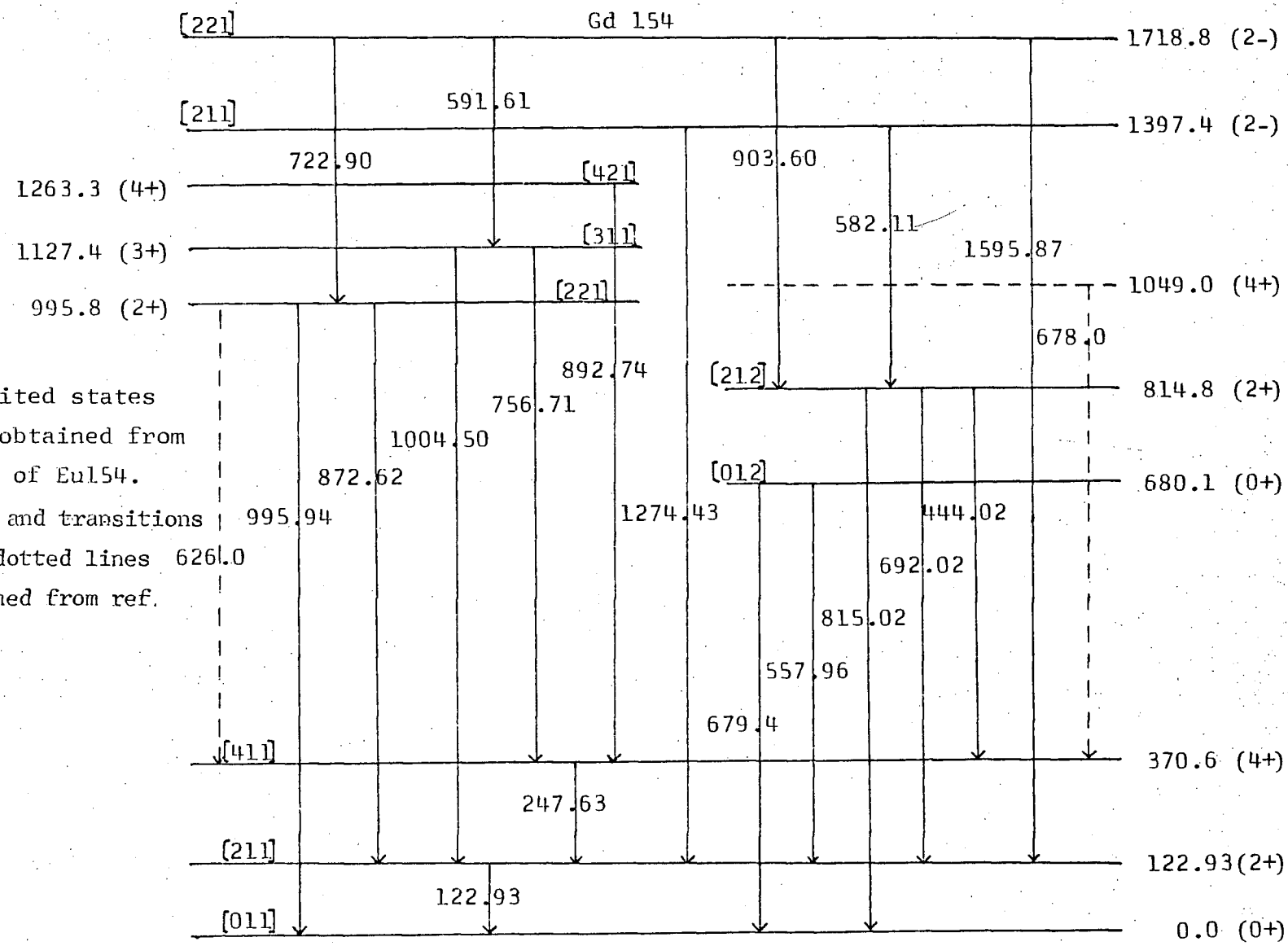

Fig.22 The excited states of Gd154 obtained from the decay of Eu154. (The level and transitions given in dotted lines are obtained from ref. 36.)

Level Name (Kev)	Transitional Intensities (Relative)			
	Input γ + C.E.	Output γ + C.E.	Difference (in %)	Beta from Continuum (%)
$[212]^-$ 1718.8	---	64.72±3.06	64.72±3.06 (26.33%)	29.1±2.5
$[211]^-$ 1397.4	---	93.80±4.30	93.80±4.30 (38.10%)	37.8±3.5
$[421]^+$ 1263.3	---	1.23 ±0.20	1.23±0.20 (0.50%)	---
$[311]^+$ 1127.4	10.58+0.55	54.31±2.04	43.73±2.59 (17.80%)	17.0±3.9
$[221]^+$ 995.8	47.43+2.06	54.25±2.50	6.82±4.56 (2.77%)	4.6±3.8
$[411]^+$ 370.6	13.75+0.95	17.73±0.80	3.98±1.75 (1.65%)	---
$[211]^+$ 122.93	192.85+8.93	220.0±4.44	27.15±13.37 (11.07%)	10.8±0.12
$[212]^+$ 814.8	3.77+0.39	6.98±0.88	3.21±1.27 (1.31%)	0.67±0.49
$[012]^+$ 680.10	0.0	0.90±0.17	0.90±0.17 (0.37%)	---

Table VIII Transitional intensities for gammas, conversion electrons and betas. Level name notation, $[LNn]^{\pi}$.

intense gamma-rays.) The energy deviations are less than ½ Kev. This energy agreement is excellent. In addition, these transitions are predicted to have no change of angular momentum but only a change of parity (E1?). For these, the beta conversion peaks should be much weaker in intensity than the gamma peaks. This is the case in the present investigation. Although the gamma transitions have been detected, none of the conversion peaks have been found. From the low output intensity of the level 814.77 Kev given in table VIII, it is obvious that these two transitions are necessarily weak, which is the reason that they have not been observed before. Consequently, these two transitions contribute the major portion of the population of the level 814.77 Kev.

Hamilton et al [36] suggested a level of 1049 Kev on the basis only of the existence of the 678K beta conversion peak. In the present work, no such peak was found either in the beta conversion spectrum or in the gamma spectrum. Also we can find no other transition from this level to any other level or vice versa. Although the 1049 Kev level was well-established in the decay of Tb 154 to Gd 154 [33], we have reasons to doubt its presence in the decay of Eu 154. On the other hand, another 4+ level of energy 1263.3 Kev was found due to the presence of 892.74 Kev gamma transition.

As will be seen in the next section, this level was predicted by the Asymmetric Rotator Model. The last point of difference from the scheme of Hamilton et al [36] is the absence of the 626 Kev transition.

In table VIII, the sum of transitional intensities of gammas plus conversion electrons to and from each level were given. After allowing for the experimental error, the difference should be contributed by a beta transition from the ground state of Eu 154 to that level. These differences are also expressed in percentage so as to compare them with the experimental values for the beta transitions given in the last column. The result of this comparison shows clearly that all the data are quite consistent.

§2. Model Fitting.

The theory for calculating the gamma transitional energies and the reduced transition probabilities base on the Asymmetric Rotator Model was given in Chapter 2. To proceed to the actual calculation, we made use of five basic programs written by Davidson [41].

The first program calculates the matrix elements of the angular momentum components given explicitly as follows,

$$\langle LMK|\hat{L}_1^2|LMK'\rangle = \begin{cases} (L(L+1) - K^2)/2, & \text{for } K' = K \\ \frac{1}{4}\left[(L\mp K-1)(L\pm K)(L\pm K+1)(L\mp K+2)\right]^{\frac{1}{2}}, & \text{for } K'=K\pm 2 \end{cases}$$

$$\langle LMK|\hat{L}_2^2|LMK'\rangle = \begin{cases} (L(L+1) - K^2)/2, & \text{for } K' = K \\ -\frac{1}{4}\left[(L\mp K-1)(L\pm K)(L\pm K+1)(L\mp K+2)\right]^{\frac{1}{2}}, & \text{for } K'=K\pm 2 \end{cases}$$

$$\langle LMK|\hat{L}_3^2|LMK'\rangle = K^2\delta_{KK'}$$

and thus calculates the matrix elements of the rotational Hamiltonian (see equation (27)) for a given γ. Then, the latter matrix is diagonalized by using the Jacobian method. The eigenvalues $\varepsilon_N(L)$ as well as the coefficients C_K are found in this way.

The second program solves equation (38) for a given μ by iteration process and calculates Z_1 from equation (39). The quantum number ν_1 is available in tabular form [41] by linear interpolation. Hence, the theoretical ratios of each state in the ground state rotational band to the first 2^+ level energy (E_{211}) are calculated by means of equation (44)

and (44a).

The third program is the same as the second except that the quantum number is replaced by ν_2, which is obtained from another table [41]. This gives the energies of the first excited beta band.

The fourth program just calculates the rotational part of the E2 transition probabilities. This is done by using equation (59) with the coefficients C_K^{LN} and γ known and with a Clebsch-Gordan Coefficients subroutine.

The last program then calculates the vibrational part of the probability. This program contains all the subroutines necessary for solving equations (68) and (69). Note that the integration in (68) is done by dividing the integral range into 20 increments.

All the above programs apply to the quadrupole case ($\lambda = 2$) and the octupole case ($\lambda = 3$).

In the present calculation, the first three programs were combined together to yield all the level energies for a given pair of γ and μ. The experimental values of all the level energies are also read in. The root-mean-square deviation of the calculated level energies from the experimental ones is found in percentage form. In this calculation, those levels having no experimental correspondence are omitted. Then the two parameters γ and μ are varied within suitable ranges which enclose a minimum root-mean-square deviation of the

level energies. Finally, this minimum is determined by iteration, and so also the corresponding level energies. By applying the last two programs, the ratios of the reduced transition probabilities are also found. The results of the energy fittings in the quadrupole case are presented in table IX. The root-mean-square deviation in this case is defined as follows,

$$D_{RMS} = \frac{\left[\sum (E^{Th}_{LNn} - E^{Exp}_{LNn})^2\right]^{\frac{1}{2}}}{\sum E^{Th}_{LNn}} \qquad (102)$$

where the summations are carried out over the last six energy levels in table IX, E^{Exp}_{LNn} are the experimental level energies (in Kev) determined, and

$$E^{Th}_{LNn} = \frac{E_{LNn} - E_{011}}{E_{211} - E_{011}} (E^{Exp}_{211} - E^{Exp}_{011}) + E^{Th}_{011} , \qquad (103)$$

the fitted theoretical level energies. Note that the E_{LNn} are in an arbitrary energy scale, and that the equation (103) is obtained under the restriction of $E^{Th}_{011} = E^{Exp}_{011}$ and $E^{Th}_{211} = E^{Exp}_{211}$. The purpose of this restriction is to obtain the same energy scale for both E^{Th}_{LNn} and E^{Exp}_{LNn}. It should also be mentioned that this method of fitting is different from the standard least square fit. We believe that the application of the latter method will meet with great computational difficulties.

The RMS deviation D_{RMS} resulting from the values in table IX is 1.503 per cent, and the corresponding values for the asymmetry parameter γ and the stiffness μ are respectively 11.52 degrees and 0.402.

Similar (unpublished) calculations have been done by Davidson[67] using another set of experimental data. The results

To follow page 110.

obtained for γ and μ are 11.62 degrees and 0.401 respectively, in good agreement with ours. A very recent publication by Aisenberg et al[68] using the method of Davydov and Chaban[12] gives γ = 11.5 and μ = 0.8. The experimental data in this publication have been determined by Yoshizawa et al[34] by means of Coulomb excitation.

Experimental Energy E^{Exp}_{LNn} (Kev)	Theoretical Energy E^{Th}_{LNn} (Kev)	Deviation (%)	L N n
0.00	0.00	---	0 1 1
122.93	122.93	---	2 1 1
995.75	1052.73	5.41	2 2 1
1127.35	1121.31	0.54	3 1 1
370.56	365.54	1.37	4 1 1
1263.30	1211.96	4.24	4 2 1
680.10	676.49	0.53	0 1 2
814.77	831.85	2.05	2 1 2

Table IX Comparison of the experimental and theoretical energies in the quadrupole case (λ=2, positive parity).

To find the ratios of the reduced transition probabilities from the experimental data, we made use of equation (51). Only four ratios were calculated, each of which consists of two transitions from the same initial state to different levels of the ground state beta band. Assuming all these transitions are E2, then from equation (51), $\ell = 2$; and hence

$$\frac{B(E2, L_i \rightarrow L_{f1})}{B(E2, L_i \rightarrow L_{f2})} = \frac{(E_{\gamma 2})^5}{(E_{\gamma 1})^5} \frac{T_1(E2)}{T_2(E2)}$$

where $E_\gamma = \hbar\omega$, the gamma energy. Substituting the experimental relative intensities for T_1 and T_2 and the corresponding gamma energies, the ratios $\frac{B(E2, L_i \rightarrow L_{f1})}{B(E2, L_i \rightarrow Lf2)}$ were found as below in table X together with the theoretical values.

Energy Ratio	Name	Expt. Value	Theo. Value
$\frac{995.94}{872.62}$	$\frac{[221] \rightarrow [011]}{[221] \rightarrow [211]}$	0.434±0.040	0.443
$\frac{444.02}{692.02}$	$\frac{[212] \rightarrow [411]}{[212] \rightarrow [211]}$	3.790±0.629	4.352
$\frac{815.02}{692.02}$	$\frac{[212] \rightarrow [011]}{[212] \rightarrow [211]}$	0.152±0.014	0.373
$\frac{1004.5}{756.71}$	$\frac{[311] \rightarrow [211]}{[311] \rightarrow [411]}$	1.026±0.104	1.004

Table X The branching ratios of gamma transitions between positive-parity levels.

Three of the four calculated ratios in Table X agree with the measured values within the experimental uncertainties. The third ratio 815/692 is less than half the value predicted. This suggests that if the 815 Kev transition is pure E2 which seems likely from the spin assignment of the levels involved, then the 692 Kev transition has a strong E0 component. The conversion coefficient data indicated this, but predicted that it was only 6 percent. To account for the low 815/692 ratio in Table X on this basis alone, the E0 component would have to equal about 60 percent of the total 692 Kev transition intensity.

The 692 Kev transition is involved in one other ratio, 444/692. While theory and experiment agree here within the error limits, the theoretical value is on the high side. If again this is caused by the 692 Kev E0 component, in this case it only requires it to be about 12 percent for the mean experimental value to match the theoretical prediction. So it is not likely that the low 815/692 ratio can be explained in this way.

For the octupole case, since we have only two negative parity levels (1718.8 and 1397.4 Kev) both with spin 2, we assigned them to be $[212]^-$ and $[211]^-$ respectively. With these quantum numbers, the asymmetry parameter γ'' and the stiffness μ'' were found to be 4.606 degrees and 0.49725. No gamma transition was found between them, although there are six transitions linking them to positive parity levels.

The monopole transition probability T(E0) for the transition ($0^+_\beta \rightarrow 0^+_{gnd}$) was calculated from equation (78). The

functions $I_{\nu'\nu}(0)$, $I_{\nu'\nu}(2)$, $I_{\nu'}(0)$ and $I_{\nu'}(2)$ were evaluated with Davidson's subroutines. The numerical values of the necessary parameters follow;-

$E = 0.55796$ Mev.

$\Omega = 0.335 \times 10^{11}$ sec^{-1} (ref.(45))

$\mu = 0.402158$

$P_{rot} = 0.964775$

$\beta_o = 0.303$ (ref.(16))

$Z = 2.53275$

$Z_1 = 2.56668$

$Z' = 2.64444$

$Z_1' = 2.75555$

$I_{\nu'}(0) = 1.7260$

$I_{\nu'}(2) = 1.7684$

$I_{\nu'\nu}(0) = 6.3418$

$I_{\nu'\nu}(2) = 1.5334$

From these data, $\frac{T(E0)}{T(E2)}\ (0^+_\beta \longrightarrow 0^+_{gnd}) = 0.085$ from (78)
$= 0.039 \pm 0.012$ (experimental)

It thus appears that the predictions of the Asymmetric Rotator model, while successful for the E2 ratios, are not reliable for monopole transitions.

We next programmed equation (78a) for the transition 692 Kev. The values of the parameters used were

$E = 0.69202$ Mev

$\Omega = 0.35 \times 10^{11}$ sec^{-1}

$\mu = 0.402158$

$P_{rot} = 0.2714$

$\beta_o = 0.303$

$Z = 2.6444$

$Z_1 = 2.7555$

$I_{\nu'\nu}(0) = 6.855$

$I_{\nu'\nu}(2) = 1.236$

Thence $\frac{T(E0)}{T(E2)}\ (2^+_\beta \longrightarrow 2^+_{gnd}) = 0.158$

from which the predicted E0 component is approximately 13 per cent of the total 692 transition. Assuming it is about twice too large (as above), it is consistent with the conversion data results.

CHAPTER VIII

CONCLUSIONS

The information deduced from the present experimental data as well as from that of the other workers leads to a fairly complete level structure of Gd 154 from the decay of Eu 154. The gamma transitions from one level to another have been exhaustively sorted out. Should there be any new gamma transitions, they must be extremely weak in intensity. It is not expected that there will be further modification to the energies of the levels to any appreciable extent. Because of the presence of some of the weaker transitions shown in table III, which apparently have no place in the decay scheme, it is hoped that new levels will be found in the future to include these transitions.

Comparison of the energies of the levels and the gamma transition probabilities with the theoretical values based on the Asymmetric Rotator Model demonstrates as a whole the validity of this model in the present chosen even-even nucleus (Gd 154). The close fits in most cases are remarkable. The error limit of the $0^+ \rightarrow 0^+$ monopole transition is relatively large. Experimentally, re-investigation

of the monopole transitions in this nucleus might be best carried out by means of Coulomb excitation, because the beta excited states in the present investigation are weakly populated. Thus the transition intensities were estimated with great difficulty.

As has been shown in the section on model fitting, (Chapter 7), the determination of the asymmetry parameter γ and the stiffness parameter μ involves the assignment of the theoretical energies of the two lowest energy levels to be equal to the corresponding experimentally determined energies. In this method, we have only two parameters (i.e. γ and μ) to vary in order to achieve a minimum RMS deviation. An alternative method would be to relax the condition of such an assignment. In consequence, two additional adjustible parameters would have to be varied in order to minimize the RMS deviation. Computation by this method would certainly be more complex. One could, of course, include the RMS values of the reduced transition probabilities in order to evaluate γ and μ. However, the uncertainty limits on these ratios are in general much larger than those of the level energies so that the accuracy of the method could be reduced over the present approach.

Finally, it is urgently to be hoped that the further development of this model of the nucleus will include the prediction of the transition probabilities between negative parity and positive parity levels. There are a sufficient

number of such transitions in even-even nuclei to make such calculations both interesting and useful.

REFERENCES

1. K. Siegbahn, Alpha-, Beta-and Gamma-ray Spectroscopy, p.557.
2. A. Bohr, Mat.Fys.Medd.Dan.Vid.Selsk 26, No.14 (1952).
3. J. Rainwater, Phys. Rev. 79, 432 (1950).
4. A. Faessler & W. Greiner, Z. Physik 168, 425 (1962).
5. A. Faessler & W. Greiner, Z. Physik 170, 105 (1962).
6. A. Faessler & W. Greiner, Z. Physik 177, 190 (1964).
7. A. Faessler, W. Greiner & R.K. Sheline, Physics Dept., Uni. Maryland, TR No. 345 (1963).
8. A. Faessler, W. Greiner & R.K. Sheline, Physics Dept.,Uni. Mary land, TR No. 372 (1964).
9. R.K. Sheline, Rev. Mod. Phys. 32, 1 (1960).
10. A.S. Davydov & G.F. Filippov, Nu. Phys. 8, 237 (1958).
11. A.S. Davydov & V.S. Rostovsky, Nu. Phys. 12, 58 (1959).
12. A.S. Davydov & A.A. Chaban, Nu. Phys. 20, 499 (1960).
12a. A.S. Davydov , Nu. Phys. 20, 682 (1961).
13. A.S. Davydov, V.S. Rostovsky & A.A. Chaban, Nu. Phys. 27, 134 (1961).
14. S.A. Williams & J.P. Davidson, Can. J. Phys. 40, 1423(1962).
15. J.P. Davidson & M.G. Davidson, Phys. Rev. 138, B316 (1964).
16. J.P. Davidson, Nu. Phys. 86, 561 (1966).
17. J.M. Cork, M.K. Brice, R.G. Helmer & D.E. Sarason, Phys. Rev. 107, 1621 (1957).

18. J.O. Juliano & F.S. Stephens, Phys. Rev. 108, 341 (1957).

19. B.S. Dzelepov, Izvest Akad.Nauk.SSSR Ser.Fiz. 21,966 (1957).

20. B.V. Bobikin, Izvest Akad.Nauk.SSSR Ser.Fiz.21,1556 (1957).

21. O. Nathan & M.A. Waggoner, Nu. Phys. 2, 548 (1957).

22. S.K. Bhattacharjee, Proc. A Indian Acad.Sci. 47,295(1958).

23. P. Debrunner, Helv. Phys. Acta. 33, 395 (1960).

24. C.V.K. Baba & S.K. Bhattacharhee, Phys. Rev. 123,865(1961).

25. L.D. Wyly, E.T. Ptronis, H. Duloney & C.H. Braden, Phys. Rev. 124, 841 (1961).

26. K.S.R. Sastry, R.F. Petry & R.G. Wilkinson, Phys. Rev. 123, 615 (1961).

27. S.K. Bhattacherjee & S.K. Mitra, Phys. Rev. 126, 1154(1962).

28. J.W. Sunier, Helv. Phys. Acta. 36, 429 (1963).

29. P.G. Hansen, H.L. Nielsen & K. Wilsky, Nu. Phys.89,571(1966).

30. B.C. Dutta, R. hess & G.Wulff,Helv.Phys.Acta.37,610(1964).

31. J. Burde, M. Rakavy, G. Rakavy, Phys. Rev. 129,2147(1963).

32. R.S. Dingus, W.L. Talbert & M.G. Stewart, Nu. Phys. 83, 545 (1966).

33. B. Harmatz & T.H. Handley, Phys. Rev. 123, 1758 (1961).

34. Y. Yoshizawa, B. Elbek, B. Herskind & M.C. Olesen, Nu. Phys. 73, 273 (1965).

35. R. Block, B. Elbek & P.O. Tjom, Nu. Phys. A91, 576 (1967).

36. J.H. Hamilton, T. Katoh, W.H. Brantley & E.F. Zganjar, Phys. Lett. 13, 43 (1964).

37. M.E. Rose, Elementary Theory of Angular Momentum, (1957).

38. A.R. Edmonds, Angular Momentum in Quantum Mechanics, (1957).

39. W. Pauli, Handbuck der Physik Bd XXIV/1 (1933).

40. J.P. Davidson, Rev. Mod. Phys. 37, 105 (1965).

41. J.P. Davidson, USNRDL, TR, 901 (1965).

42. T. Tamura & L.G. Komai, Phys. Rev. Lett. 3, 344 (1959).

43. T. Tamura & T. Udagawa, Nu. Phys. 16, 460 (1960).

44. T. Tamura & H. Yoshida, Nu. Phys. 30, 579 (1962).

45. E.L. Church & J. Wenesser, Phys. Rev. 103, 1035 (1956).

46. K.C. Mann & R.P. Chaturvedi, Can. J. Phys. 41, 932 (1963).

47. J.M. Blatt & V.F. Weisskopf, Theoretical Nuclear Physics.

48. R.D. Evans, The Atomic Nucleus, p.676.

49. Nuclear Data Sheets (April, 1964).

50. K. Siegbahn, Beta- and Gamma-ray Spectroscopy, p.549.

51. S.G. Nilsson, Dan.Vid.Sel.Mat.Fys.Med. 29, No.16 (1955).

52. G. Alaga, Nu. Phys. 4, 625 (1957).

53. C.J. Gallagher, Nu. Phys. 16, 215 (1960).

54. G. Alaga, K. Adler, A. Bohr, & R.B. Mottelson, Kgl. Dan. Vid. Sel. Mat. Fys. Med. 29, 9 (1955).

55. C.S. Wu, Rev. Mod. Phys. 22, 389 (1950).

56. H.M. Taylor & N.F. Mott, Proc. Roy. Soc. (London) 142A, 215 (1933).

57. M.E. Rose, Internal Conversion Coefficients.

58. L.A. Sliv & I.M. Band, Coefficients of Internal Conversion

of Gamma Radiation.

59. Nucleon Data, Set A, 1, No.6 (1966), Acad. Press.

60. E. Segre, Experimental Nuclear Physics, Vol. III, p.368.

61. W. Parker, M. De Croes, K. Sevier,Jr., Nu. Inst. & Meth. 7, 22 (1960).

62. E. Bruninx & G. Rudstam, Nu. Inst. & Meth. 13, 131 (1961).

63. E. Fuschini, C. Maroni, C. Porceddu, & P. Veronesi, Nu. Inst. & Meth. 26, 301 (1964).

64. W. Parker, H. Bildstein, N. Getoff, H. Fischer-Colbrie & H. Regal, Nu. Inst. & Meth. 26, 61 (1964).

65. T. Walton, M.Sc. Thesis, Physics Dept., Uni. of B.C.

66. J.F. Suarez & E.Y. de Aisenberg, Nu. Phys. A90, 449 (1967).

67. J.B. Davidson, private communication.

68. E.Y. de Aisenberg & J.F. Suarez, Nu. Phys. A97, 529 (1967).